

December 2017

# Electrochemical Detection of Low-concentration Lead (II) Ions from Water

Mohammad Rizwen Ur Rahman  
*University of Wisconsin-Milwaukee*

Follow this and additional works at: <https://dc.uwm.edu/etd>

 Part of the [Mechanical Engineering Commons](#)

---

## Recommended Citation

Rahman, Mohammad Rizwen Ur, "Electrochemical Detection of Low-concentration Lead (II) Ions from Water" (2017). *Theses and Dissertations*. 1680.  
<https://dc.uwm.edu/etd/1680>

This Thesis is brought to you for free and open access by UWM Digital Commons. It has been accepted for inclusion in Theses and Dissertations by an authorized administrator of UWM Digital Commons. For more information, please contact [open-access@uwm.edu](mailto:open-access@uwm.edu).

# ELECTROCHEMICAL DETECTION OF LOW- CONCENTRATION LEAD (II) IONS FROM WATER

by

Mohammad Rizwen Ur Rahman

A Thesis Submitted in  
Partial Fulfillment of the  
Requirements for the Degree of

Master of Science  
in Engineering

at

The University of Wisconsin-Milwaukee

December 2017

## ABSTRACT

### ELECTROCHEMICAL DETECTION OF LOW-CONCENTRATION LEAD (II) IONS FROM WATER

by

Mohammad Rizwen Ur Rahman

The University of Wisconsin-Milwaukee, 2017  
Under the Supervision of Dr. Woo-Jin Chang

The aim of this study was to develop an electrochemical sensor for speedy, selective and sensitive detection of lead ion ( $\text{Pb}^{2+}$ ) using graphene oxide and pyrrole nanocomposite. Different combinations of graphene oxide and pyrrole in layers and mixtures were tested for the finest sensitive detection of lead ion ( $\text{Pb}^{2+}$ ). Reduced graphene oxide and polypyrrole (rGO-PPY as layer) nanocomposite modified screen printed electrode (SPE) showed the best signal in response to the differential pulse anodic stripping voltammetry (DPASV) with a limit of detection to 5 ppb. The rGO-PPY modified electrode possessed a large effective surface area because of the unique 3D porous architectures and displayed good selectivity for determination of  $\text{Pb}^{2+}$  in presence of  $\text{Cu}^{2+}$ . The differential pulse anodic stripping voltammetry signals were analyzed and relevant parameters were optimized. The developed rGO-PPy nanocomposite modified SPE sensor was tested with the spiked tap water solution to validate its applicability in real sample analysis. The sensor structure and the fabrication method of the developed sensor is rapid and simple to follow compared to complex and time consuming electrochemical synthesis process. Moreover, this fabrication process can be easily modified and implemented using a printing device for inexpensive mass production.

© Copyright by Mohammad Rizwen Ur Rahman, 2017  
All Rights Reserved

To  
all my family members and friends

# TABLE OF CONTENTS

|   |      |
|---|------|
| List of Figures .....   | viii |
| List of Abbreviations .....   | xii  |
| ACKNOWLEDGEMENTS .....  | xiii |
| Chapter 1: Introduction .....   | 1    |
| 1.1 Organization of the thesis .....  | 2    |
| 1.2 Motivation/Literature Review .....  | 3    |
| 1.3 Mechanism of stripping voltammetry .....  | 15   |
| 1.4 Mechanism of lead ion ( $Pb^{2+}$ ) detection using stripping voltammetry .....                                   | 21   |
| Chapter 2: Experimental Section .....   | 23   |
| 2.1 Materials and Reagents .....  | 24   |
| 2.2 Devices, Instruments and Measurements .....   | 24   |
| 2.3 Fabrication Method .....  | 26   |
| 2.3.1 Synthesis of graphene oxide-pyrrole nanocomposite .....   | 26   |
| 2.3.2 Graphene Oxide - Polypyrrole (GO-PPy) as layer .....  | 27   |
| 2.3.3 Reduced Graphene Oxide - Polypyrrole (rGO-PPy) as layer .....   | 28   |
| 2.3.4 Graphene Oxide - Pyrrole (GO/Py) as mixture.....  | 29   |
| 2.3.5 Reduced Graphene Oxide - Pyrrole (rGO/Py) as mixture .....  | 29   |
| 2.3.6 Electrochemical polymerization of Graphene Oxide and Pyrrole mixture (GO/PPy)<br>.....                          | 30   |
| 2.3.7 Electrochemical polymerization and subsequent reduction of Graphene Oxide and<br>Pyrrole mixture (rGO/PPy)..... | 30   |
| Chapter 3: Sensor Structure and Fabrication Methods .....   | 32   |
| 3.1 SEM image for surface morphologic characterization of graphene oxide and pyrrole<br>composite film.....           | 33   |
| 3.1.1 Bare SPE (no additional nanomaterials) .....  | 35   |
| 3.1.2 Graphene Oxide - Polypyrrole (GO-PPy) as layer .....  | 37   |
| 3.1.3 Reduced Graphene Oxide - Polypyrrole (rGO-PPy) as layer .....   | 38   |
| 3.1.4 Graphene Oxide - Pyrrole (GO/Py) as mixture.....  | 39   |
| 3.1.5 Reduced Graphene Oxide - Pyrrole (rGO/Py) as mixture .....  | 40   |
| 3.1.6 Electrochemical polymerization of Graphene Oxide and Pyrrole mixture (GO/PPy)<br>.....                          | 41   |

|            |   |    |
|------------|---|----|
| 3.1.7      | Electrochemical polymerization and subsequent reduction of Graphene Oxide and Pyrrole mixture (rGO/PPy).....  | 42 |
| Chapter 4: | Performance Analysis and Operating Parameters Optimization.....   | 44 |
| 4.1        | Quantitative determination of Pb <sup>2+</sup> .....  | 45 |
| 4.2        | Importance of pH in electrochemical detection of heavy metals ions .....  | 45 |
| 4.3        | Effect of pH on electrochemical detection of Pb <sup>2+</sup> using graphene oxide and pyrrole modified SPE.....  | 49 |
| 4.4        | Effect of graphene oxide concentration on Pb <sup>2+</sup> detection using rGO-PPy modified SPE .....   | 51 |
| 4.5        | Effect of deposition time on Pb <sup>2+</sup> detection using rGO-PPy modified SPE .....  | 52 |
| 4.6        | Effect of deposition potential on Pb <sup>2+</sup> using rGO-PPy modified SPE .....   | 54 |
| 4.7        | Detection of Pb <sup>2+</sup> in 0.1 M sodium-acetate buffer, pH 4.4 using bare SPE sensor (without any nanocomposites) .....                                       | 55 |
| 4.8        | Detection of Pb <sup>2+</sup> in 0.1 M sodium-acetate Buffer, pH 4.4: layers and mixture of GO and 0.1 M pyrrole.....   | 56 |
| 4.8.1      | Graphene Oxide - Polypyrrole (GO-PPy) as layer .....  | 56 |
| 4.8.2      | Reduced Graphene Oxide - Polypyrrole (rGO-PPy) as layer .....   | 57 |
| 4.8.3      | Graphene Oxide - Pyrrole (GO/Py) as mixture.....  | 57 |
| 4.8.4      | Reduced Graphene Oxide - Pyrrole (rGO/Py) as mixture .....  | 58 |
| 4.8.5      | Electrochemical polymerization of Graphene Oxide and Pyrrole mixture (GO/PPy) .....   | 59 |
| 4.8.6      | Electrochemical polymerization and subsequent reduction of Graphene Oxide and Pyrrole mixture (rGO/PPy).....  | 59 |
| 4.9        | Electrochemical detection of Pb <sup>2+</sup> in 0.1 M sodium-acetate buffer, pH 4.4 using bare Sensor (i.e. without any modification).....                         | 60 |
| 4.10       | Electrochemical detection of Pb <sup>2+</sup> in 0.1 M sodium-acetate buffer, pH 4.6 using sGO/PPy .....  | 61 |
| 4.11       | Electrochemical detection of Pb <sup>2+</sup> in 0.1 M sodium-acetate buffer, pH 4.4 using rGO-PPy modified SPE .....   | 62 |
| 4.12       | Effect of physical parameters (temperature) on electrochemical detection of Pb <sup>2+</sup> in 0.1 M sodium-acetate buffer, pH 4.4 using rGO-PPy modified SPE..... | 68 |
| 4.13       | Selectivity test of rGO-PPy modified SPE in presence of Cu <sup>2+</sup> (as interfering metal ions) on electrochemical detection of Pb <sup>2+</sup> : .....       | 73 |
| 4.13.1     | Selectivity test in presence of Cu <sup>2+</sup> on electrochemical detection of Pb <sup>2+</sup> using rGO-PPy modified SPE .....                                  | 74 |
| 4.14       | Electrochemical detection of Pb <sup>2+</sup> using rGO-PPy modified SPE in tap water test .....  | 76 |

|                            |    |
|----------------------------|----|
| Chapter 5: Conclusion..... | 82 |
| 5.1 Overall summary .....  | 83 |
| 5.2 Future direction ..... | 84 |
| References.....            | 87 |

## LIST OF FIGURES

|  |    |
|--|----|
| Figure 1: Disposition/Pre-concentration step in a stripping voltammetry .....  | 16 |
| Figure 2: Stripping/Dissolution step in a stripping voltammetry.....   | 18 |
| Figure 3: Working method of the stripping voltammetry process with the three-electrode setup:<br>(1) working electrode; (2) counter electrode; (3) reference electrode ..... | 19 |
| Figure 4: A three-electrode Screen Printed Electrode (SPE) sensor (50 x 13 mm / h x w).....  | 25 |
| Figure 5: CHI-6012E, a computer-controlled electrochemical analyzer (CHI, USA) .....   | 26 |
| Figure 6: Atomic structure of pyrrole (left) and polypyrrole (right) .....   | 26 |
| Figure 7: Cyclic voltammetry (CV) technique used for polymerization of polypyrrole using the<br>electrochemical station.....   | 28 |
| Figure 8: Differential pulse voltammetry (DPV) technique for reduction of graphene oxide using<br>the electrochemical station.....   | 29 |
| Figure 9: 3-dimensional graphite structure showing the covalent bonds and van der Waals bond<br>.....  | 34 |
| Figure 10: SEM image of the working electrode of a bare (graphite powder only) SPE Sensor .  | 35 |
| Figure 11: Atomic structure (top) and SEM image (bottom) of the graphite, graphene oxide and<br>reduced graphene oxide. ....   | 36 |
| Figure 12: SEM image of the working electrode of with graphene oxide (left) and reduced<br>graphene oxide (right) modified SPE Sensor.....                                   | 37 |
| Figure 13: SEM image of the working electrode of with GO-PPy (as layer).....   | 38 |
| Figure 14: SEM image of the working electrode of with rGO-PPy (as layer) .....   | 39 |
| Figure 15: SEM image of the working electrode of with GO/Py (as mixture).....  | 40 |
| Figure 16: SEM image of the working electrode of with reduced rGO/Py (as mixture).....   | 41 |
| Figure 17: SEM image of the working electrode of GO/PPy (mixture electrodeposition) modified<br>SPE Sensor.....  | 42 |
| Figure 18: SEM image of the working electrode of rGO/PPy (mixture electrodeposition and<br>subsequent reduction) modified SPE Sensor .....                                   | 43 |
| Figure 19: Effect of pH on Pb <sup>2+</sup> detection using SPE sensor, 1000 ppb Pb <sup>2+</sup> in 0.1 M sodium-<br>acetate buffer with different pH.....                  | 51 |

|  |    |
|--|----|
| Figure 20: Effect of graphene oxide concentration on the Pb <sup>2+</sup> detection using rGO-PPy modified SPE sensor in 500 ppb Pb <sup>2+</sup> in sodium-acetate buffer (pH 4.4) with different concentration of graphene oxide.....  | 52 |
| Figure 21: Effect of deposition time in lead ion Pb <sup>2+</sup> detection using DPASV method with rGO-PPy modified screen printed electrode (SPE) in 1000 ppb Pb <sup>2+</sup> in sodium-acetate buffer (pH 4.4) with different deposition cycle .....   | 53 |
| Figure 22: Effect of deposition potential in lead ion Pb <sup>2+</sup> detection using DPASV method with rGO-PPy modified screen printed electrode (SPE) in 250 ppb Pb <sup>2+</sup> in sodium-acetate buffer (pH 4.4) with different deposition potential .....                                 | 54 |
| Figure 23: Comparison between bare sensor (the original graphite powder without any nanocomposites) before and after the cleaning and pre-treatment cycle with 0 ppb Pb <sup>2+</sup> and 50 ppb Pb <sup>2+</sup> in sodium acetate buffer (pH 4.4) with 10 min (600 sec) deposition cycle ..... | 55 |
| Figure 24 GO-PPy (as layer) modified SPE sensor in detection of 0 ppb Pb <sup>2+</sup> and 50 ppb Pb <sup>2+</sup> in sodium acetate buffer (pH 4.4) with 10 min (600 sec) deposition cycle .....  | 56 |
| Figure 25: rGO - PPy (as layer) modified SPE sensor in detection of 0 ppb Pb <sup>2+</sup> and 50 ppb Pb <sup>2+</sup> in sodium-acetate buffer (pH 4.4) with 10 min (600 sec) deposition cycle.....   | 57 |
| Figure 26: GO/Py (as mixture) modified SPE sensor in detection of 0 ppb Pb <sup>2+</sup> and 50 ppb Pb <sup>2+</sup> in sodium-acetate buffer (pH 4.4) with 10 min (600 sec) deposition cycle.....   | 58 |
| Figure 27: rGO/Py (as mixture) modified SPE sensor in detection of 0 ppb Pb <sup>2+</sup> and 50 ppb Pb <sup>2+</sup> in sodium-acetate buffer (pH 4.4) with 10 min (600 sec) deposition cycle.....  | 58 |
| Figure 28: GO/PPy (electrodeposited as mixture) modified SPE sensor in detection of 0 ppb Pb <sup>2+</sup> and 50 ppb Pb <sup>2+</sup> in sodium-acetate buffer (pH 4.4) with 10 min (600 sec) deposition cycle.....   | 59 |
| Figure 29: rGO/PPy (electrodeposition and subsequent reduction of mixture) modified SPE sensor in detection of 0 ppb Pb <sup>2+</sup> and 50 ppb Pb <sup>2+</sup> in sodium-acetate buffer (pH 4.4) with 10 min (600 sec) deposition cycle .....   | 60 |
| Figure 30: Bare SPE (no modification) sensor in detection of various concentration of Pb <sup>2+</sup> in sodium-acetate buffer (pH 4.4) with 10 min (600 sec) deposition cycle.....   | 61 |
| Figure 31: Cysteine-Functionalized Graphene Oxide/Polypyrrole Nanocomposite modified sensor [28] in detection of various concentration of Pb <sup>2+</sup> in sodium-acetate buffer (pH 4.4) with 10 min (600 sec) deposition cycle .....  | 62 |

|   |    |
|---|----|
| Figure 32: rGO-PPy modified SPE sensor in detection of Pb <sup>2+</sup> in 0 – 250 ppb concentrated solution of Pb <sup>2+</sup> in 0.1 M sodium-acetate buffer (pH 4.4) with 10 min (600 sec) deposition cycle .....   | 63 |
| Figure 33: rGO-PPy modified SPE sensor in detection of Pb <sup>2+</sup> in 250 – 1000 ppb concentrated solution of Pb <sup>2+</sup> in 0.1 M sodium-acetate buffer (pH 4.4) with 10 min (600 sec) deposition cycle .....  | 64 |
| Figure 34: Plot of the peak current from the DPASV rGO-PPy modified SPE sensor in detection of Pb <sup>2+</sup> in 0 ppb - 25 ppb concentrated solution of Pb <sup>2+</sup> in 0.1 M sodium-acetate buffer (pH 4.4) with 10 min (600 sec) deposition cycle .....                          | 64 |
| Figure 35: Plot of the peak current from the DPASV rGO-PPy modified SPE sensor in detection of Pb <sup>2+</sup> in 25 ppb - 100 ppb concentrated solution of Pb <sup>2+</sup> in 0.1 M sodium-acetate buffer (pH 4.4) with 10 min (600 sec) deposition cycle.....                         | 65 |
| Figure 36: Plot of the peak current from the DPASV rGO-PPy modified SPE sensor in detection of Pb <sup>2+</sup> in 250 ppb - 1000 ppb concentrated solution of Pb <sup>2+</sup> in 0.1 M sodium-acetate buffer (pH 4.4) with 10 min (600 sec) deposition cycle.....                       | 66 |
| Figure 37: Plot of the peak current from the DPASV rGO-PPy modified SPE sensor in detection of Pb <sup>2+</sup> in 0 ppb - 1000 ppb concentrated solution of Pb <sup>2+</sup> in 0.1 M sodium-acetate buffer (pH 4.4) with 10 min (600 sec) deposition cycle.....                         | 67 |
| Figure 38: Effect of temperature on Pb <sup>2+</sup> detection: 1000 ppb Pb <sup>2+</sup> in 0.1 M sodium-acetate buffer, pH 4.4 with rGO-PPy SPE deposition and stripping at the same temperature .....  | 69 |
| Figure 39: Peak current from the DPASV step for 1000 ppb Pb <sup>2+</sup> in 0.1 M sodium-acetate buffer, pH 4.4, with rGO-PPy SPE deposition and stripping at the same temperature .....   | 70 |
| Figure 40: Effect of temperature on Pb <sup>2+</sup> detection: 1000 ppb Pb <sup>2+</sup> in 0.1 M sodium-acetate buffer, pH 4.4 with rGO-PPy SPE deposition at room temperature and stripping at different temperature .....   | 71 |
| Figure 41: Peak current from the DPASV step for 1000 ppb Pb <sup>2+</sup> in 0.1 M sodium-acetate buffer, pH 4.4, with rGO-PPy SPE deposition at room temperature and stripping at different temperature .....  | 71 |
| Figure 42: Comparison between the peak current from the DPASV step for 1000 ppb Pb <sup>2+</sup> in 0.1 M sodium-acetate buffer, pH 4.4, with rGO-PPy SPE deposition at room temperature and stripping at different temperature and deposition and stripping at the same temperature .... | 72 |

Figure 43: Tap water test report on “Lead/Copper Samples” by Wisconsin Department of Natural Resources ..... 74

Figure 44: Electrochemical detection of  $Pb^{2+}$  in presence of  $Cu^{2+}$  using rGO-PPy modified SPE sensor in 0.1 M sodium-acetate buffer (pH 4.4) with 10 min (600 sec) deposition cycle (Blue line: 1,000 ppb  $Pb^{2+}$  in presence of 5,000 ppb  $Cu^{2+}$  and Orange line: 500 ppb  $Pb^{2+}$  in presence of 2,500 ppb  $Cu^{2+}$ ) ..... 75

Figure 45: Electrochemical detection of  $Pb^{2+}$  in presence of  $Cu^{2+}$  using rGO-PPy modified SPE sensor in 0.1 M sodium-acetate buffer (pH 4.4) with 10 min (600 sec) deposition cycle (with smaller maximum value in y-axis to zoom in the peak current for the orange line: 500 ppb  $Pb^{2+}$  in presence of 2,500 ppb  $Cu^{2+}$ ) ..... 75

Figure 46: Tap water test report on “Lead/Copper” by Milwaukee Water Works [87] ..... 76

Figure 47: Electrochemical detection of  $Pb^{2+}$  in tap water with spiked  $Pb^{2+}$  and  $Cu^{2+}$  using rGO-PPy modified SPE with 10 min (600 sec) deposition cycle (blue line: 1 ppb  $Pb^{2+}$ , orange line: 10 ppb  $Pb^{2+}$ , black line: 25 ppb  $Pb^{2+}$ , yellow line: 50 ppb  $Pb^{2+}$ , red line: 50 ppb  $Pb^{2+}$  in presence of 200 ppb  $Cu^{2+}$ ) ..... 77

Figure 48: : Tap water test report on “Fluoride Sample History” by Wisconsin Department of Natural Resources [85] ..... 79

Figure 49: Tap water test report on “Disinfection Byproducts” as a results of the chemical applied to the natural water (lake/river/ground water) by Wisconsin Department of Natural Resources [85] ..... 80

Figure 50: Solubility of lead salt ( $PbCl_2$ ) in water with different pH, pH 4.4 buffer in the jar (on the left) and tap water pH 7.38 in the conical flask (on the right) with same of amount lead salt in 100 mL water ..... 85

## LIST OF ABBREVIATIONS

|         |   |
|---------|---|
| DPASV   | Differential Pulse Anodic Stripping Voltammetry   |
| LOD     | Limit of Detection  |
| GO      | Graphene Oxide  |
| Py      | Pyrrole   |
| PPy     | Polypyrrole   |
| CV      | Cyclic Voltammetry  |
| i-t     | Open Current Amperometric   |
| SPE     | Screen Printed Electrode  |
| GCE     | Glassy Carbon Electrode   |
| DI      | Deionized Water   |
| SEM     | Scanning Electron Microscope  |
| GO-PPy  | Graphene Oxide - Polypyrrole as layer   |
| rGO-PPy | Reduced Graphene Oxide - Polypyrrole as layer   |
| GO/Py   | Graphene Oxide - Pyrrole as mixture   |
| rGO/Py  | Reduced Graphene Oxide - Pyrrole as mixture   |
| GO/PPy  | Electrochemical polymerization of Graphene Oxide and Pyrrole mixture                          |
| rGO/PPy | Electrochemical polymerization and subsequent reduction of Graphene Oxide and Pyrrole mixture |
| IUPAC   | International Union of Pure and Applied Chemistry   |
| WHO     | World Health Organization   |
| EPA     | United States Environmental Protection Agency   |
| ppb     | Parts per Billion (ppb) (1 ppb = 1 $\mu\text{g/L}$ )  |

## ACKNOWLEDGEMENTS

I am ever grateful to God, the Creator and the Almighty, and to whom I owe my very existence. First, I would like to thank my advisor, Dr. Woo-Jin Chang for giving me the opportunity to work in his research group. He has helped me to go through the process of restarting my academic chapter for my graduate studies after I returned to the academia from a full time industrial position. With his continuous support and guidance throughout my graduate studies. I am also grateful to my lab mate Tae-Joon Kwak for helping me to learn synthesis and fabrication of nanocomposites. It was also fun and encouraging to work with Hwangjae Lee, MiSong Ryu, alumni of the lab. The valuable training by Dr. Steven Hardcastle (Manager, Advanced Analysis Facility) on the scanning electron microscope (SEM) has helped me to analyze the surface of the nanocomposites.

I am also thankful to Dr. Yongjin Sung and Dr. Junjie Niu for being the members of my thesis committee. I appreciate their time to evaluate my work. I am always indebted to my friends for their encouragement and support especially at times when things were going tough. I am grateful to my family, their care, love and best wishes, which despite of their physical absence has helped me to finish this study.

# **Chapter 1: Introduction**

## 1.1 Organization of the thesis

The work performed in this thesis focuses on electrochemical detection of heavy metals ions, particularly lead (II) ions or  $Pb^{2+}$  in water. Differential Pulse Anodic Stripping Voltammetry (DPASV), one of the electroanalytical techniques is been used in this study for trace analysis of heavy metals ions. The fabrication method, working principle of the electrochemical sensor is discussed in detail. Comparison between different structures of the sensors, effect of different operating condition, is also demonstrated.

Chapter 1 presents a brief literature review based on the similar electrochemical sensor structure for detection of heavy metals ions. The material selection for the target analytes and fabrication techniques of the electrochemical sensor is discussed in this chapter. The working mechanism of the electrochemical sensor for heavy metal ions detection, specially  $Pb^{2+}$  is also included in Chapter 1. Chapter 2 is based on the analysis and comparison between the different sensor structures. This chapter also includes the fabrication methods, information on the materials and devices used in this study. Performance of the proposed structures for the nanocomposites, comparison between them for the best DPASV response from the different sensors is discussed in Chapter 3. One of the most important section in chapter 3 is the importance of pH in electrochemical detection of heavy metals. The parameters for the optimum operating condition is also covered in this chapter. Chapter 4 features the comparison between ideal operating condition with respect to the physical parameters, evaluation of mutual interfering ions and the tap water-sample application. The comparison between the ideal operating conditions and the tap water (as real application) is also included in this chapter. Chapter 5 consists of conclusion where the overall

application, limitation as an overall summary of the developed sensor. The future direction of the proposed electrochemical sensor and its application is also included at the end of this chapter.

## 1.2 Motivation/Literature Review

Metals with relatively high densities, atomic weights, or atomic numbers are commonly referred as heavy metals. A less common definition of heavy metal is any metal with a potential negative health effect or environmental impact, such as lead (Pb), Arsenic (As), Mercury (Hg), Chromium (Cr), and even metal like iron (Fe) and copper (Cu) above a certain range [1]. Metals with a density more than  $5 \text{ g/cm}^3$  are sometimes quoted as criterion to define heavy metals. The most common use of the term “heavy metals” refer to any metal that can cause health problems of any living organism or capable of environmental damage [2, 3]. Mercury (Hg), cadmium (Cd), arsenic (As), and lead (Pb) are mostly referred example of heavy metals. There are some high-density metals are not toxic, but some of the light metals or metalloids are known for their toxicity [2, 4]. Cadmium considered as a heavy metal can be used a as good example. With a density of  $8.65 \text{ g/cm}^3$ , atomic number of 48 and specific gravity of 8.65, cadmium is known for its toxicity. Even though the density of gold is  $19.30 \text{ g/cm}^3$ , atomic number 79 and specific gravity 18.88, typically gold is not considered as toxic. The term "heavy metal" may be a "meaningless term" according to the International Union of Pure and Applied Chemistry or IUPAC, because there is no standardized definition for a heavy metal [2]. Toxicity for any given metal varies widely depending on the physical form (i.e. complex form, ionic form or suspended form) or the oxidation state of the metal based on the environmental condition. For example, Hexavalent chromium (+6 oxidation state) is deadly, which is used in textile dyes, wood preservation and anti-corrosion

products, while trivalent chromium is nutritionally significant in many organisms for its role related to human's metabolism and storage of carbohydrate, fat and protein [3, 5].

Certain heavy metals, such as copper, iron, cobalt, chromium, zinc, manganese, magnesium, selenium, and molybdenum, may be dense and/or toxic, but necessary in low concentration for the normal functioning and needed to support biological functions in many key enzymes, act as cofactors, or act in oxidation-reduction reactions [5]. While excess exposure to some of the heavy metal elements can cause cellular damage and disease, some of the heavy metals are essential for health and nutrition for some life. Most heavy metals show a great tendency to form complex compounds, particularly with those biological macromolecules (protein, DNA) which contain nitrogen, sulfur, and oxygen ligands. As a result, changes in the molecular structure of proteins, the fracture of hydrogen bonds, or inhibition of enzymes can occur [6, 7]. Interaction with those ligands can cause altering the cell cycle, leading to cell death or causing carcinogenesis [8].

With a more specific identification, heavy metals are the relatively dense metals or metalloids known for their potential risk and toxicity to living organism and to the environmental contexts. The term has specific application to cadmium, mercury, lead and arsenic, all of which appear in the World Health Organization's list of chemicals of major public health concern [9]. Antimony, chromium, cobalt, copper, manganese, nickel, selenium, silver, thallium and zinc are also considered as toxic heavy metals and part of that list. In this essay, only lead is targeted for detection and quantification in aqueous solution.

Metals are naturally occurring constituents in the environment and vary in concentrations across geographic regions. All environmental media have naturally occurring mixtures of metals, and often introduced into the environment in different forms as complex mixtures. Metals are neither created nor destroyed by biological or chemical processes, only transformed from one form to another depending on the chemical reaction and the environmental condition. The toxico-kinetics and toxico-dynamics of metals depend on the metal, the specific form of the metal or metal compound in that instance, and the organism's ability to regulate and/or absorb the metal [4]. So, the environmental chemistry of metals strongly influences their fate and effects on human and ecological receptors. Human civilization and a concomitant increase in industrial activities has gradually redistributed many toxic metals from the earth's crust to the environment and increased the possibility of human exposure due to contamination of soil, groundwater, and air. Common sources of the toxic heavy metals are from industrial and mining wastes, aging water supply infrastructure from the early 20<sup>th</sup> century with lead containing water pipe, up to come level in some paints, lead-acid batteries, vehicle emissions by using lead containing gasoline, fertilizers, treated woods [10, 11], and microplastics floating in the world's oceans [12]. In some children's toys arsenic, cadmium and lead may be used following a strict regulatory standard. In toy manufacturing, lead is used as a anti-corrosive agent, stabilizer and color enhancer[10]. Cadmium is used sometime in toy jewelry make it shiny, to increase the mass and as a stabilizer. Arsenic is thought to be used in coloring dyes. Tin-lead alloy was widely used to solder the distilling apparatus or joining the copper water pipes, still a great source of lead poisoning trough drinking water. Tough the tin-antimony alloy is now the replacement for tin-lead alloy because of the potential toxic effect of lead, tin-lead alloy is still in use for soldering of electronic circuit. Arsenic can also be found in some rat poison used in grain and mash stores [11, 12].

Among those heavy metal ions, lead is of great concern because of the high toxicity of its compounds, nonbiodegradable and accumulation in various organisms. It is a strong neurotoxin and a carcinogen, and causes lung disease, stroke, kidney problems, high blood pressure, etc. [5, 6, 13, 14]. Based on a research in 2015, the Institute for Health Metrics and Evaluation (IHME) has reported that, lead exposure accounted for 494,550 deaths and loss of 9.3 million disability-adjusted life years (DALYs) due to long-term effects on health. In the same report, they have estimated that lead exposure accounted for 12.4% of the global burden of idiopathic developmental intellectual disability, 2.5% of the global burden of ischemic heart disease and 2.4% of the global burden of stroke [15]. Since 2014, lead contamination in drinking water has been an issue in Flint, one of the largest city in Michigan, USA. In one of the samples had lead levels that reached a staggering 13,200 parts per billion (ppb) which is almost 900 times as high as the 15-ppb regulatory limit set by the United States Environmental Protection Agency (US EPA) [14, 16]. Though, the World Health Organization (WHO) has established a guideline limiting lead concentration in drinking water as 10 ppb ( $\mu\text{g/L}$ ) [14]. The source of the contamination in Flint, Michigan has been attributed to "corrosion in the lead and iron pipes that distribute water to city residents" [16]. According to the United States Environmental Protection Agency (U.S. EPA), 10–20% of adults and 40–60% of infants are exposed to lead contamination via drinking water [17]. A research conducted on the lead poisoning in Nigeria revealed that immediate and acute consequence of lead toxicity in young children through lead contaminated soil, water, and food [18]. With the strict and reduced use of lead for industrial use, it is essential to detect and carefully monitor the total amount of lead present in drinking water.

The recommended and standard trace metal analysis of drinking water by U.S. EPA is method 200.8 using the inductively coupled plasma mass spectrometry (ICP-MS) in standard, collision and reaction modes, estimated detection limit (scanning mode  $\mu\text{G/L}$ ): Arsenic 0.9, Cadmium 0.1, Chromium 0.07, Copper 0.03, Lead 0.08 [4, 19]. The method 200.8 is suitable to determine a total twenty one (21) elements as dissolved elements in drinking water, surface waters, ground waters, wastewaters, sludges, and soils samples. Some of the EPA approved current analytical methods for the detection of heavy metals include atomic absorption spectroscopy, inductively coupled plasma (ICP)-atomic emission spectrometry (AES) [20], inductively coupled plasma (ICP)-mass spectrometry (MS) [21], fluorescence spectroscopy, X-ray fluorescence analysis [22, 23]. The main advantages of these EPA approved analytical methods are their versatility as the same method can be used for trace analysis for a large panel of elements, their very low limit of detection (LOD) and their sensitivity. Though these are most reliable methods for trace metal analysis, there are some disadvantages also. The major drawback is the cost involved in these processes, a laboratory with expensive materials are required and the multi-step sample preparation and complex analytical procedures cannot be performed without trained operators [19], which makes these unsuitable for rapid on-site measurements. In some cases, an on-site, continuous monitoring is necessary to prevent possible contaminations at the source.

Due to its advantages over the conventional analytical methods electrochemistry is an interesting alternative for detection heavy metals ions in water [24, 25], though EPA has not approved any of the electrochemical techniques for reliable trace metal analysis. Electrochemical devices, particularly stripping voltammetry for metal ion detection in water are selective towards electroactive species, inexpensive, user-friendly (instrumental simplicity) and provide choices for

different sensing materials based on the target molecules or the analytes [26-29]. In most cases, the electrochemical devices can be used by following simple instructions without any prior training. The procedures for these devices make it possible for a miniature device which can be used in on-site and for rapid measurements [30]. This also allow a fast analysis comparing to the analytical method, with experimental data obtained mostly few minutes. This method can be improved for better sensitivity, lower detection limit (LOD), detecting multiple target molecules in one run and on-line monitoring for an automated system [31-36].

In electrochemical detection of heavy metal ions, carbon materials (graphite or glassy carbon) are generally used as the electrode materials due to their low cost, chemical stability, wide potential window, relatively inert electrochemistry, and electro-catalytic activity for a variety of redox reactions [37]. The basic carbon based working electrode along with the reference and a counter electrode was tested using stripping voltammetry techniques for analysis of heavy metals [38], but the sensitivity was very low and the detection limit cannot meet the requirements specified by WHO and the US Environmental Protection Agency (US EPA) [14]. The researches focus on the improving the sensitivity, selectivity and linearity of the working electrode by doping it with other materials for improved conductivity, reduced noise and better affinity toward the target heavy metal molecules.

In recent years, graphene has been used as novel electrode material for the working electrode for its tremendous potential for electrochemical applications heavy metal ions sensing [37, 39]. Graphene based electrochemical sensors have been developed for the detection of heavy-metal ions the excellent properties of graphene, such as large surface-to volume ratio, high conductivity

and electron mobility at room temperature, robust mechanical properties, and flexibility [30, 40-43]. Comparing to graphite and glassy carbon electrodes, the electrochemical responses of graphene electrodes have more favorable electron-transfer kinetics [37]. The main advantage of graphene as an electrode is the availability of a large, active surface area and fast electron transfer rate. The presence of oxygen-containing groups on its edges or surface, resulting in easy discrimination of target analytes based on their respective peaks, which commonly overlap on conventional graphite electrodes [44]. In addition to graphene, functionalized nanomaterials/ conducting polymer nanocomposite is a reliable approach to enhance the selectivity/affinity of target metal ions on electrode surface for electrochemical detection of heavy metals.

Li et al. [38] reported that electrochemical sensors based on Nafion–graphene (Nafion-G) composite film exhibited improved sensitivity for metal ion ( $\text{Pb}^{2+}$  and  $\text{Cd}^{2+}$ ) detection, and improved interference due to the synergistic effect of graphene nanosheets and Nafion. The cation exchange capacity of Nafion enhanced electron conduction of GO resulted the high sensitivity [45-47]. Linear calibration curves have been reported for 0.5 to 50  $\text{mgL}^{-1}$   $\text{Pb}^{2+}$  and for 1.5 to 30  $\text{mgL}^{-1}$   $\text{Cd}^{2+}$ . A highly sensitive electrochemical platform for the determination of  $\text{Zn}^{2+}$ ,  $\text{Cd}^{2+}$ ,  $\text{Pb}^{2+}$ , and  $\text{Cu}^{2+}$  by square-wave anodic stripping voltammetry (SWASV) was also reported by Willemse et al. [48] using a Nafion-G nanocomposite solution in combination with an in situ plated mercury film electrode. The electrode of a Nafion-G nanocomposite was found suitable for the simultaneous detection of  $\text{Zn}^{2+}$ ,  $\text{Cd}^{2+}$ ,  $\text{Pb}^{2+}$ , and  $\text{Cu}^{2+}$ . For individual metal ion detection, the lower detection limits were reported 0.07  $\mu\text{gL}^{-1}$  (0.338 nM) for  $\text{Pb}^{2+}$ , 0.08  $\mu\text{gL}^{-1}$  (1.23 nM) for  $\text{Zn}^{2+}$ , 0.13  $\mu\text{gL}^{-1}$  (2.03 nM) for  $\text{Cu}^{2+}$ , and 0.08  $\mu\text{gL}^{-1}$  (0.71 nM) for  $\text{Cd}^{2+}$ . Although the Nafion-Graphene composite electrochemical sensors discussed above showed high sensitivity for the detection of

metal ions, this simple mixture method to make nanocomposites could easily lead to irreversible agglomerates and even restacking of graphene to form graphite after the drying of dispersion solutions, due to van der Waals forces and  $\pi$ - $\pi$  stacking interactions between each of the graphene sheets [49, 50].

Shim et. al reported an ethylene-diamine-tetra-acetic acid (EDTA)-bonded conducting polymer modified electrode [24] for simultaneous detection of  $\text{Pb}^{2+}$ ,  $\text{Cu}^{2+}$ , and  $\text{Hg}^{2+}$  ions with normalized detection limit  $6.0 \times 10^{-10}$ ,  $2.0 \times 10^{-10}$ , and  $5.0 \times 10^{-10}$  M, respectively. The stability of the EDTA-CPME was remarkably improved by coating the surface with the Nafion film. Lan et. al. reported a new disposable bismuth-coated porous screen-printed carbon electrode (Bi-P-SPCE) for trace heavy metal ions detection [51]. With the rough surface, large active area and low background noise of P-SPCE, the electrode exhibited significantly enhanced sensitivity for  $\text{Pb}^{2+}$  and  $\text{Cd}^{2+}$  detection compared to screen-printed carbon electrode (SPCE) and glassy carbon electrode (GCE). the detection limits obtained on the proposed Bi-P-SPCE are  $0.03 \mu\text{g/L}$  and  $0.34 \mu\text{g/L}$  for  $\text{Pb}^{2+}$  and  $\text{Cd}^{2+}$ , respectively.

Chang et. al. reported a cysteine-functionalized graphene oxide (sGO) using carbonyl-diimidazole as a cross-linker via amide and carbamate linkages [30]. The sGO/polypyrrole (PPy) nanocomposite film was grown on the working electrode surface of a screen-printed electrode (SPE) and was used to detect lead ions ( $\text{Pb}^{2+}$ ) in water using differential pulse voltammetry (DPV). The measurable detection limit of the sensor was 0.07 ppb (linear range). Z. Zhao et. al. [52] synthesized a polypyrrole/reduced graphene oxide nanocomposite as the working electrode of glassy carbon electrode. The GCE sensor was tested to detect mercury ions ( $\text{Hg}^{2+}$ ) in the presence

of other metal ions, such as  $\text{Pb}^{2+}$ ,  $\text{Cd}^{2+}$ ,  $\text{Cu}^{2+}$ , and  $\text{Zn}^{2+}$  with sensitivity ( $0.124 \text{ mA nM}^{-1}$ ) and LOD (15 nM). H. Zhao et al. [53] reported a similar polypyrrole-graphene (PPY-rGO) nanocomposite by electrochemical synthesis with glassy carbon electrode. The modified electrode with an optimum relevant parameters for square wave anodic stripping voltammetry (SWASV) showed very good affinity towards the lead ion ( $\text{Pb}^{2+}$ ) with promising linear range of  $5 \times 10^{-9}$  to  $7.5 \times 10^{-7}$  mol/L, with LOD of  $4.7 \times 10^{-11}$  mol/L. The same was tested in the presence of other metal ions, such as  $\text{Cu}^{2+}$ ,  $\text{Hg}^{2+}$ ,  $\text{Zn}^{2+}$  and  $\text{Cd}^{2+}$  showed good selectivity towards  $\text{Pb}^{2+}$  against other relevant metal ions in aqueous water. Choi and Jang [54] synthesized porous carbon materials and their derivatives combined with PPy using vapor infiltration polymerization of pyrrole monomers. The functionalized polymer layer was successfully coated onto the pore surface of carbon without collapse of mesoporous structure enhanced the adsorption of heavy metal ions from water. Wei et. al. [26] reported the use of polypyrrole/carbonaceous nanospheres modified screen-printed electrode for detection of  $\text{Hg}^{2+}$  and  $\text{Pb}^{2+}$  with a detection limit of 0.0041 nM for  $\text{Pb}^{2+}$  and 0.0214 nM for  $\text{Hg}^{2+}$ . Wang et. al. [55] reported about a  $\text{Pb}^{2+}$  detection sensor based on Nitrogen (N) and sulfur (S) co-doped carbonaceous materials. The composite material exhibited a large surface area, high conductivity, adjustable porous structures, and fast electron transport. Based on a differential pulse anodic stripping voltammetry method the LOD obtained in  $0.064 \mu\text{g/L}$ .

Bismuth nanoparticles has been reported as a good choice with graphene for electrochemical detection of heavy metal ions. Liu et. al. [56] synthesized bismuth nanoparticles modified graphene ultrathin film electrodes and polyaniline porous layers for detection of lead ( $\text{Pb}^{2+}$ ) and cadmium ( $\text{Cd}^{2+}$ ). The working electrode was made of graphene films and further modified with bismuth (Bi) nanoparticles deposition and by a porous layer of polyaniline (PANI). Zhang et. al. [34] also

reported a bismuth-modified working electrodes for detection of lead ( $\text{Pb}^{2+}$ ) and cadmium ( $\text{Cd}^{2+}$ ) in sea water that works in three steps. In the optimum operating conditions, the linear range values for  $\text{Cd}^{2+}$  and  $\text{Pb}^{2+}$  in seawater were 0.1–3.2  $\mu\text{g/L}$  and 0.2–3.2  $\mu\text{g/L}$ , respectively. It has been noted that flexible graphene oxide (GO)-PANI and graphene-PANI hybrid offer remarkable combination of excellent electrochemical performance and biocompatibility. Gismera et. al. [57] reported a disposable screen-printed electrode (SPE) modified with bismuth-PSS composites as high sensitive sensor for cadmium and lead determination. Bismuth was incorporated in screen-printed carbon electrode modified with polystyrene sulfonate (PSS) and carbon nano-powder (CnP). The working electrode was modified with the bismuth oxide particle and tested with optimized parameter by differential pulse anodic stripping voltammetry (DPASV) for detection of lead ( $\text{Pb}^{2+}$ ) and cadmium ( $\text{Cd}^{2+}$ ) in aqueous solution. The limits of detection were 0.27  $\mu\text{g L}^{-1}$  ( $1.3 \times 10^{-9}$  M) for  $\text{Pb}^{2+}$  and 0.10  $\mu\text{g L}^{-1}$  ( $9.0 \times 10^{-10}$  M) for  $\text{Cd}^{2+}$ .

Gong et al. [42] fabricated monodispersed gold nanoparticles (AuNPs) onto the graphene nanosheet matrix, which could greatly facilitate electron-transfer processes between  $\text{Hg}^{2+}$  and the electrode, showed a good performance for the detection of  $\text{Hg}^{2+}$  in practical water samples. The sensor had a high sensitivity of 708.3  $\mu\text{A/ppb}$ , and its lower detection limit (6 ppt) was far below the guideline value of drinking water specified by the World Health Organization (1 ppb) [58]. Wei et al. reported an  $\text{SnO}_2$ /reduced GO nanocomposite modified glassy carbon electrode, which was used for the simultaneous and selective electrochemical detection of ultra-trace amounts of  $\text{Cd}^{2+}$ ,  $\text{Pb}^{2+}$ ,  $\text{Cu}^{2+}$ , and  $\text{Hg}^{2+}$  ions in drinking water [59]. Simultaneous analysis by SWASV of  $\text{Cd}^{2+}$ ,  $\text{Pb}^{2+}$ ,  $\text{Cu}^{2+}$ , and  $\text{Hg}^{2+}$  ions using an  $\text{SnO}_2$ /reduced GO nanocomposite electrode at increasing concentrations with the lower detection limits of the  $\text{SnO}_2$ /reduced GO nanocomposite modified

glassy carbon electrode for  $\text{Cd}^{2+}$ ,  $\text{Pb}^{2+}$ ,  $\text{Cu}^{2+}$ , and  $\text{Hg}^{2+}$  were 0.1015, 0.1839, 0.2269, and 0.2789 nM, respectively, which were well below the guideline value specified by the World Health Organization [58]. Xia et. al. [60] developed an electrochemical micro-sensor for simultaneous detection of  $\text{Cu}^{2+}$  and  $\text{Pb}^{2+}$  using an l-aspartic acid/l-cysteine/gold nanoparticle modified microelectrode using Micro Electro-Mechanical System (MEMS) technique. The fabrication of this electrochemical sensing platform toward  $\text{Pb}^{2+}$  and  $\text{Cu}^{2+}$  was done by combining the unique properties of nanomaterials with the specific complexing ability of amino acid. Gold nanoparticles were induced to enlarge the surface area and to increase the loading amount of L-cys; the L-asp molecules were crosslinked with L-cys to increase the complexing sites. The limit of detection reported was  $1 \mu\text{g L}^{-1}$  for both  $\text{Cu}^{2+}$  and  $\text{Pb}^{2+}$  and showed good selectivity in the presence of  $\text{Co}^{2+}$ ,  $\text{Cd}^{2+}$ ,  $\text{Ca}^{2+}$  and  $\text{Ni}^{2+}$  as interfering ion in aqueous solution. Fu et al. [61] developed a cysteine self-assembled AuNP/single wall carbon nanotubes (SWCNT) on working electrode surface for the detection of  $\text{Cu}^{2+}$ . Zhu et al. [62] reported AuNP-graphene- cysteine composite modified Bi-film electrode for simultaneous determination of  $\text{Cd}^{2+}$  and  $\text{Pb}^{2+}$  using square wave anodic stripping voltammetry (SWASV).

Morton et. al. [63] developed a cysteine-functionalized multi-walled carbon nanotubes (MWCNT)-modified glassy carbon electrode (GCE) as a sensor to improve detection of  $\text{Pb}^{2+}$  and copper ions ( $\text{Cu}^{2+}$ ) dissolved in water. Tolani et al. [64] reported the cysteine-modified polymer nanowires to evade the drawbacks of other functionalized materials used for effective detection and removal of heavy metal ions.

From the review of the recent advancement on electrochemical approach, it is obvious that the high affinity by functionalized nanomaterials/ conducting polymer nanocomposite is a reliable approach to enhance the accumulation of target metal ions on electrode surface for electrochemical detection of heavy metals. While some of those functionalized nanomaterials/ conducting polymers showed increased conductivity, some has disadvantages while using in electrochemical detection. For example, ion exchange resins lack the selectivity to target metal ions, weak binding ability, toxicity from crown ether compounds, and biopolymers are costly and biodegradable [30]. Cysteine binds well with graphene and pyrrole, but the synthetization and activation of graphene is a complex process. As one of the most promising materials, polypyrrole (PPY) shows great potential in constructing electrochemical sensors [53]. Aside from its biocompatibility, it also exhibits other advantages such as easy preparation, low cost and relatively high conductivity. Up to now, there have been several researches about functionalized PPY for the detection of  $Pb^{2+}$  [26, 30, 31, 64]. However, most of these modification methods are complex, require long synthetization process and comparatively difficult for mass production. Thus, it is quite essential to establish a rapid and simple modification method for polypyrrole (PPY) to realize ultra-sensitive and selective detection of  $Pb^{2+}$ . As discussed above, a lot of research has demonstrated that the combination between PPY and carbon nanomaterials, specially graphene oxide could significantly improve the sensitivity of the as formed PPY -based sensors. Graphene oxide- polypyrrole (GO/PPy) nanocomposite offers large surface area, fast electron transfer rate, increased mass transport rate, enhanced electro-catalytic properties, lower solution resistance, and higher signal-to-noise ratio. In addition, reduced graphene oxide (rGO) as a collection of nanoelectrodes for electrochemical applications has advantages over conventional macroelectrodes [37, 65-67], including (1) a high signal-to noise ratio because of the ultrahigh electron mobility of graphene

and its unique structural properties, such as one atom thickness; (2) a low power that enables stripping analysis in a high resistive media, which makes the supporting electrolyte unnecessary, and hence, reduces interference effects; (3) graphene-based electrodes serve as an ideal platform for accommodating metal ions and facilitating metal ion electron transfer; (4) graphene-based electrochemical electrodes can detect an individual ion as well as simultaneously monitor multiple metal ions with a low detection limit; and (5) the capability of on-site measuring of the metal ion concentration change in groundwater samples. In the present study, we investigated the best combination between graphene oxide as the base template and pyrrole as the conducting polymer. The aim of this study was to fabricate a simple and effective electrochemical sensor to detect  $\text{Pb}^{2+}$  in water. Reduced graphene oxide (rGO) and polypyrrole (PPY) was also part of the study with combination of mixture and layer structure between the two primary materials.

### 1.3 Mechanism of stripping voltammetry

For monitoring of industrial materials, scientific studies and the environmental analysis, the electroanalytical methods, based on the electrochemical principles are widely used for its advantages over the conventional analytical techniques. Among the different electroanalytical methods voltammetry one of the most used method for trace metal analysis is [30, 68-71]. Voltammetry is known as the study of current as a function of applied potential in system with at least two electrodes in an analytical solution. Information about the analyte in the solution can be obtained by measuring the resulting current with the varying potential. The different types of voltammetry techniques have simple theoretical relations and represent different aspects of dependence between the current resulting from the applied potential such as the shape of curve, height and position of peak. Anodic stripping voltammetry (ASV), cathodic stripping voltammetry

(CSV), square-wave anodic stripping voltammetry (SWASV), differential pulse anodic stripping voltammetry (DPASV), linear sweep voltammetry (LSV) are different techniques of voltammetry with more specific use such as - to determining diffusion coefficients and half-cell reduction potentials, quantitative, analytical method for trace analysis of metal cations. Stripping voltammetry methods consists of two-stage electroanalytical process, namely pre-concentration or deposition step and dissolution or stripping step.

Step 1. Deposition/Pre-concentration: The deposition step is the concentration of analytes from the sample solution of target molecules on the surface of the working electrode at a constant potential deposition. Based on the target analyte the fixed potential can be used for oxidation or reduction to attract the molecules for deposition on the working surface. Figure 1 shows typical deposition/pre-concentration step which is the “Amperometric i-t Curve (i-t)” process using the CHI-660D, a computer-controlled electrochemical analyzer. The deposition potential was -1.2 V and the deposition time was 600 seconds i.e. 10 min. The sampling interval time, quiet time and sensitivity can also be changed based on the requirement or the operating condition.

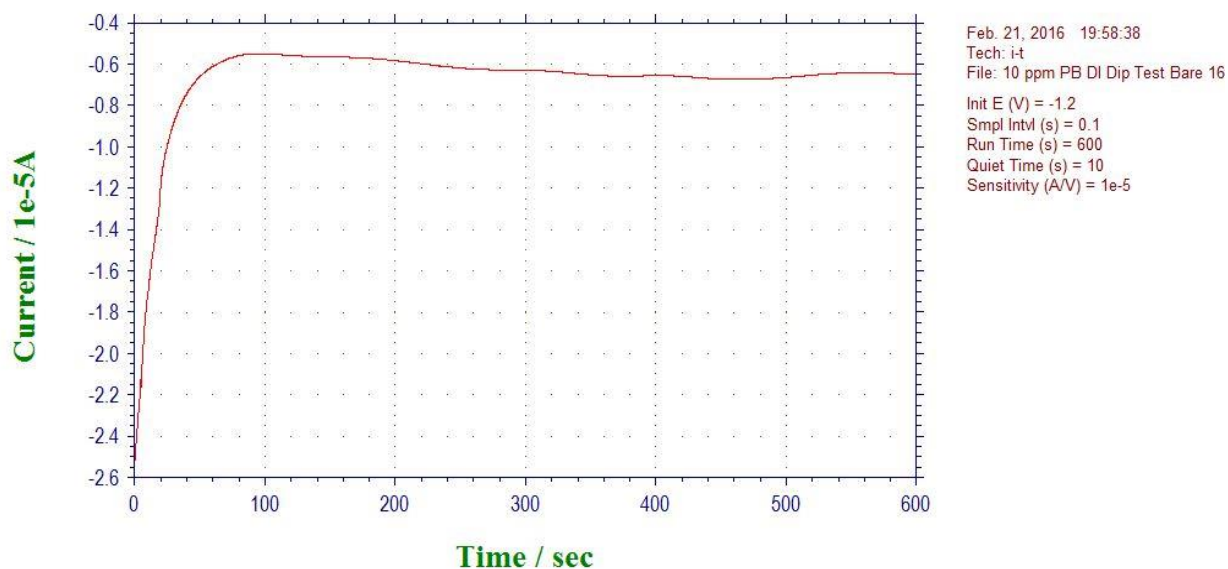


Figure 1: Disposition/Pre-concentration step in a stripping voltammetry

Step 2. Stripping/Dissolution: It is the dissolution of the target electrically active molecules from the surface of the working electrode with a potential scan. This process is done by applying a potential sweep using the working electrode or by electric pulses on the working electrode. The electrical signal in response to the potential is measured as the dependent variable of the potential. The shape of the electric signal in respect to the potential is commonly referred as the stripping curve, which mainly depends on the method of the potential scan, whether the solution is stirred or not (for increased mass transfer/diffusion), depositional potential, depositional time and the type of the electrolytes. The electrical signal in response to the applied obtained in this step is related to the concentration of metal, and by the position of the peak potential a specific metal is identified [72]. A typical stripping/dissolution step is shown in Figure 2. The initial potential was -1.2 V and the final potential was 0.2 V with 0.004 V increment voltage and 0.15 second as the pulse width for the Differential Pulse Anodic Stripping Voltammetry (DPASV) method.

As mentioned earlier, anodic stripping voltammetry is one of the most commonly used voltammetric methods for detection and quantification for trace metal analysis [68]. The target analyte from the electrolyte solution is electroplated on the working electrode during a deposition step with a negative potential, and oxidized from the electrode during the stripping step. The current is measured during the stripping step in response to the applied potential, which can be either linear, staircase, square wave, or pulse. As the stripping step initiates the oxidation of the analytes accumulated in the working electrode, it is recorded as a peak in the signal i.e. current at the potential at which the analytes begin to be oxidized. The height of the current, i.e the peak current is the quantitative parameter related to the concentration of the analyte and can be maximize by altering the operating parameter to improve sensitivity of the detection. The

electrochemical reaction is the source of the signal in the voltammetry techniques. For a reversible reaction, the potential related to the peak current is equal to potential of the standard reaction. And for an irreversible electrode reaction, position of maximum current peak is shifted toward negative potential values in relation to formal electrode potential of tested redox system.

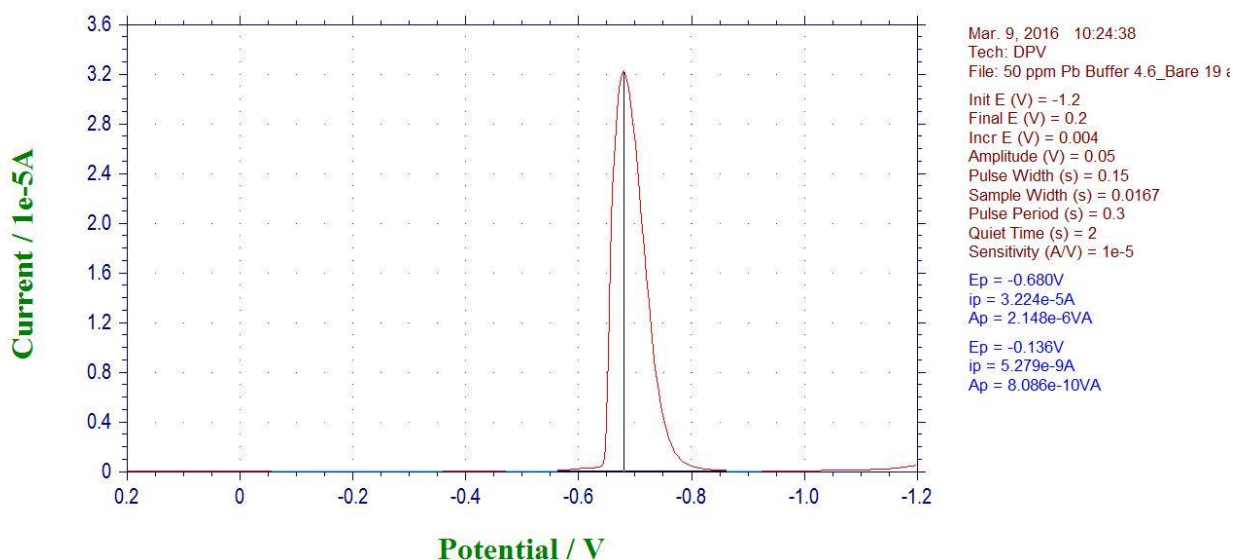
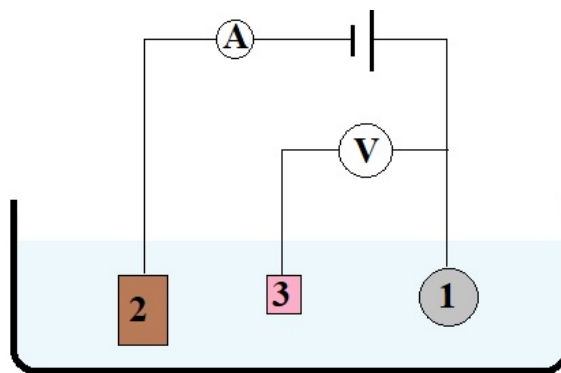


Figure 2: Stripping/Dissolution step in a stripping voltammetry

The standard anodic stripping voltammetry usually includes three electrodes, a working electrode, a counter electrode (also referred as auxiliary electrode), and a reference electrode (Figure 3). The working electrode, is the main electrode that goes through all the modification to facilitate the transfer of charge to and from the analyte with the applied desired potential in a controlled way to attract the analytes on its surface.



*Figure 3: Working method of the stripping voltammetry process with the three-electrode setup: (1) working electrode; (2) counter electrode; (3) reference electrode*

The reference electrode is a half cell with a known reduction potential and act as reference in measuring and controlling the working electrode's potential. The counter electrode facilitates all the current needed to balance the current recorded at the working electrode in response to the applied potential. To maximize the current from the potential sweep, a wide range of potential often used based on the supporting electrolytes, where it oxidizes or reduces the analytes in the supporting electrolyte. The role of the supporting electrolyte is to work as a solvent for the analytes of interest and to minimize solution resistance during the electrochemical process. The electrochemical processes without a supporting electrolyte is also possible, but the accuracy and sensitivity of the results will be greatly reduced because of added resistance. With the great variety of electrode reactions, available electrode materials, electrode designs, and conditions of electrode polarization, stripping voltammetry can be used in detection of wide ranges of analytes. The advantages of stripping electroanalytical methods used to determine trace metal analysis are [71]:

- High selectivity, good accuracy, low detection limits and reproducibility
- Possibility of determining a considerable number of elements based on their redox behavior
- Inexpensive and relatively simple operation

Differential Pulse Anodic Stripping Voltammetry (DPASV), which works on the same principle as the Anodic Stripping Voltammetry is one of the most applied technique nowadays for detection of different heavy metals using electrochemical technique [34, 62, 73]. With these techniques, it is possible to identify chemically active free ions and differentiate species based on their redox potential. The measured current during the stripping steps in DPASV is directly dependent on the concentration of the active free ions in the electrolytes [72]. In DPASV, the potential between the working electrode and the reference electrode is changed as a pulse from an initial potential to an inter-level potential with a specific pulse width (millisecond). The pulse is repeated by changing the inter-level final potential with a constant difference between the initial and the interlevel potential till it reaches to the final potential of the potential scan. The current measured between the working electrode and counter electrode before and after the potential pulse are used to analyze their differences and compared against the applied potential sweep.

The peak current and the sensitivity of the DPASV technique greatly dependent on the amount of metal which is being deposited during the deposition step/pre-concentration step on the electrode surface. However, the amount of deposited metal depends on the parameters such as total metal concentration & available chemically active ions, time/rate of deposition, surface of electrodes, temperature and the complex metal species on intermediate stages of electrodes – solution. The important factor of metal complexes in height of the stripping voltammetry.

#### 1.4 Mechanism of lead ion ( $Pb^{2+}$ ) detection using stripping voltammetry

In this study, Differential Pulse Anodic Stripping Voltammetry (DPASV) is used for the electrochemical detection of lead ion ( $Pb^{2+}$ ) in water. The proposed sensor and method can detect the presence of lead, in particular lead in free cationic form i.e.  $Pb^{2+}$  (lead in active +2-oxidation state i.e. non-complexed) such that they can be used to measure the concentration of  $Pb^{2+}$  in the sample of interest, even when very low levels of  $Pb^{2+}$  are present.

As explained earlier, the analysis comprises a first step of applying a negative voltage to the sample of interest to reduce  $Pb^{2+} / Pb (II)$  to  $Pb / Pb (0)$  and a second step of applying a voltage towards positive to oxidize  $Pb / Pb (0)$  to  $Pb^{2+} / Pb (II)$ . By comparing the peak current generated in the sample of interest and the reference sample with the known peak current confirms the presence of lead in the sample of interest.

The first step is the electrochemical reduction, the deposition/pre-concentration is done with a suitable negative potential for a set duration to accumulate the free lead cationic i.e.  $Pb^{2+}$  on the surface of the working electrode.



Following the deposition step, the second step is the electrochemical oxidation, the potential is "swept positive" to electrochemically "stripped" the lead metal i.e.  $Pb (0)$  from the electrode surface which was deposited in the first step.



The oxidation to  $Pb^{2+} / Pb(II)$  initiates a peak in the current in the voltammogram, the height and the area of the current versus the potential is dependent to the concentration of  $Pb^{2+}$  in the solution of interest. The sensitivity and the limit of detection (LOD) of the electrochemical method can be greatly improved by optimizing the potential and time of potential application during the steps discussed earlier.

The deposition time is one of the important factors, longer time in the deposition step will deposit more material on the working electrode surface which subsequently will cause the stripping peak to be larger (i.e. more material accumulated to be stripped). Other approaches to improve the sensitivity of the electrochemical method using forced convection (i.e. stirring), determining the optimum deposition potential, different operating conditions and so on.

## **Chapter 2: Experimental Section**

## 2.1 Materials and Reagents

Graphite flakes (+100 mesh), Pyrrole were purchased from Sigma-Aldrich. Graphene Oxide water dispersion (concentration 4 mg/mL) was purchased from Graphenea Inc. All the other chemicals (Acetone, Isopropyl Alcohol, Sodium Acetate Trihydrate, Acetic Acid, Metals Salts) used were of analytical grade and were purchased from Sigma-Aldrich as well. All solutions were prepared with deionized water supplied in the Global Water Center by Water Council (a non-profit organization, a globally connected epicenter for water research, innovation, education and business development).

## 2.2 Devices, Instruments and Measurements

Screen-printed electrodes (SPEs), which is a good alternative of the glassy carbon electrode (GCE), classical bulky electrodes and cells and the use of electrochemical methods less influenced by oxygen interference. With the significant improvement with respect to both their format and their printing materials over the past decade, are used as economical electrochemical substrates [69]. SPEs have been successfully utilized for the rapid in situ analysis of the environmental pollutants because of their advantageous material properties, such as disposability, simplicity, and rapid responses [26, 30, 57, 70, 73]. Considering the ease of handling and manipulation in a disposable manner of the SPEs, it is now possible to eliminate problems associated with carryover of contamination or biofouling and reducing the fear of damage associated with an expensive reusable sensor. Figure 4 shows a three-electrode Screen Printed Electrode (SPE) sensor based graphite powder used in this study. The microfabrication technology for screen-printed thick-film electrochemical transducer makes it inexpensive and durable for electrochemical analysis in

environmental, clinical or agri-food areas. The most common screen-printing technique uses a woven mesh to support an ink-blocking stencil, and a roller or squeegee is moved across the screen stencil to force or pump ink or other printable materials such as carbon, gold, platinum, silver or carbon nanotubes inks past the threads of the woven mesh in the open areas. This technology allows the mass production of reproducible yet inexpensive and mechanically robust solid strip electrodes.

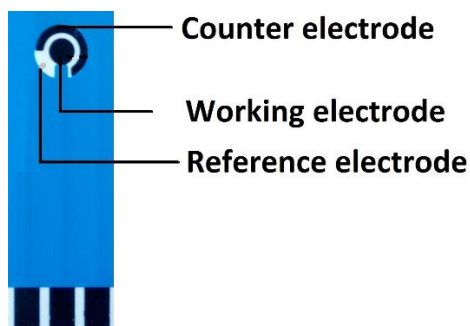


*Figure 4: A three-electrode Screen Printed Electrode (SPE) sensor (50 x 13 mm / h x w)*

A conventional screen-printed three-electrode system (from eDAQ Pty Ltd.) consisting of graphitic carbon powder as working electrode (central circle, diameter=3 mm), graphitic carbon powder (outer annular crescent) as counter electrode, and Ag/AgCl pellet as reference electrode was used. All electrochemical measurements were performed using CHI-6012E (Figure 5), a computer-controlled electrochemical analyzer (CHI, USA). The Scanning Electron Microscope (SEM) images were taken using the JEOL JSM-6460 LV with Energy Dispersive Spectroscopy and the Plasma Sputter Coating equipment in Advanced Analysis Facility (AAF) at the College of Engineering & Applied Science, University of Wisconsin-Milwaukee.



Figure 5: CHI-6012E, a computer-controlled electrochemical analyzer (CHI, USA)

## 2.3 Fabrication Method

### 2.3.1 Synthesis of graphene oxide-pyrrole nanocomposite

As described in chapter 1, Graphene Oxide (GO) has been selected as the base layer and the pyrrole is selected as the polymer to enhance the affinity of the lead ion  $Pb^{2+}$  towards the working electrode. The graphene oxide improves the electrical conductivity and effective surface area of the working electrode of the SPE [28, 30, 37, 40, 44]. And pyrrole, a type of conducting organic polymer with interesting redox behavior and good environmental stability [30, 54, 74, 75] improves the selectivity and sensitivity of the working electrode because of the complexation affinity between  $Pb^{2+}$  and amine groups ( $=N/=N+H$ ) [54].

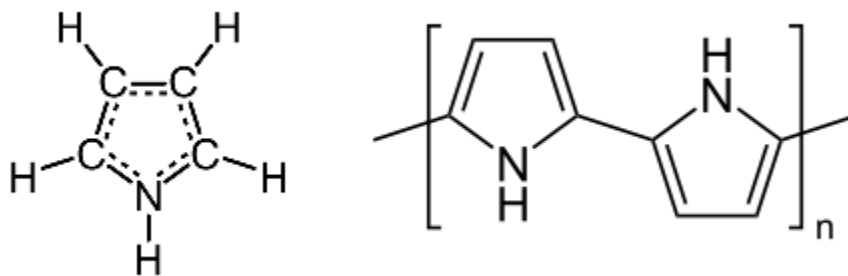


Figure 6: Atomic structure of pyrrole (left) and polypyrrole (right)

Six different concentration of GO was created from the base solution 4 mg/mL. The base concentration was diluted with deionized water was sonicated for 3 hours to form homogeneous dispersion 0.5 mg/mL, 1 mg/mL, 1.5 mg/mL, 2 mg/mL, 2.5 mg/mL, 3 mg/mL. The concentration of pyrrole was fixed (0.1 M). Six different structures were tested using the combination layers and mixture between the GO and pyrrole. And those are-

1. Graphene Oxide - Polypyrrole (GO-PPy) as layer
2. Reduced Graphene Oxide - Polypyrrole (rGO-PPy) as layer
3. Graphene Oxide - Pyrrole (GO/Py) as mixture
4. Reduced Graphene Oxide - Pyrrole (rGO/Py) as mixture
5. Electrochemical polymerization of Graphene Oxide and Pyrrole mixture (GO/PPy)
6. Electrochemical polymerization and subsequent reduction of Graphene Oxide and Pyrrole mixture (rGO/PPy)

All the new SPE sensors were cleaned with deionized water, isopropyl alcohol, acetone and deionized water (fixed the sequence) using squeeze wash bottle. The SPE sensor was dried at room temperature for 1 hour. The following steps were carried out for the above mentioned six nanocomposite structures-

### 2.3.2 Graphene Oxide - Polypyrrole (GO-PPy) as layer

About 8  $\mu$ L of GO was drop casted on the working electrode. Then it was dried for 8 hours at the room temperature. Then a layer of polypyrrole (PPy) was polymerized potentiostatically using cyclic voltammetry (CV) technique. The parameter for the CV technique was  $-0.2$  V

(initial voltage) and +0.9 V (final voltage) up to 20 complete cycles at scan rate of 50 mV/s (Figure 7). The GO sheets served as a template for PPy deposition during the electrochemical polymerization process. The modified electrode (GO-PPy SPE) was washed with deionized water to remove any physically adsorbed nanocomposite film and dried at ambience for the next 24 hours before use.

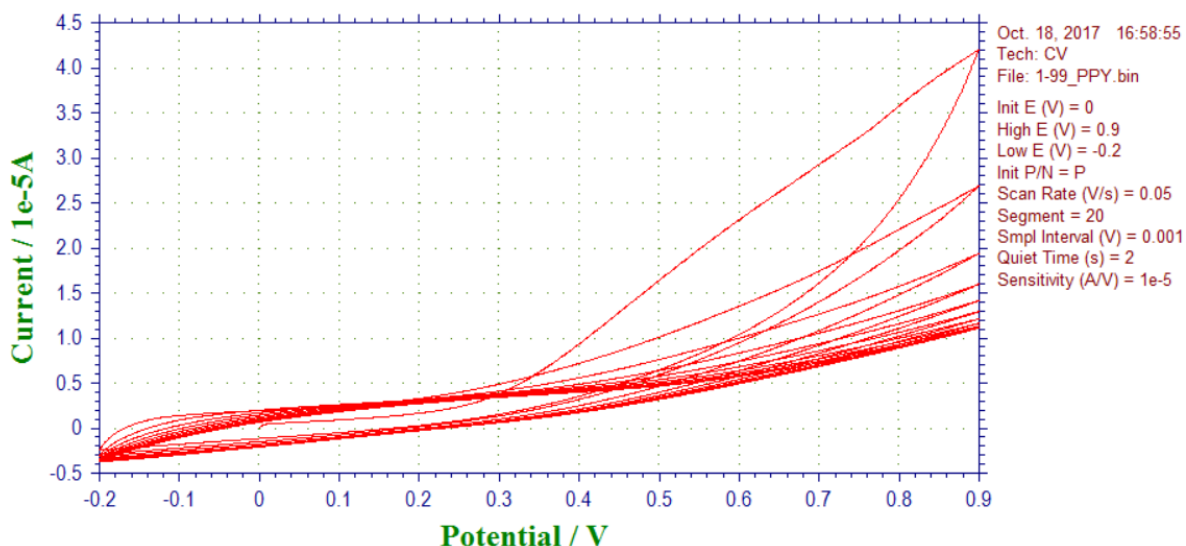


Figure 7: Cyclic voltammetry (CV) technique used for polymerization of polypyrrole using the electrochemical station

### 2.3.3 Reduced Graphene Oxide - Polypyrrole (rGO-PPy) as layer

About 8  $\mu\text{L}$  of GO was drop casted on the working electrode. Then it was dried for 8 hours at the room temperature. Then GO was effectively reduced to reduced graphene oxide (rGO) through in-situ electrochemical reduction method (Figure 8). After that a layer of polypyrrole (PPy) was polymerized potentiostatically using cyclic voltammetry (CV) technique. The parameter for the CV technique was  $-0.2$  V (initial voltage) and  $+0.9$  V (final voltage) up to 20 complete cycles at scan rate of 50 mV/s. The rGO sheets served as a template for PPy deposition during the electrochemical polymerization process. The modified electrode (GO-

PPy SPE) was washed with deionized water to remove any physically adsorbed nanocomposite film and dried at ambience for the next 24 hours before use.

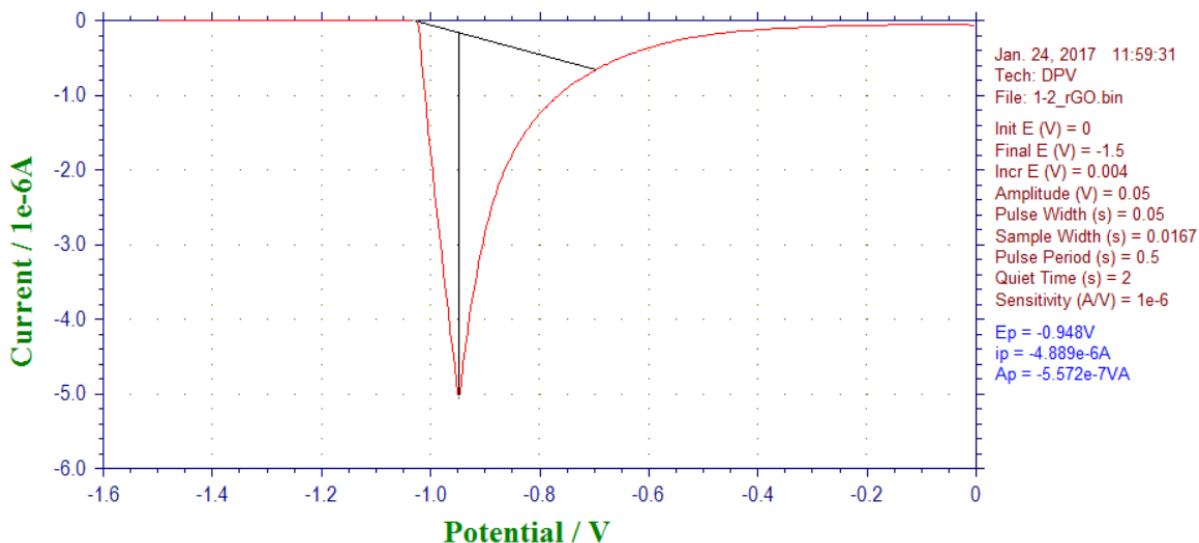


Figure 8: Differential pulse voltammetry (DPV) technique for reduction of graphene oxide using the electrochemical station

### 2.3.4 Graphene Oxide - Pyrrole (GO/Py) as mixture

Pyrrole (concentration 0.1 M) was added to the GO aqueous solution with the ratio 1:1 and the solution was subjected to magnetic stirring for 60 min to make a stable intermixture. About 8  $\mu$ L of GO-Py was drop casted on the working electrode. Then it was dried for 24 hours at the room temperature before use it for the detection of lead ions.

### 2.3.5 Reduced Graphene Oxide - Pyrrole (rGO/Py) as mixture

Pyrrole (concentration 0.1 M) was added to the GO aqueous solution with the ratio 1:1 and the solution was subjected to magnetic stirring for 60 min to make a stable intermixture. About 8  $\mu$ L

of GO-Py was drop casted on the working electrode. Then it was dried for 8 hours at the room temperature. After that GO-Py layer was effectively reduced to reduced graphene oxide (rGO) through in-situ electrochemical reduction method. Then it was dried for 24 hours at the room temperature before use it for the detection of lead ions.

### 2.3.6 Electrochemical polymerization of Graphene Oxide and Pyrrole mixture (GO/PPy)

Pyrrole (concentration 0.1 M) was added to the GO aqueous solution with the ratio 1:1 and the solution was subjected to magnetic stirring for 60 min to make a stable intermixture. After that a layer of polypyrrole (PPy) was polymerized potentiostatically using cyclic voltammetry (CV) technique. The parameter for the CV technique was  $-0.2$  V (initial voltage) and  $+0.9$  V (final voltage) up to 20 complete cycles at scan rate of 50 mV/s. The modified electrode (GO & PPy SPE) was washed with deionized water to remove any physically adsorbed nanocomposite film and dried at ambience for the next 24 hours before use.

### 2.3.7 Electrochemical polymerization and subsequent reduction of Graphene Oxide and Pyrrole mixture (rGO/PPy)

Pyrrole (concentration 0.1 M) was added to the GO aqueous solution with the ratio 1:1 and the solution was subjected to magnetic stirring for 60 min to make a stable intermixture. After that a layer of polypyrrole (PPy) was polymerized potentiostatically using cyclic voltammetry (CV) technique. The parameter for the CV technique was  $-0.2$  V (initial voltage) and  $+0.9$  V (final voltage) up to 20 complete cycles at scan rate of 50 mV/s. The modified electrode (GO & PPy SPE) was washed with deionized water to remove any physically adsorbed nanocomposite film and dried at ambience for the next 8 hours. After that the GO and Polypyrrole composite layer was

effectively reduced to reduced graphene oxide and polypyrrole (rGO & PPy) through in-situ electrochemical reduction method.

In the fabrication processes of the graphene oxide and pyrroles based nanocomposite modified SPE, both the polymerization and electrochemical reduction were carried out in a common three-electrode system. Pyrrole is used as monomer (for the drop casted model) and as a polymer (using the electrochemical polymerization process). All of the six types of SPE sensors were cleaned electrochemically in sodium acetate buffer solution of pH 4.4 using the Differential Pulse Anodic Stripping Voltammetry (DPASV) method to remove any physically adsorbed nanocomposite film or loose particle that may produce noise or signal interference before testing with analytical solution. The initial potential was -1.2 V and the final potential was 0.2 V with 0.004 V increment voltage and 0.15 second as the pulse width for the DPASV method.

# **Chapter 3: Sensor Structure and Fabrication Methods**

### 3.1 SEM image for surface morphologic characterization of graphene oxide and pyrrole composite film

The surface morphology of the working electrode of the bare SPE, graphene oxide (GO), reduced-graphene oxide (rGO), GO-Polypyrrole as layer, rGO-Polypyrrole as layer, GO-Pyrrole as mixture, Reduced GO-Pyrrole as mixture, Electrodeposition GO and Polypyrrole mixture, Electrodeposition and subsequent reduction GO and Polypyrrole mixture – all the six combinations of layers and mixtures nanocomposite modified working electrode of the SPE were characterized by scanning electron microscopy (SEM) image.

The working electrode of the screen printed used in this study is made of graphite powder, a form of extremely high-grade carbon and is the most stable under standard conditions [37]. Graphite, a 3-dimensional carbon-based material made up of planar and layered structure; each of the layer contains carbon atoms linked together in a hexagonal lattice. These links are made from an extremely strong chemical bond that involves the sharing of electron pairs between atoms, known as covalent bonds. The crystalline flake form of graphite is made up of millions of individual layers of linked carbon atoms stacked together. And bond between the carbon atoms in layers are the van der Waals bond - the residual attractive or repulsive forces between molecules or atomic groups that do not arise from a covalent bond.

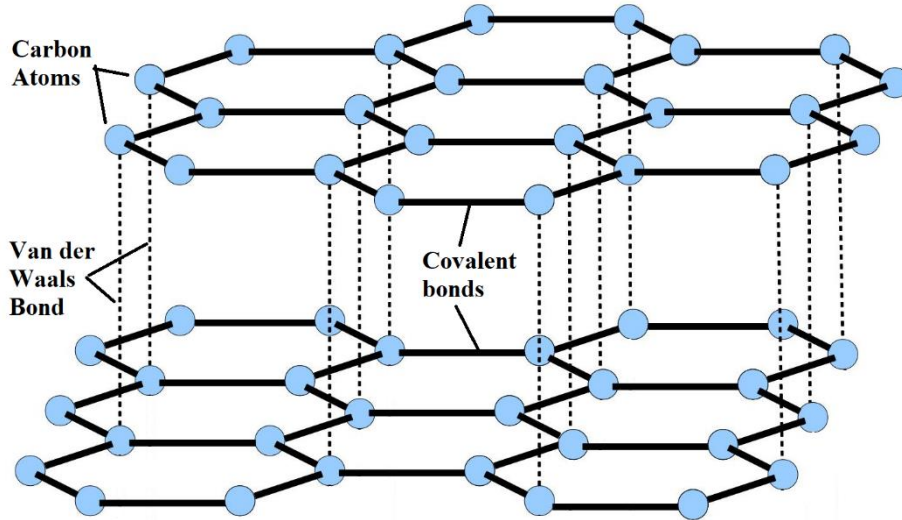


*Figure 9: 3-dimensional graphite structure showing the covalent bonds and van der Waals bond [76]*

By the oxidation of graphite using a strong oxidizing agents, oxygenated functionalities can be introduced in the graphite structure which expand the layer separation and makes the material hydrophilic (dissolve in water) [37, 44, 77]. It enables graphite oxide to be exfoliated in water using sonication to produce graphene oxide (GO) which is single or few layer graphene. The number of layers of those hexagonal lattices mainly differs between graphite oxide and graphene oxide. The standard procedure to synthesize graphene oxide (GO) begins with graphite powder as the source of carbon. The Hummer's method is most widely used process to synthesize graphite oxide using the graphite powder with a mixture of sodium nitrate, potassium permanganate, and sulfuric acid [78, 79]. Graphene oxide is produced by sonicating the graphite oxide to further exfoliate the graphene oxide layers.

As mentioned earlier, due to the presence of the oxygen functionalities in the graphene oxide, it is easily dispersible in water and other organic solvents. This makes graphene oxide a very good choice to improve electrical and mechanical properties when mixing it with ceramic or polymer

matrixes for metal ion detection. Graphene oxide has many oxygen-containing functional groups, such as epoxides, carbonyls, hydroxyl groups, and carboxyl groups. These functional groups disrupt the conjugated  $\pi$  system and hinder it from gaining its maximum strength as well the maximum conductivity [77]. Reducing the graphene oxide to form reduced graphene oxide (rGO) can be done by eliminating these oxygen-containing functional groups [80], which improve its strength and conductivity. The reduced graphene oxide (rGO) becomes more difficult to disperse in water/solvent due to its tendency to create aggregates after most of the oxygen groups are removed in this process of removal of oxygen-containing functional groups.

### 3.1.1 Bare SPE (no additional nanomaterials)

The SEM image of the bare (no additional nanomaterials) working electrode of the SPE is showed in Figure 10. As mentioned in the instrument section, the working electrode is based on graphite powder.

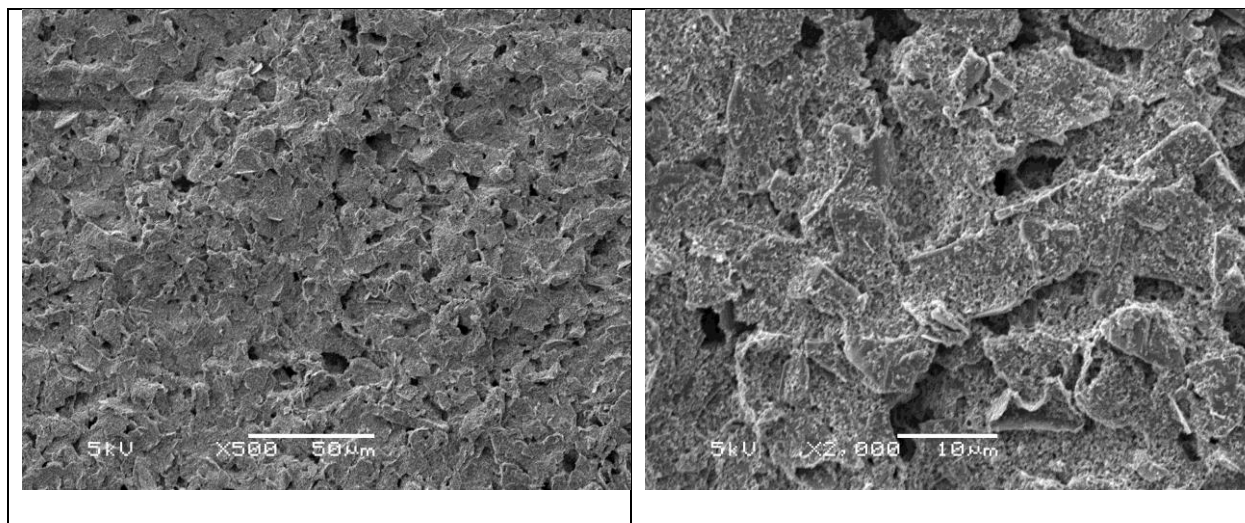


*Figure 10: SEM image of the working electrode of a bare (graphite powder only) SPE Sensor*

To summarize, graphene - a single layer originated (separated) from graphite, graphite oxide - an oxidized product of graphite with more than 8 layers (approx.), graphene oxide - an oxidized product of graphite with 1~8 layers and reduced graphene oxide- reduced product (oxygen groups) of graphene oxide.

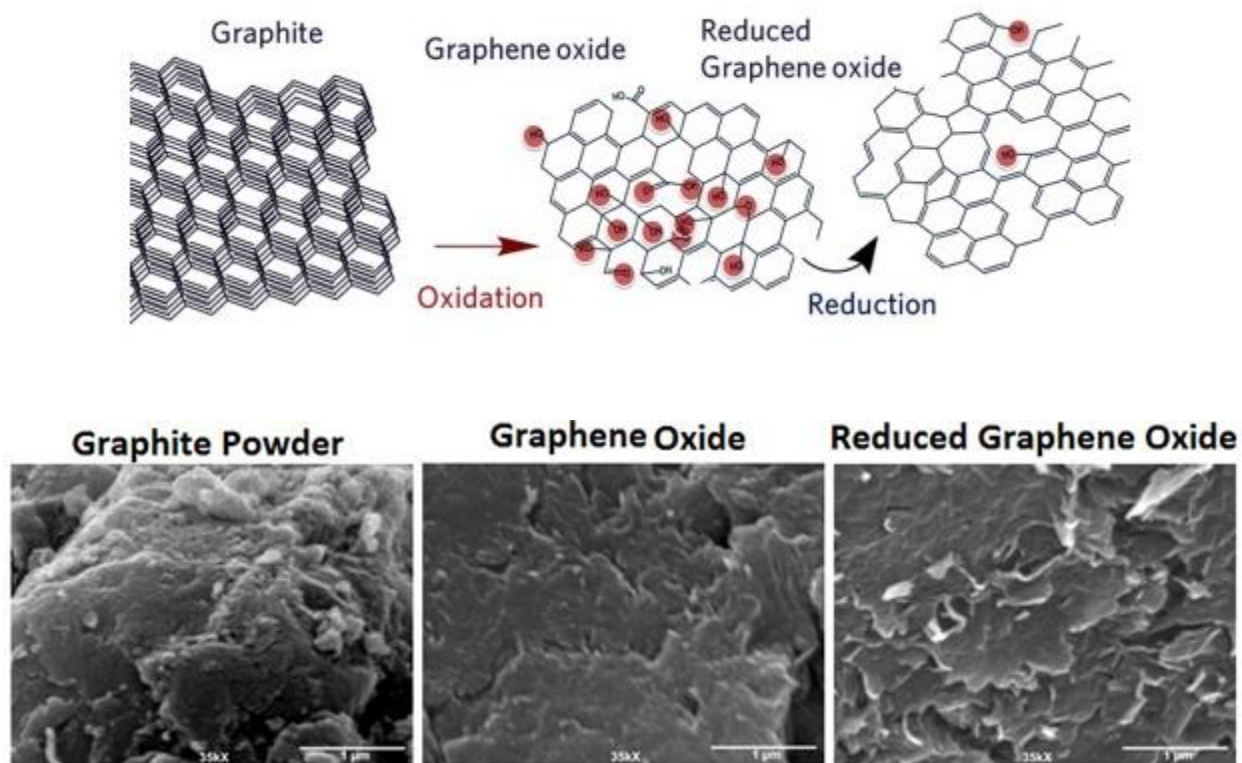


*Figure 11: Atomic structure (top) and SEM image (bottom) of the graphite, graphene oxide and reduced graphene oxide. Images from Gensheimer et. al. [81] and Kauppila et. al. [82]*

The Figure 11, shows the SEM images and the structure of the graphite, graphene oxide and reduced graphene oxide. As shown in Figure 12 the comparison between the SEM images of the graphene oxide and the reduced graphene oxide (rGO) material. The rGO images shows more wrinkles compared to the GO sheets. The electrochemical reduction of GO was consisted of

crumpled sheets which were closely aggregated with each other as a result of the reduction of the oxygen groups.

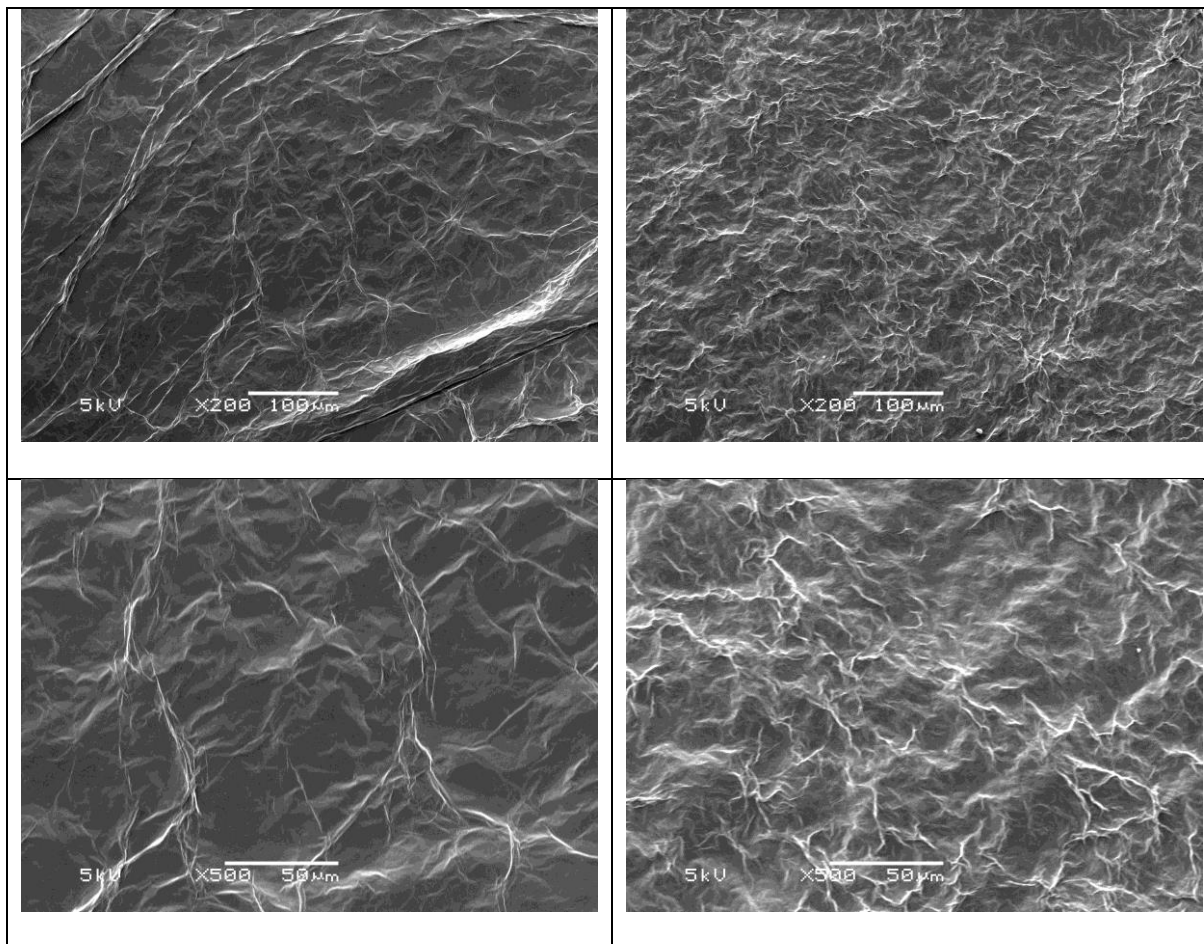


*Figure 12: SEM image of the working electrode of with graphene oxide (left) and reduced graphene oxide (right) modified SPE Sensor*

### 3.1.2 Graphene Oxide - Polypyrrole (GO-PPy) as layer

The unique structure of the graphene oxide (drop casted) and polypyrrole (PPy) showed a unique structure different from the graphene oxide or the polypyrrole structure (Figure 13). The electrochemically grown PPy nanocomposite film made the graphene oxide layer more uniform.

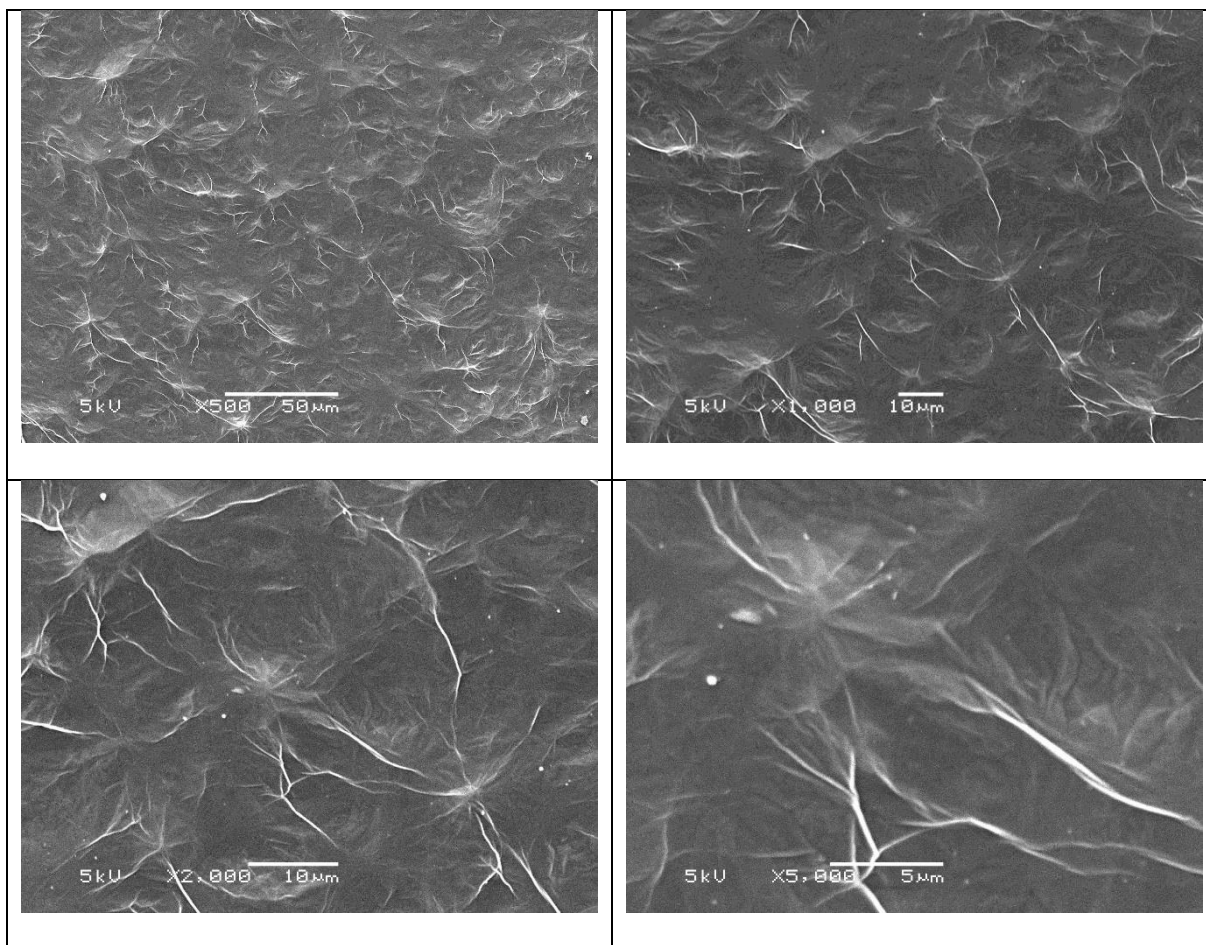


*Figure 13: SEM image of the working electrode of with GO-PPy (as layer) modified SPE Sensor*

### 3.1.3 Reduced Graphene Oxide - Polypyrrole (rGO-PPy) as layer

As for the rGO - Polypyrrole (as layer) modified SPE Sensor (Figure 14), the architecture of this nanocomposite showed many wrinkled sheets reflecting the physical nature of rGO and the uniform layered-structure indicated the formation of PPy along graphene sheets. The incorporation of rGO nanosheets enormously altered the distribution of PPy in the obtained nanocomposite and conducted to produce a 3D nanocomposite by covering with PPy. It also revealed that unique 3D structure of rGO - PPy nanocomposite was more porous than PPy film, which could provide more binding sites with  $Pb^{2+}$  and contribute to improve the detection sensitivity.

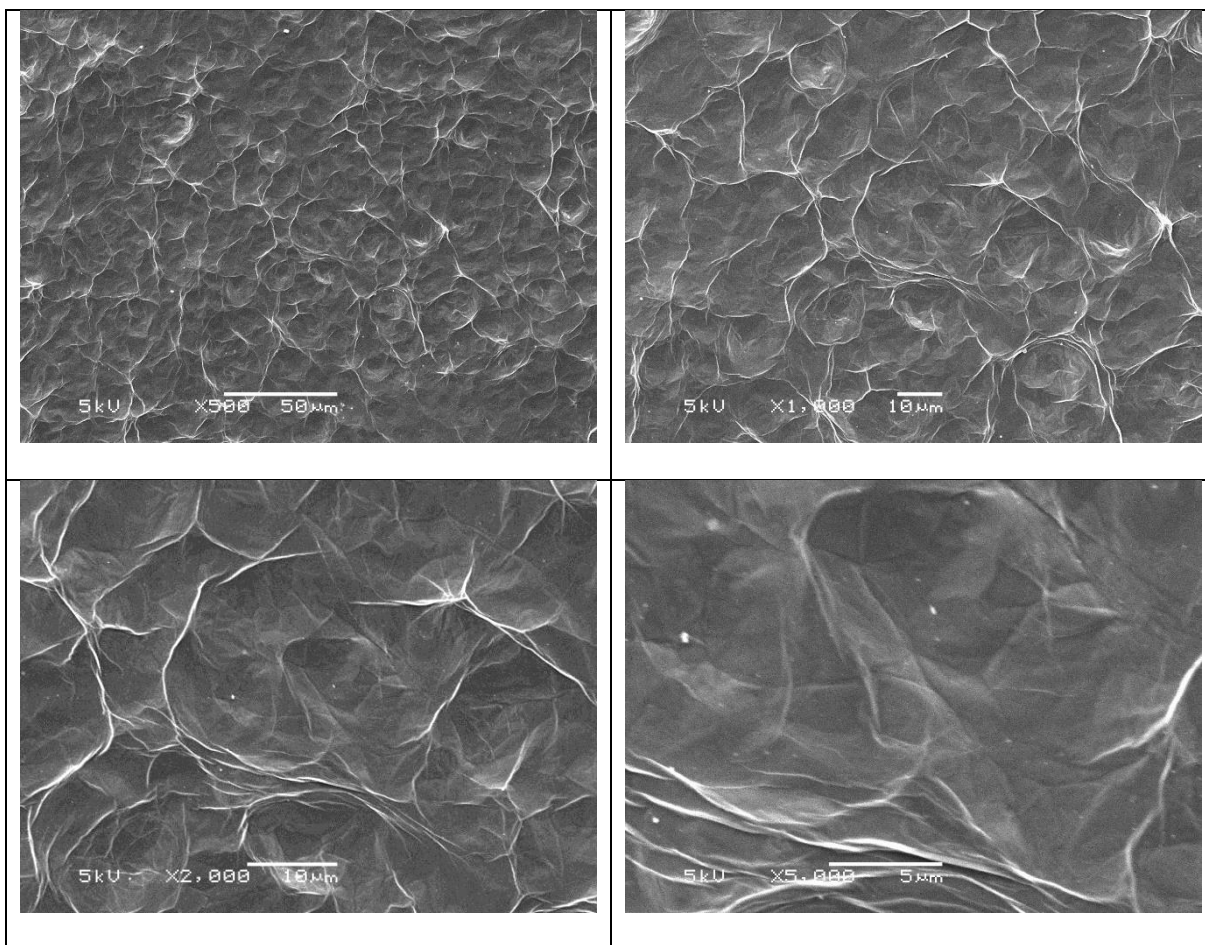


*Figure 14: SEM image of the working electrode of with rGO-PPy (as layer) modified SPE Sensor*

#### 3.1.4 Graphene Oxide - Pyrrole (GO/Py) as mixture

The SEM image of the GO and Py as mixture (drop casted) modified working electrode of the SPE sensor revealed gel like structure. The mixture caused the graphene oxides layers to be closer and reduced surface area. The pyrrole suppressed the unique structure of the graphene oxide and made it less porous. Figure 15 shows SEM images of this structure with four different magnification. Comparing with above two structures of the layers, this structure seemed less porous and solid.

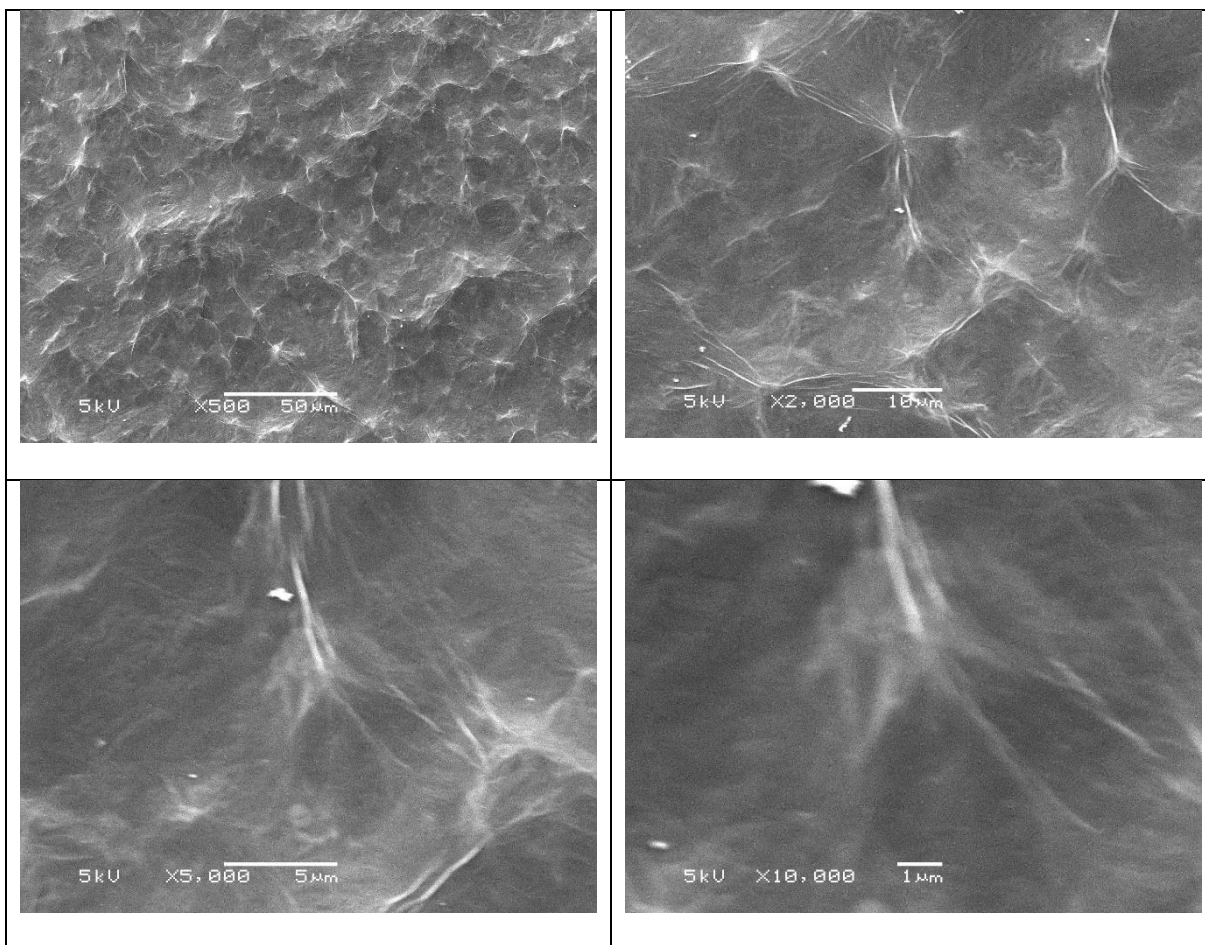


*Figure 15: SEM image of the working electrode of with GO/Py (as mixture) modified SPE Sensor*

### 3.1.5 Reduced Graphene Oxide - Pyrrole (rGO/Py) as mixture

The wrinkled sheets represent the characteristics of the reduced graphene oxide in the SEM image (Figure 16) of the working electrode of with rGO and Pyrrole as mixture (drop casted) modified SPE Sensor. The reduction of this nanocomposite increased the surface, but this structure was found unstable and a tendency to become porous during experimental investigation.

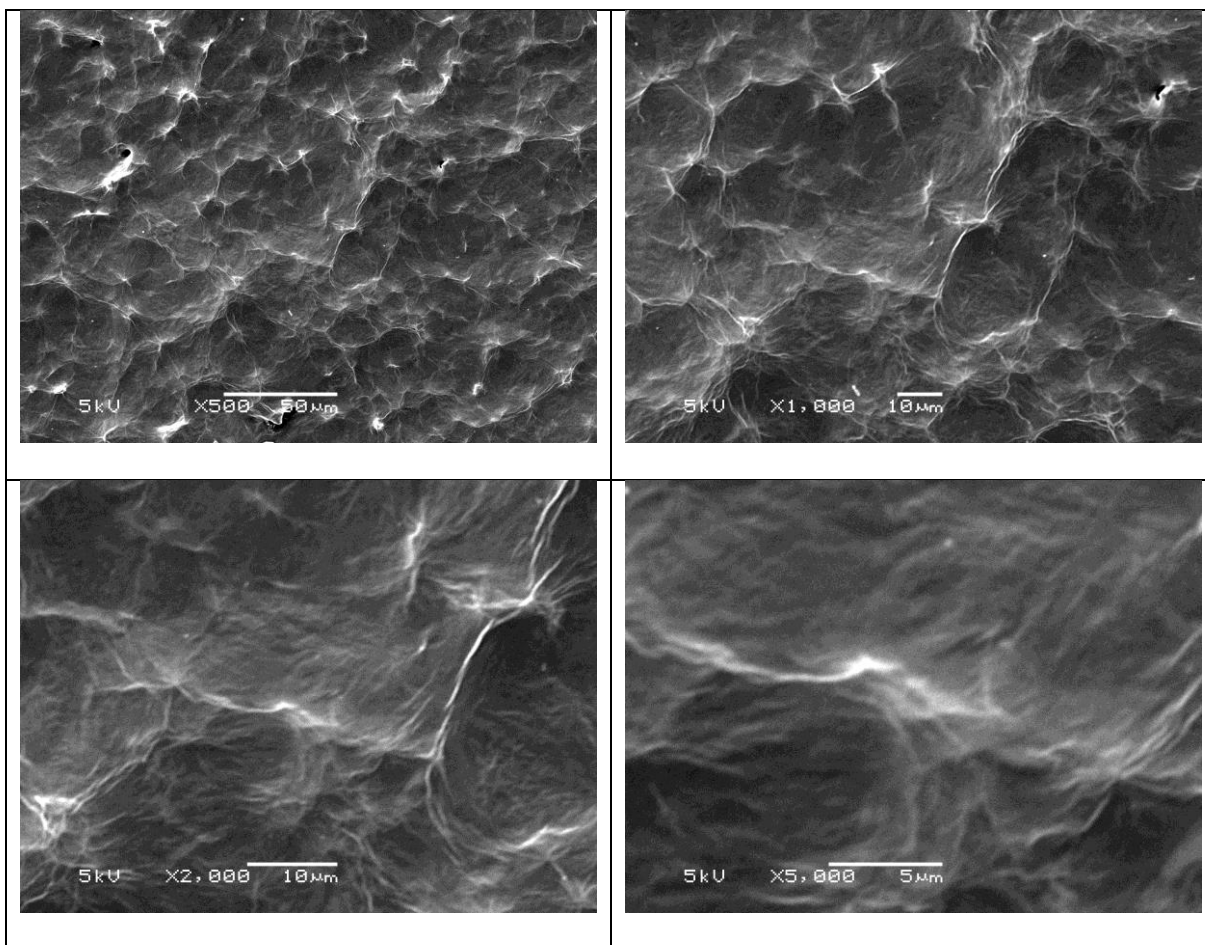


*Figure 16: SEM image of the working electrode of with reduced rGO/Py (as mixture) modified SPE Sensor*

### 3.1.6 Electrochemical polymerization of Graphene Oxide and Pyrrole mixture (GO/PPy)

The SEM image of the working electrode of GO and Polypyrrole mixture (electrodeposition) modified SPE sensor showed in Figure 17. The electro polymerization of the graphene oxide and pyrrole created a viscous layer of polypyrrole and graphene oxide. It can be seen from the image that the polypyrrole has suppressed the porous layer of the graphene oxide properties and created a uniform layer of the polymer.

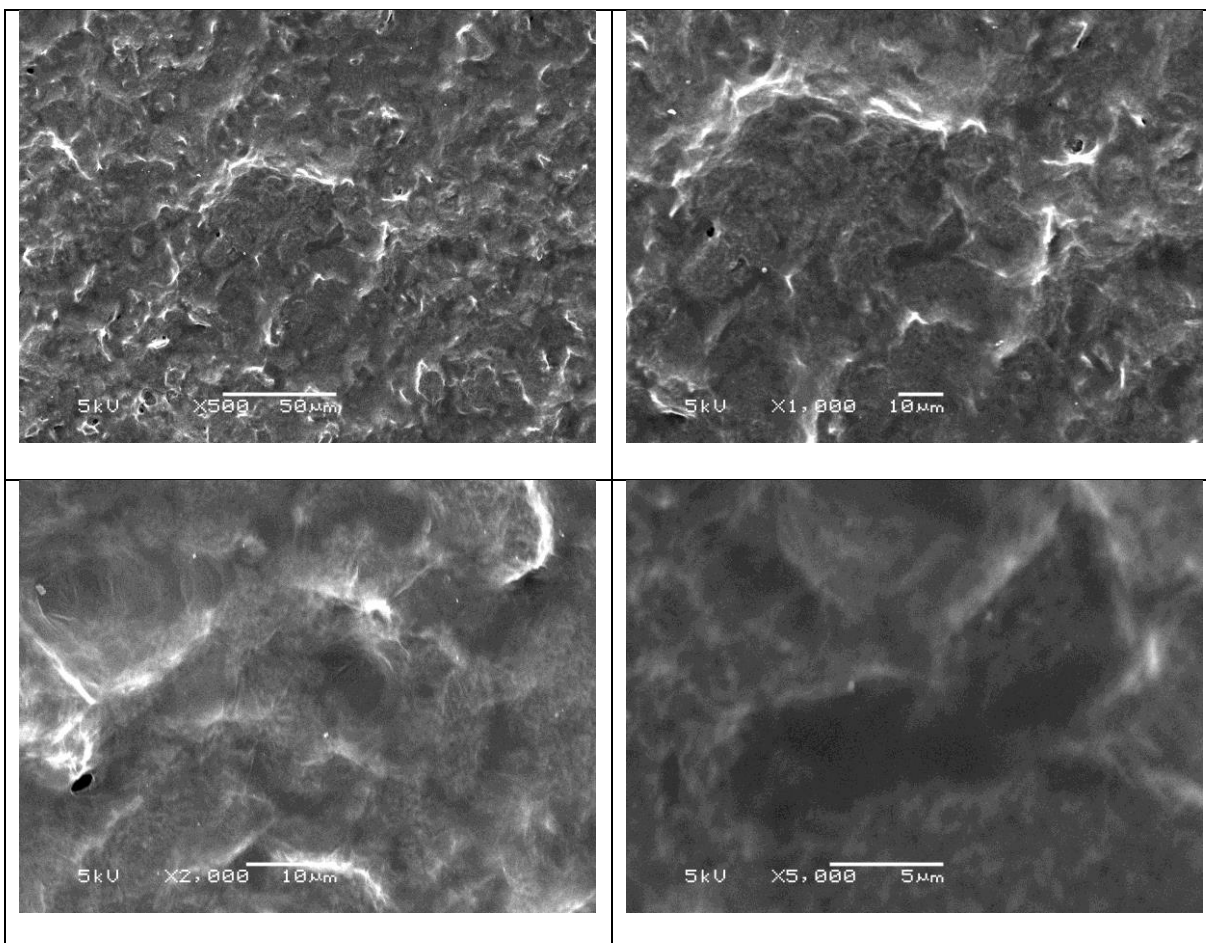


*Figure 17: SEM image of the working electrode of GO/PPy (mixture electrodeposition) modified SPE Sensor*

### 3.1.7 Electrochemical polymerization and subsequent reduction of Graphene Oxide and Pyrrole mixture (rGO/PPy)

As for the working electrode of reduced GO and Polypyrrole mixture (electrodeposition and subsequent reduction) modified SPE Sensor (Figure 18), the architecture of this nanocomposite showed some wrinkled sheets reflecting the physical nature of rGO as compare to the similar structure without the electrochemical reduction of the composite layer. The viscous layered-structure indicated the formation of PPy through the graphene sheets.

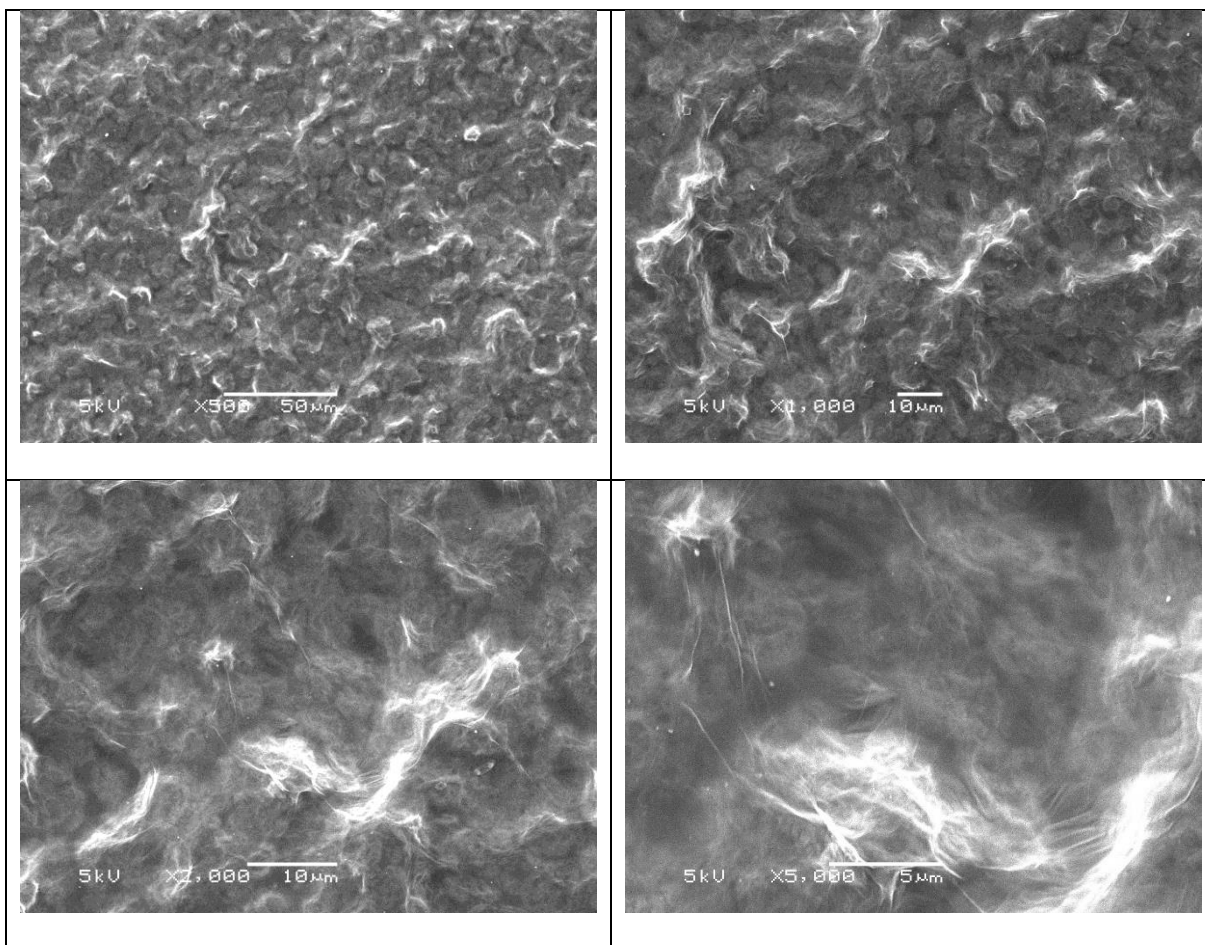


*Figure 18: SEM image of the working electrode of rGO/PPy (mixture electrodeposition and subsequent reduction) modified SPE Sensor*

## **Chapter 4: Performance Analysis and Operating Parameters Optimization**

## 4.1 Quantitative determination of $\text{Pb}^{2+}$

An electrochemical sensor for speedy, selective and sensitive detection of  $\text{Pb}^{2+}$  was developed using reduced graphene oxide and polypyrrole (rGO-PPY) nanocomposite by drop casting and electrochemical synthesis. The rGO-PPY modified electrode possessed a large effective area because of unique 3D porous architectures and displayed excellent selectivity for determination of  $\text{Pb}^{2+}$ . As mentioned in the sensor structure and fabrication the motivation was to fabricate an electrochemical sensor with rapid and simple process compared to complex and time consuming electrochemical synthesis process used. Moreover, this fabrication process can be easily modified and implemented using a printing device for inexpensive mass production. As discussed earlier in the chapter 1, the researches on electrochemical detection of heavy metal ions are based on a supporting electrolyte with a controlled pH to ensure the lability of active metal ions in the solution of interest. The optimization method of the operating parameters and the materials selected was based on that principle.

## 4.2 Importance of pH in electrochemical detection of heavy metals ions

Heavy metal species dissolved in water may occur as free ions, or aquo-ions, or as inorganic and organic complexes. In natural surface water from various source (i.e. rain, river, lake or underground) the heavy metals are being quickly degraded and deposited in the form of hard soluble carbons in presence of carbonates or bicarbonates, sulfates and sulfides on the bottom [71]. In water, free metal cations are generally surrounded by coordinating water molecules and so have been termed “aquo-cations,” although by convention the water molecules are ignored when writing chemical reactions involving metal cations. The total analytical concentration of a given metal in

water is the sum of the concentrations of its free ion and its complexes and any metal associated with suspended solids, whether organic or mineral. For any aqueous solution of lead, the total molal concentration of lead  $\Sigma Pb$ , in a natural water might equal [4]:

$$\sum Pb = mPb^{2+} + mPbOH^+ + mPbCO_3^0 + mPbHCO_3^+ + mPbSO_4^0 + mPb \text{ (Suspended Solid)}$$

In most natural waters, the concentration of free lead ion  $mPb^{2+}$ , is less than the sum of the molal concentrations of its complexes, which in this case are lead complexes with hydroxyl, carbonate, bicarbonate, and sulfate ions. Complexes are formed between metals (acids) and ligands (bases) present in a solution based on the source of the water. Other metals that are found in natural waters most often as complexes and not as free ions include  $Al^{3+}$ ,  $Ag^+$ ,  $Cu^{2+}$ ,  $Fe^{3+}$ , and  $Hg^{2+}$ . Complexes that incorporate metals play a major role in controlling the availability and fate of metals in the environment. Heavy metals in water available in a wide range of different chemical forms and in different oxidizing conditions based on the formation and characteristics of the complexes. Metal complexing has a direct influence on metal adsorption to organic matter or mineral surfaces. The product of the ion activity coefficient and the molal concentration of each species equals the activity of the ion [83]. Which means for a given total Pb concentration, the greater the amount of Pb that is complexed, the lower the concentration of free Pb ion. This means that as the extent of Pb complexing increases, the total Pb concentration must also increase to reach saturation equilibrium with the given lead salt.

Several factors influence the sorption of metals in aquatic systems. Speciation/ complexation is the distribution of a given constituent among its possible chemical forms, including metal

complexes, which have differing tendencies to be adsorbed or desorbed; precipitation is the process by which dissolved species exceed the solubility limits of their solids, so that some of the species precipitate from solution; colloid formation can result in metals being sorbed or coprecipitated with colloidal-sized particles; bio-fixation occurs when biological processes (usually involving microorganisms or plants) result in the binding of metals to solid materials; interactions with natural organic matter can also result in sorption. In addition to these factors, sorption is influenced by changes in pH, oxidation potential, salinity, concentrations of competing ions, the nature of sorbent phases and their surface areas, and surface site densities [4].

To what extent will heavy metals in water/solvent be mobile, depends from number of parameters [71]:

- pH of water or the solvent solution
- content of organic and inorganic matter (can form metal complexes and so provide alternative binding sites for the metal ion) such as carbonates, phosphates, hydrated oxides of iron, sulfide ions and pyrite
- different operating conditions (such as temperature, pressure)

Among those parameters, the pH of the aqueous solution is probably the single most important variable that influences the behavior of metals in the environment [4]. Metal complexes with sulfate, fluoride, chloride, and phosphate are most stable and important below pH 7, whereas metal carbonate and hydroxide complexes become increasingly more important above pH 6–8. Hydrogen ion competes with metal cations for adsorption sites, so that adsorption of metal cations by hydrous ferric oxide (HFO), for example, is low in acid systems but increases with increasing

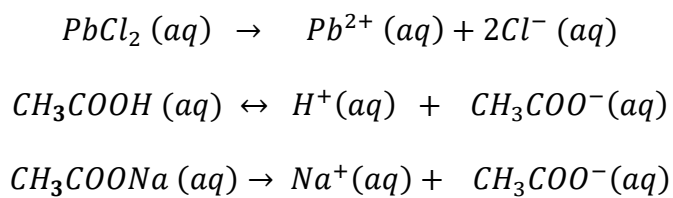
pH. In contrast, oxyanions of As, Mo, Se, and Cr tend to be desorbed from HFO with increasing pH because of competition between the oxyanions and OH<sup>-</sup> ion for sorption sites. Furthermore, the solubility of most metal-containing minerals is greatest under acid conditions, decreasing with increasing pH [4, 71, 84].

In the electrochemical methods using the stripping voltammetry, the peak current is directly related to the pH values of the solution of interest. The maximum value of the current in the oxidizing process decreases with the increase of pH value. Increase of the pH, increase more hydroxyl ions (OH<sup>-</sup>) in the solution which significantly diminish the number of solution phase metal ions by forming metal hydroxide complex. These reduction in solution phase metal decrease the number the active metal ions to be deposited on the surface of the working electrode in the deposition step. But at too lower pH values, protons may compete with lead ions for the binding sites so as to influence on the sensors linear range as well as reproducibility [84]. In electrochemical analysis, protons (H<sup>+</sup>) play a key role in different electrochemical reactions, often by acting as a catalyst or by simply retarding competing side reactions.

Since in heavy metal detection, pH is important as it controls metal ion availability (lability) which in turn affects the magnitude of the detection response, we have used a buffer solution as a supporting electrolyte/solvent for the lead salt (PbCl<sub>2</sub>). For our proposed sensor structure, we will optimize the pH of the solvent which is discussed in the following section.

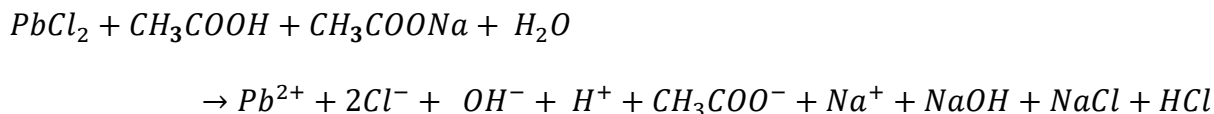
### 4.3 Effect of pH on electrochemical detection of $Pb^{2+}$ using graphene oxide and pyrrole modified SPE

It is already discussed in the previous chapter about the importance of pH on the electrochemical/electro analysis methods. Lead (II) chloride has been used in this study as source of lead ion ( $Pb^{2+}$ ). Sodium acetate and acetic acid was used to make buffer which was the supporting electrolyte/analyte solvent used in the electrochemical detection of lead ion. The following equation (not balanced) showed what happened to the lead (II) chloride, sodium acetate and acetic acid in an aqueous solution.



A buffer solution is one that resists a change in its pH when  $H^+$  or  $OH^-$  ions are added or removed when some other reaction taking place in the same solution. The essential component of a buffer system is a conjugate acid-base pair whose concentration is higher compare to the concentrations of added/produced  $H^+$  or  $OH^-$  it is expected to buffer against. The buffer system used in this study was 0.1 M solution of sodium acetate and the conjugate pair here is acetic acid and its conjugate base, the acetate ion. The idea is that this conjugate pair "pool" will be available to gobble up any small addition of  $H^+$  or  $OH^-$  that may result from other processes going on in the solution.

Combining all the reactant in the same equation i.e. when lead (II) chloride was added to sodium acetate-acetic acid buffer, the following chemical reaction might take place with the buffer made of the deionized water. The reaction is not balanced and assumed to have all the possible products from the reactants.



Adding lead (II) chloride to buffer solution created  $Pb^{2+}$ ,  $Cl^-$ ,  $H^+$ ,  $CH_3COO^-$  and  $Na^+$ . Because of the conjugate pair, and the availability of  $H^+$  and  $OH^-$ , the resultant products might have some  $Pb^{2+}$  as ion in the solution. The ions available in the solution can be attracted and stripped off to determine to presence of lead in the solution.

Figure 19 shows the stripping voltammetric behaviors of 1000 ppb (or 1 ppm)  $Pb^{2+}$  in 0.1 M sodium acetate-acetic acid (0.1 M NaAc-HAc) solution with respect to different pH values. The preconcentration step was 10 min (600 sec) with stirring solution (with a magnetic stir) and the peak current was recorded from the stripping step (DPASV). With the range of pH from 4.0-5.2, the peak current increased with pH and reaches to the peak at pH 4.4. It sharply went down at pH 4.6 and it remained similar without any significant change. Increase of the pH, increase more hydroxyl ions ( $OH^-$ ) in the solution which significantly diminish the number of solution phase metal ions by forming metal hydroxide complex. These reduction in solution phase metal decrease the number the active metal ions to be deposited on the surface of the working electrode in the deposition step that reduced the height of the peak current in the DPASV step [38]. It was reported by Zhu et. al.

[84] at too lower pH values, protons may compete with lead ions for the binding sites which may influence on the sensor linear range as well as reproducibility. The sensor developed in this study was not tested with analytes with pH less than 4.0. The optimum pH was selected 4.4 for this study to test the graphene oxide and pyrrole nanocomposite modified electrode.

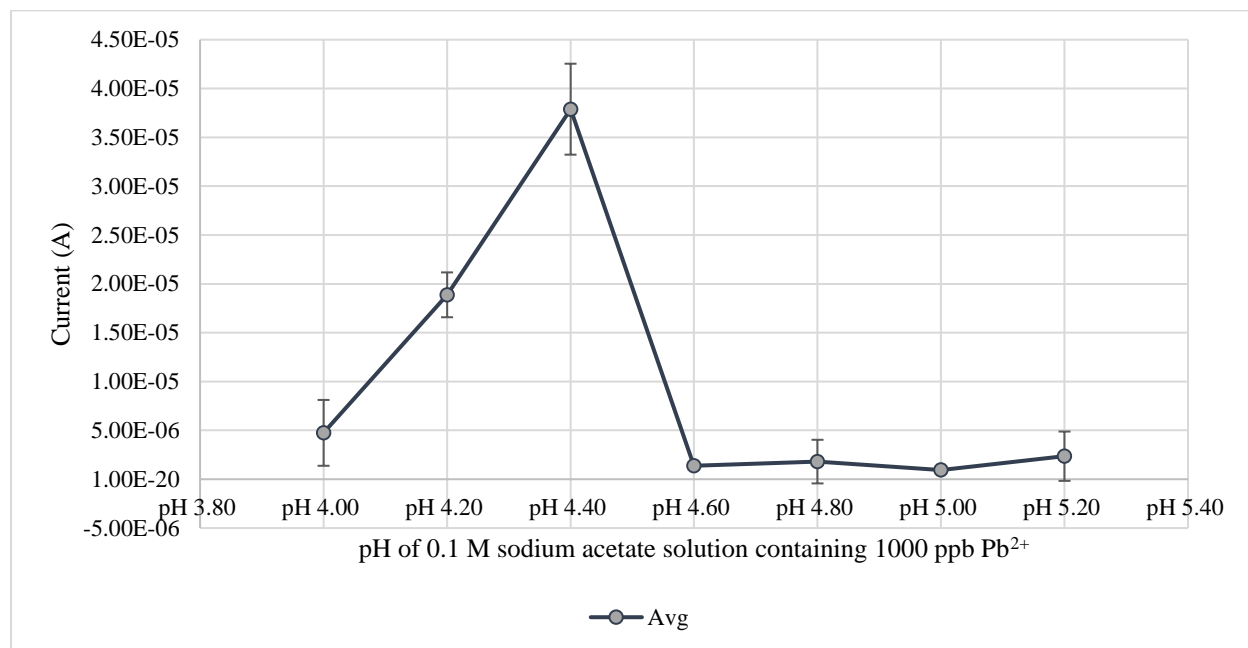
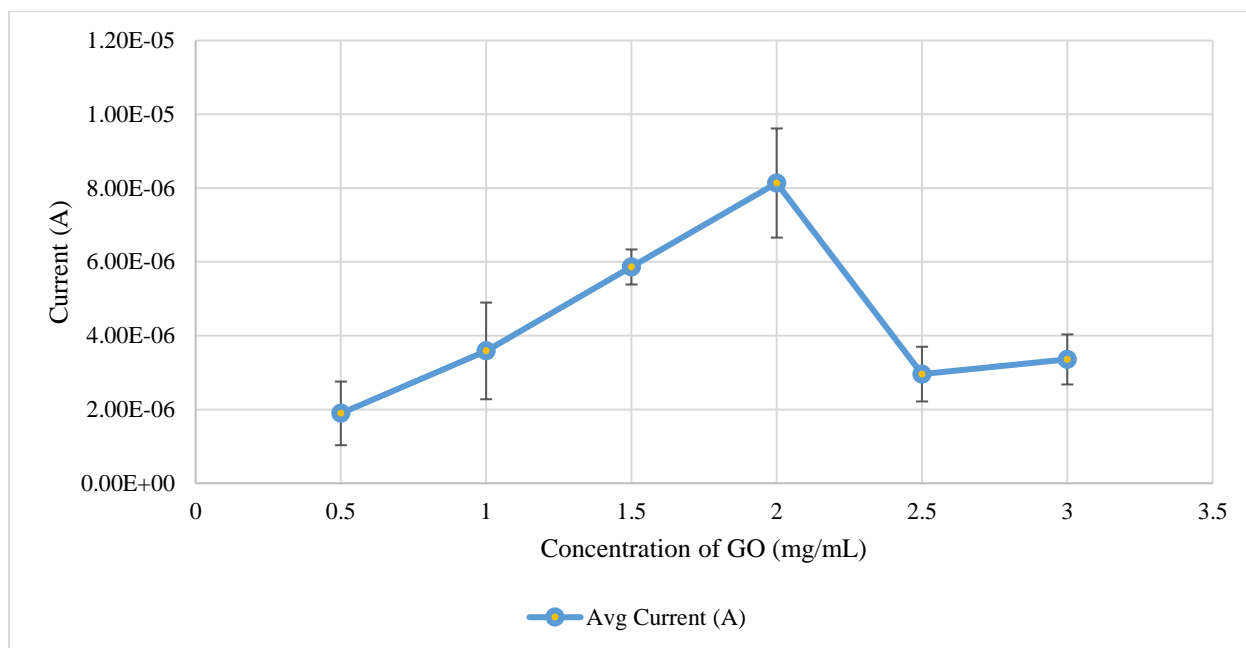


Figure 19: Effect of pH on  $Pb^{2+}$  detection using SPE sensor, 1000 ppb  $Pb^{2+}$  in 0.1 M sodium-acetate buffer with different pH

#### 4.4 Effect of graphene oxide concentration on $Pb^{2+}$ detection using rGO-PPy modified SPE

The voltammetric response of  $Pb^{2+}$  was studied with in respect to the concentration of the graphene oxide (GO) solution to prepare the graphene oxide-pyrrole nanocomposite. The concentration range of graphene oxide (GO) was selected 0.5-3 mg/mL to find out the optimum value for the proposed sensor structure. From Figure 20, it can be seen that the peak current was maximum with GO concentration 2.0 mg/mL. The GO layer increased the surface area and the acted as a base structure for the phlegmatization of pyrrole. Though the range was small on the scale, the average

peak current found to be decrease after 2.0 mg/mL of GO while it was increasing from 0.5 mg/mL to the peak at 2.0 mg/mL.



*Figure 20: Effect of graphene oxide concentration on the  $Pb^{2+}$  detection using rGO-PPy modified SPE sensor in 500 ppb  $Pb^{2+}$  in sodium-acetate buffer (pH 4.4) with different concentration of graphene oxide*

After investigating the effect of the concentration of the GO on  $Pb^{2+}$  detection using the SPE, 2 mg/mL was selected as the optimum concentration of GO for the proposed sensor structure.

#### 4.5 Effect of deposition time on $Pb^{2+}$ detection using rGO-PPy modified SPE

The sensitivity (in terms of the peak current) of the proposed method for detection of lead ion  $Pb^{2+}$  was certainly increased with the increase of the deposition/pre-concentration time because of the increased amount of lead on the graphene oxide and pyrrole modified working electrode. For a deposition potential -1.2 V, the deposition potential was steadily increasing with the increase of deposition time. However, doubling the deposition time from 5 min (300 sec) to 10 min (600 sec) significantly changed the slope positively. While increasing the deposition time from 10 min (600

sec) to 20 min (1200 sec), the plot tended to be curved with diminished slope value, as shown in Figure 28 for the peak current in DPASV step with rGO-PPy modified screen printed electrode (SPE) in 1000 ppb  $Pb^{2+}$  in sodium-acetate buffer (pH 4.4) for different deposition cycle. The sensitivity of the DPASV cycle increased with the increase in deposition time, but it also lowers the upper detection limit due to the rapid surface saturation at high lead concentrations. Therefore 10 min (600 sec) was selected as the optimum operating condition for this study.

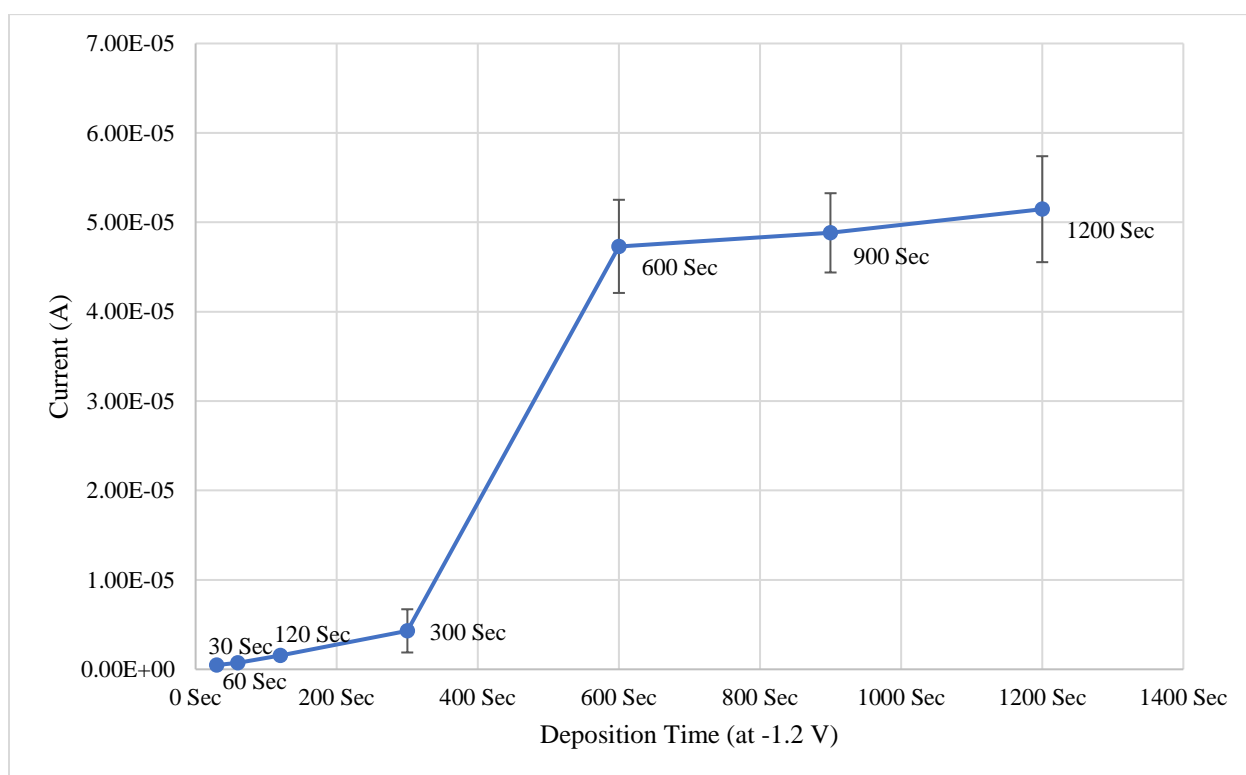


*Figure 21: Effect of deposition time in lead ion  $Pb^{2+}$  detection using DPASV method with rGO-PPy modified screen printed electrode (SPE) in 1000 ppb  $Pb^{2+}$  in sodium-acetate buffer (pH 4.4) with different deposition cycle*

#### 4.6 Effect of deposition potential on $Pb^{2+}$ using rGO-PPy modified SPE

Figure 29 displays the effect of the deposition potential on the stripping peak current of lead ion i.e.  $Pb^{2+}$  detection in 250 ppb of  $Pb^{2+}$  sodium-acetate buffer (pH 4.4) with different deposition potential after 10 min (600 sec) deposition. With the range from -0.1 V, it was increasing with the higher slope till -0.6 V and after it was steadily increasing till -1.0 V. It reached to the peak current while the deposition potential was -1.2 V and then it went down sharply. Because of the enhanced kinetics and the attraction of the cation ( $Pb^{2+}$ ) to negative potential, the stripping peak current increased with the decrease in potential. Thus, -1.2 V was used as the optimal deposition potential.

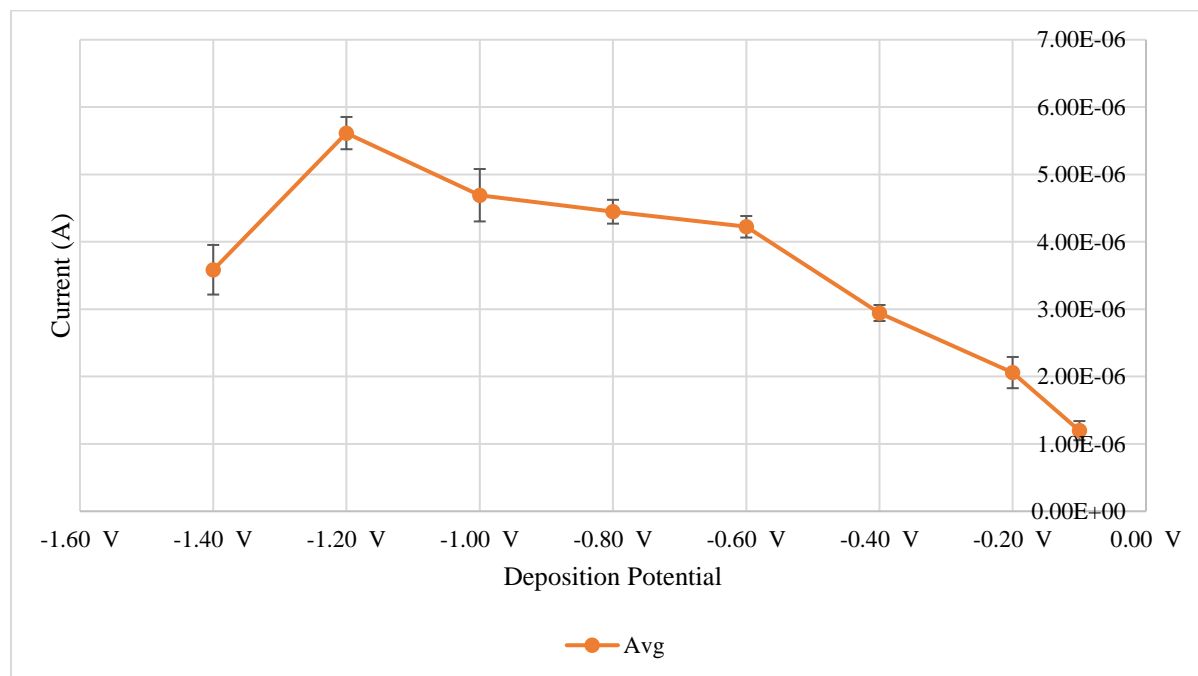


Figure 22: Effect of deposition potential in lead ion  $Pb^{2+}$  detection using DPASV method with rGO-PPy modified screen printed electrode (SPE) in 250 ppb  $Pb^{2+}$  in sodium-acetate buffer (pH 4.4) with different deposition potential

#### 4.7 Detection of $Pb^{2+}$ in 0.1 M sodium-acetate buffer, pH 4.4 using bare SPE sensor (without any nanocomposites)

As the screen-printed electrode (SPE) was used as the base sensor in this study, a bare sensor i.e. the original graphite powder without any nanocomposites was tested with 0 ppb  $Pb^{2+}$  and 50 ppb  $Pb^{2+}$  in sodium acetate buffer (pH 4.4). The deposition cycle was for 10 min (600 sec) for DPASV detection of  $Pb^{2+}$ . A bare sensor and a bare sensor after the pre-treatment (i.e. cleaning) were tested in the same operating condition. From Figure 21, it can be observed that the treatment process improved the detection and removed the noise. A pre-treatment step for a new SPE sensor is found to be necessary as there might be dust/impurities attached to the electrode surface during the packaging or shipping.

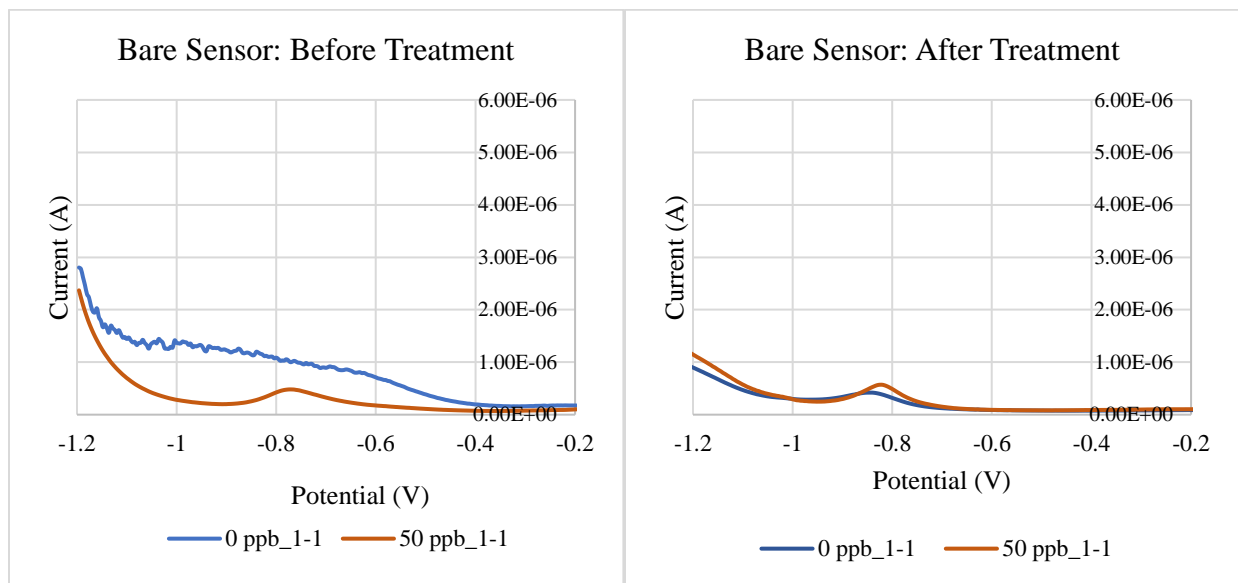


Figure 23: Comparison between bare sensor (the original graphite powder without any nanocomposites) before and after the cleaning and pre-treatment cycle with 0 ppb  $Pb^{2+}$  and 50 ppb  $Pb^{2+}$  in sodium acetate buffer (pH 4.4) with 10 min (600 sec) deposition cycle

#### 4.8 Detection of $\text{Pb}^{2+}$ in 0.1 M sodium-acetate Buffer, pH 4.4: layers and mixture of GO and 0.1 M pyrrole

All the six types of sensors mentioned earlier in chapter 3, was tested in the same operating condition with 0 ppb  $\text{Pb}^{2+}$  and 50 ppb  $\text{Pb}^{2+}$  in sodium-acetate buffer (pH 4.4). These tests were important to find out the best possible combination from the graphene oxide and pyrrole to use as the nanocomposite for detection of  $\text{Pb}^{2+}$ .

##### 4.8.1 Graphene Oxide - Polypyrrole (GO-PPy) as layer

As it can be seen from Figure 22, the signal from the 0 ppb  $\text{Pb}^{2+}$  i.e sodium-acetate buffer (pH 4.4) without any lead had the higher peak current than the 50 ppb  $\text{Pb}^{2+}$ . This highly conductive graphite based structure might have higher affinity to the available proton ions ( $\text{H}^+$ ) which might have caused higher current for the buffer solution without any  $\text{Pb}^{2+}$  in the solution.

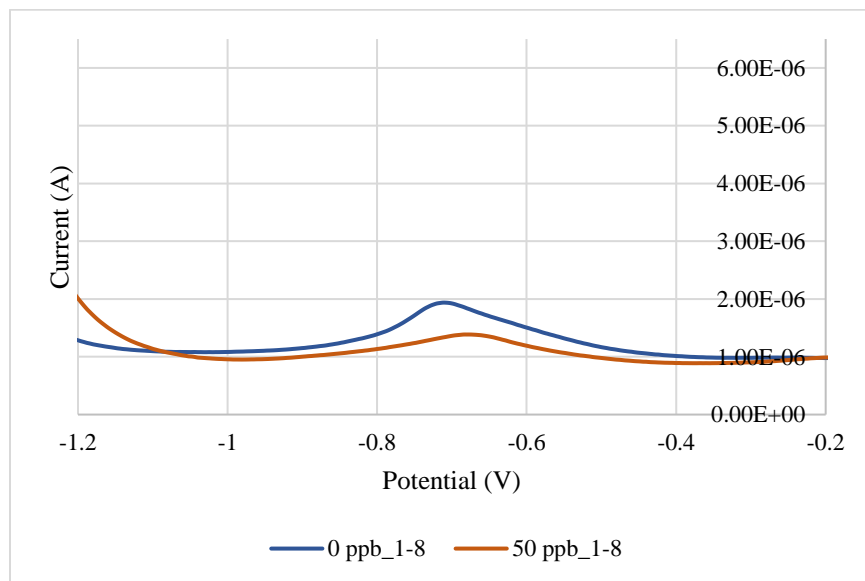
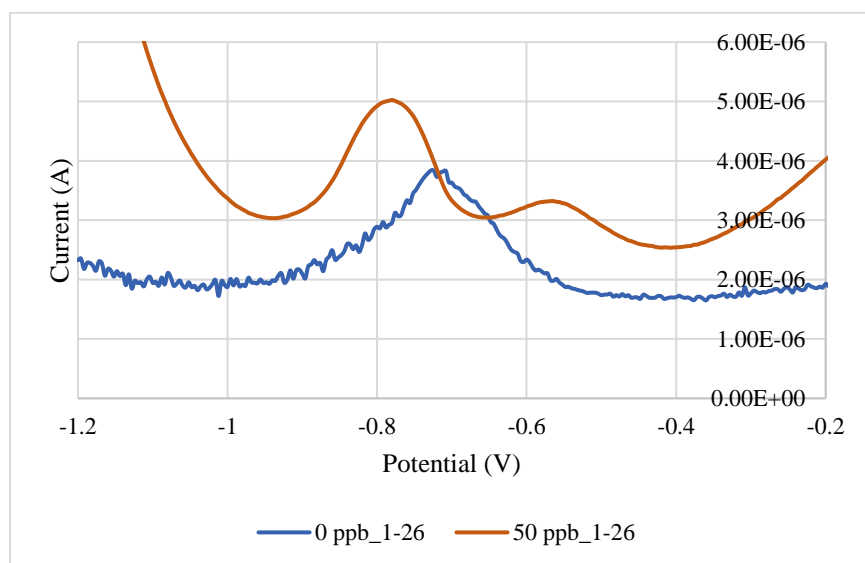


Figure 24 GO-PPy (as layer) modified SPE sensor in detection of 0 ppb  $\text{Pb}^{2+}$  and 50 ppb  $\text{Pb}^{2+}$  in sodium acetate buffer (pH 4.4) with 10 min (600 sec) deposition cycle

#### 4.8.2 Reduced Graphene Oxide - Polypyrrole (rGO-PPy) as layer

This structure is the reduced graphene oxide (rGO) version of the sensor with GO-PPy as layer. As from Figure 23, it can be seen that the peak current is significantly improved compared to the similar nanostructure discussed above. The reduction of the graphene oxide layer improved the noise to signal ratio and made a noticeable difference between the peak current from the 0 ppb  $Pb^{2+}$  and the 50 ppb  $Pb^{2+}$  in sodium-acetate buffer (pH 4.4). Technically, there shouldn't be any noticeable peak current with the 0 ppb  $Pb^{2+}$  analytes, but the improved conductivity might have produce some noise during the DPASV cycle.



*Figure 25: rGO - PPy (as layer) modified SPE sensor in detection of 0 ppb  $Pb^{2+}$  and 50 ppb  $Pb^{2+}$  in sodium-acetate buffer (pH 4.4) with 10 min (600 sec) deposition cycle*

#### 4.8.3 Graphene Oxide - Pyrrole (GO/Py) as mixture

It was the first sensor modified with the mixture of graphene oxide and pyrrole. As it shows in the Figure 23, the nanocomposite was not very stable in terms of noise. The peak current between the 0 ppb  $Pb^{2+}$  and the 50 ppb  $Pb^{2+}$  was very close.

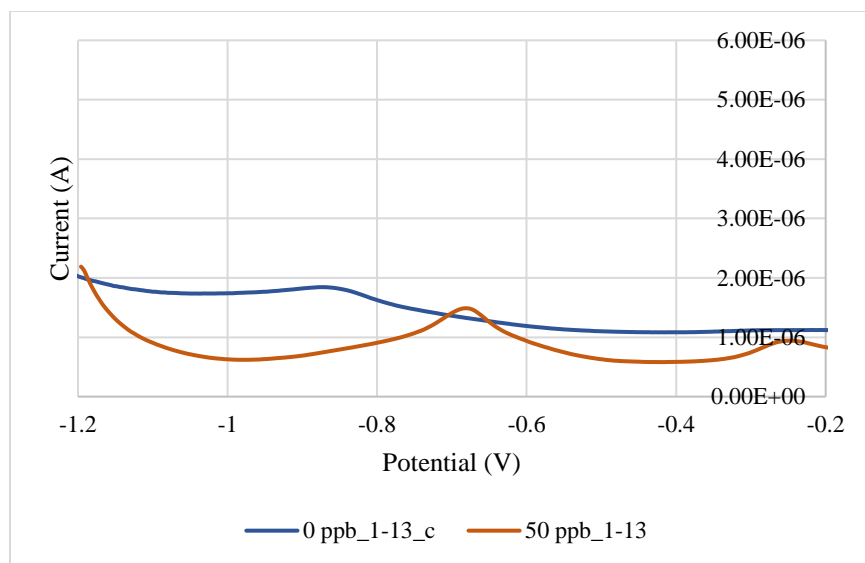


Figure 26: GO/Py (as mixture) modified SPE sensor in detection of 0 ppb  $Pb^{2+}$  and 50 ppb  $Pb^{2+}$  in sodium-acetate buffer (pH 4.4) with 10 min (600 sec) deposition cycle

#### 4.8.4 Reduced Graphene Oxide - Pyrrole (rGO/Py) as mixture

It was evident from the SEM image and the Figure 25, that the reduced form of the graphene oxide and pyrrole was not very stable structure as it was becoming severely porous during the DPASV cycle. Though it showed a very well defined peak current for the 50 ppb  $Pb^{2+}$ , but because of the weak structure, it produced noise during the test with 0 ppb  $Pb^{2+}$ .

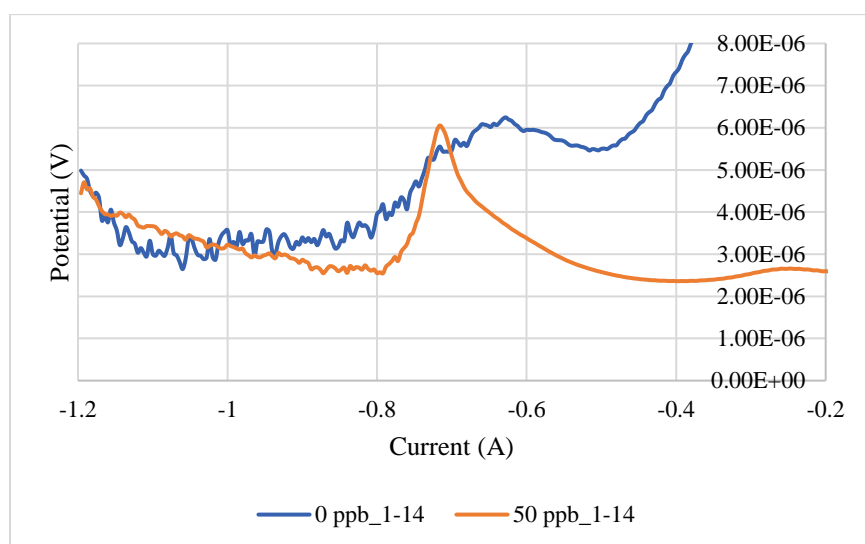


Figure 27: rGO/Py (as mixture) modified SPE sensor in detection of 0 ppb  $Pb^{2+}$  and 50 ppb  $Pb^{2+}$  in sodium-acetate buffer (pH 4.4) with 10 min (600 sec) deposition cycle

#### 4.8.5 Electrochemical polymerization of Graphene Oxide and Pyrrole mixture (GO/PPy)

The conductivity of the polymerized nanocomposite of the mixture of GO and pyrrole changed the conductivity of the working electrode. The current started to increase abruptly after the -0.7 V for the 0 ppb  $\text{Pb}^{2+}$  solution. Technically it should be flat line with minor bulging near -0.7 V. Though it showed a peak current for the 50 ppb  $\text{Pb}^{2+}$  solution, it was not selected for further study for its tendency to change rapidly after the peak current. Change in redox potential in a different operating condition might force the peak to merge with that noise (Figure 26).

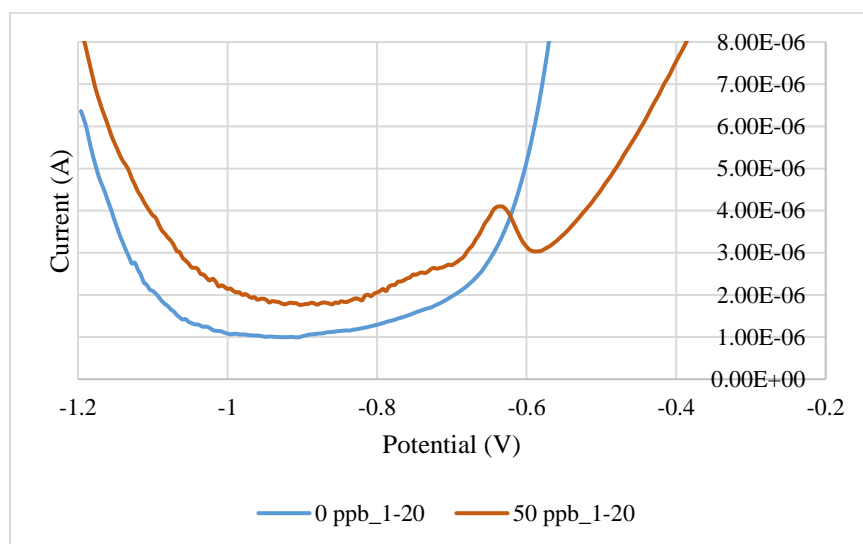
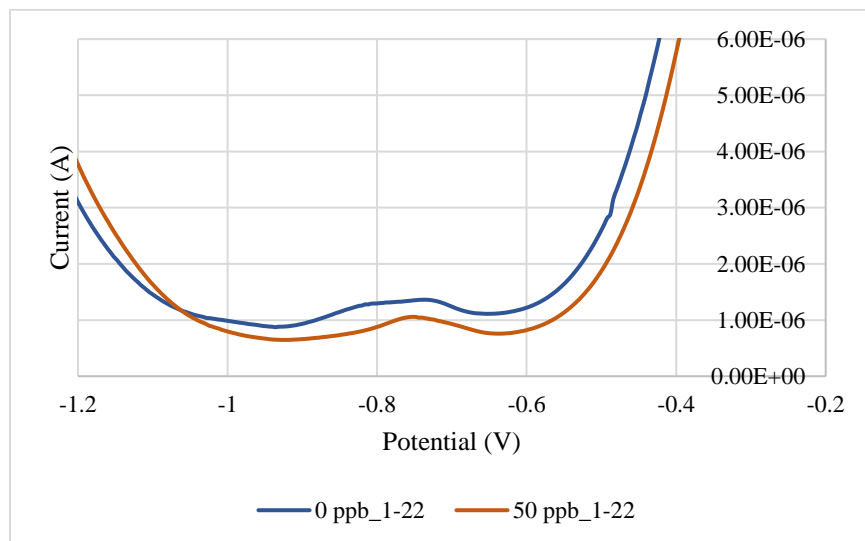


Figure 28: GO/PPy (electrodeposited as mixture) modified SPE sensor in detection of 0 ppb  $\text{Pb}^{2+}$  and 50 ppb  $\text{Pb}^{2+}$  in sodium-acetate buffer (pH 4.4) with 10 min (600 sec) deposition cycle

#### 4.8.6 Electrochemical polymerization and subsequent reduction of Graphene Oxide and Pyrrole mixture (rGO/PPy)

Comparing with the polymerized nanocomposite of the mixture of GO and pyrrole, the reduced layer of the polymerized nanocomposite of the mixture of GO and pyrrole showed better trend for both the 0 ppb  $\text{Pb}^{2+}$  and the 50 ppb  $\text{Pb}^{2+}$  solution. But the increased noise-to-signal ratio from the 0 ppb  $\text{Pb}^{2+}$  solution overpass the peak current from the 50 ppb  $\text{Pb}^{2+}$  solution (Figure 27). The

structure was studied with different values of the parameters and showed a similar trend. This structure was not selected for further analysis.



*Figure 29: rGO/PPy (electrodeposition and subsequent reduction of mixture) modified SPE sensor in detection of 0 ppb  $Pb^{2+}$  and 50 ppb  $Pb^{2+}$  in sodium-acetate buffer (pH 4.4) with 10 min (600 sec) deposition cycle*

#### 4.9 Electrochemical detection of $Pb^{2+}$ in 0.1 M sodium-acetate buffer, pH 4.4 using bare Sensor (i.e. without any modification)

After reviewing the SEM images and observing the effect of the graphene oxide and pyrrole modified screen printed electrode sensor in detection of 0 ppb  $Pb^{2+}$  and 50 ppb  $Pb^{2+}$  in sodium-acetate buffer (pH 4.4) with 10 min (600 sec) deposition cycle, the reduced graphene oxide-polypyrrole (as layers) was considered the best among all the six nanocomposites. The sensitivity and the limit of detection (LOD) was studied in this section using the rGO-PPY modified SPE sensor under the optimum operating conditions.

Before starting testing the selected sensor structure, a bare SPE (i.e. no modification of the working electrode) sensor was tested with different concentration of  $Pb^{2+}$  in sodium-acetate buffer (pH 4.4) with 10 min (600 sec) deposition cycle. It is shown in Figure 30, that the LOD of a bare sensor is close to 25 ppb (roughly) and the oxidization potential was changing during the DPASV cycle for peak current. With unpredictable change in the potential range for the peak current, it is unreliable to use such sensor for detection of  $Pb^{2+}$  in sodium-acetate buffer (pH 4.4).

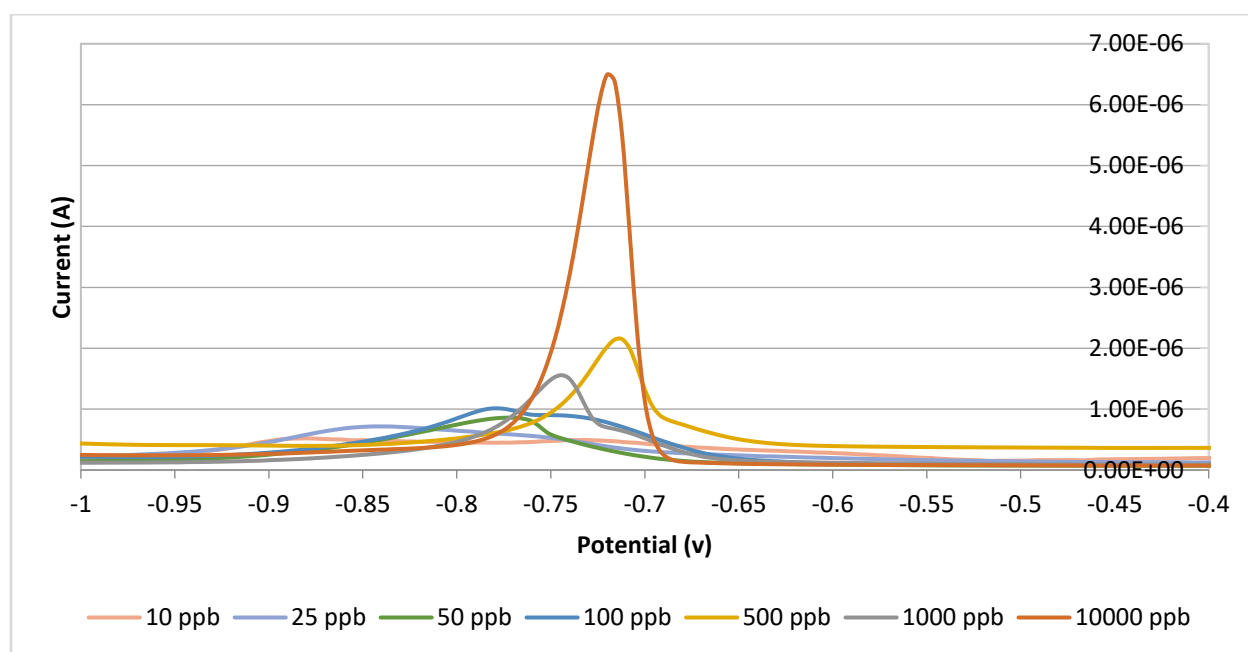
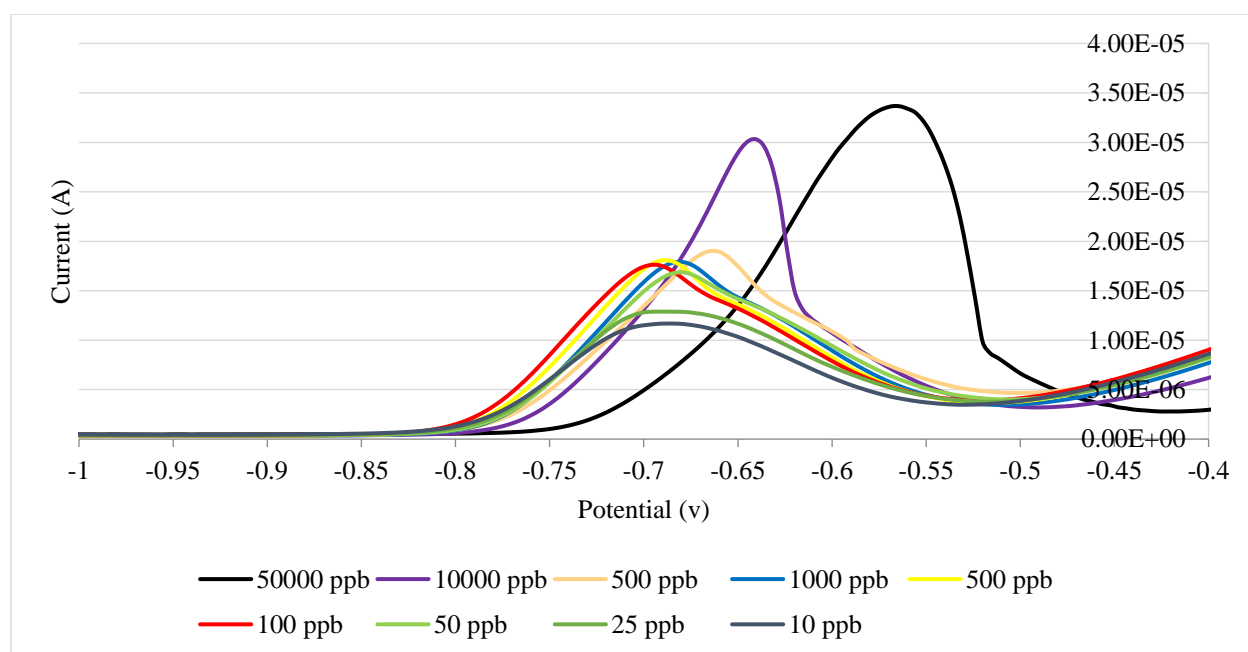


Figure 30: Bare SPE (no modification) sensor in detection of various concentration of  $Pb^{2+}$  in sodium-acetate buffer (pH 4.4) with 10 min (600 sec) deposition cycle

#### 4.10 Electrochemical detection of $Pb^{2+}$ in 0.1 M sodium-acetate buffer, pH 4.6 using sGO/PPy

In the next step, the fabrication technique of Cysteine-Functionalized Graphene Oxide/Polypyrrole Nanocomposite developed by Chang et. al. [30] was followed using the reported optimum operating condition. The goal was to test the result from that sensor to the developed one in terms

of the sensitivity and ease of fabrication. The fabrication of the functionalized graphene oxide was time consuming and needed skilled personnel. However, the LOD and the sensitivity was better than the sensor developed in this study. Comparing the results with the results mentioned by Chang et al. [30], it was found that the fabrication of the sGO/PPy electrode was not successful. Figure 31 shows the results of the sensor tested with different concentration of  $Pb^{2+}$  in sodium-acetate buffer (pH 4.6) with 10 min (600 sec) deposition cycle.



*Figure 31: Cysteine-Functionalized Graphene Oxide/Polypyrrole Nanocomposite modified sensor [30] in detection of various concentration of  $Pb^{2+}$  in sodium-acetate buffer (pH 4.4) with 10 min (600 sec) deposition cycle*

#### 4.11 Electrochemical detection of $Pb^{2+}$ in 0.1 M sodium-acetate buffer, pH 4.4 using rGO-PPy modified SPE

Under the optimized experimental conditions, the DPASV measurements were performed using rGO-PPy modified SPEs for the detection of  $Pb^{2+}$  in varying concentrations (0 ppb – 1000 ppb) of  $Pb^{2+}$  in 0.1 M sodium-acetate buffer at pH 4.4 as supporting electrolyte (Figure 32 and Figure 33).

The deposition step performed for effective accumulation of  $Pb^{2+}$  on the working electrode surface with the deposition potential of  $-1.2$  V for 10 min in open circuit condition. Then DPASV measurements were performed by scanning the stripping voltammetric potential from  $-1.2$  to  $+0.2$  V with an increment potential of 4 mV with a pulse amplitude of 50 mV, pulse width of 0.2 s and pulse period of 0.3 s. The current response elevated gradually with the increase of  $Pb^{2+}$  concentration. The well-defined stripping peak of  $Pb^{2+}$  is seen between the  $-0.8$  to  $-0.7$  V with the increase in peak current. Figure 32 shows the detection of  $Pb^{2+}$  in 0 – 250 ppb  $Pb^{2+}$  concentrated solution and Figure 33 shows the detection of  $Pb^{2+}$  in 250 – 1000 ppb  $Pb^{2+}$  concentrated solution with 0.1 M sodium-acetate buffer (pH 4.4) with 10 min (600 sec) deposition cycle.

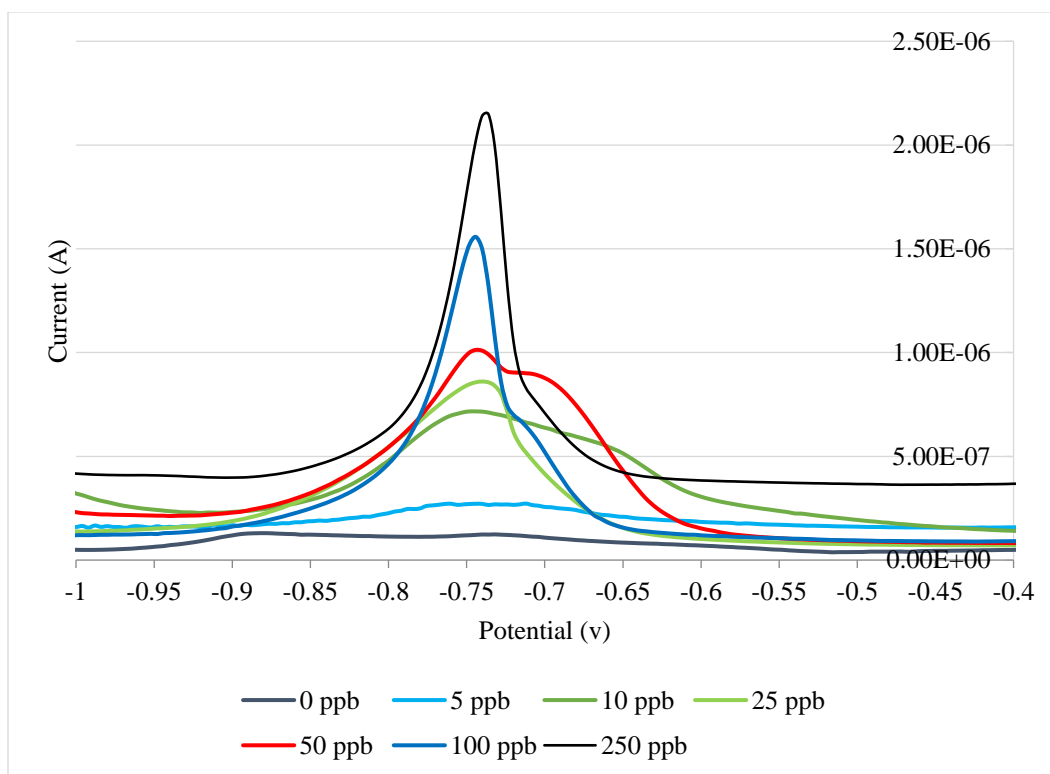


Figure 32: rGO-PPy modified SPE sensor in detection of  $Pb^{2+}$  in 0 – 250 ppb concentrated solution of  $Pb^{2+}$  in 0.1 M sodium-acetate buffer (pH 4.4) with 10 min (600 sec) deposition cycle

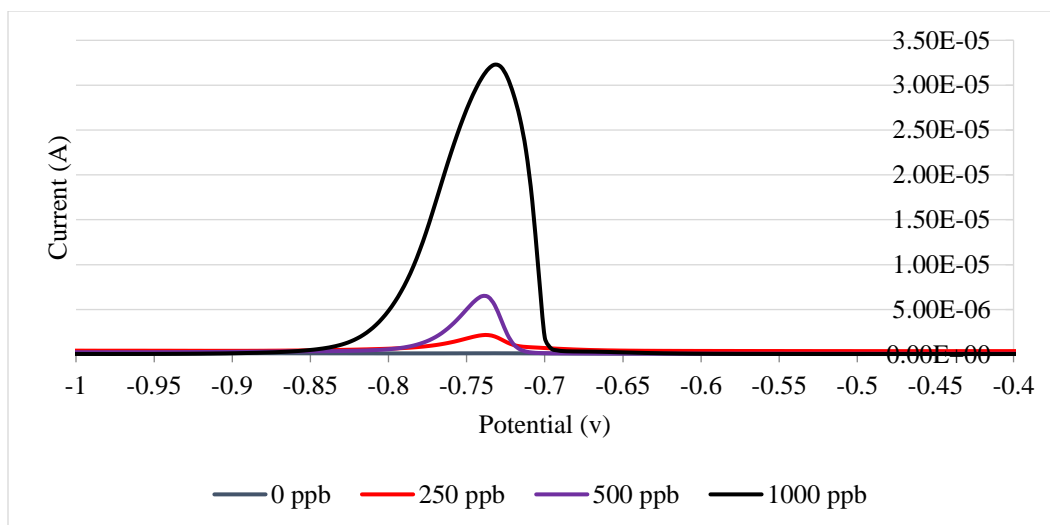


Figure 33: rGO-PPy modified SPE sensor in detection of Pb<sup>2+</sup> in 250 – 1000 ppb concentrated solution of Pb<sup>2+</sup> in 0.1 M sodium-acetate buffer (pH 4.4) with 10 min (600 sec) deposition cycle

The peak current from the DPASV steps during the test using rGO-PPy modified SPEs for the detection of Pb<sup>2+</sup> in varying concentrations (0 ppb – 1000 ppb) of Pb<sup>2+</sup> in 0.1 M sodium-acetate buffer at pH 4.4 was recorded from the data points and peak definition from the CHI software for the electrochemical station.

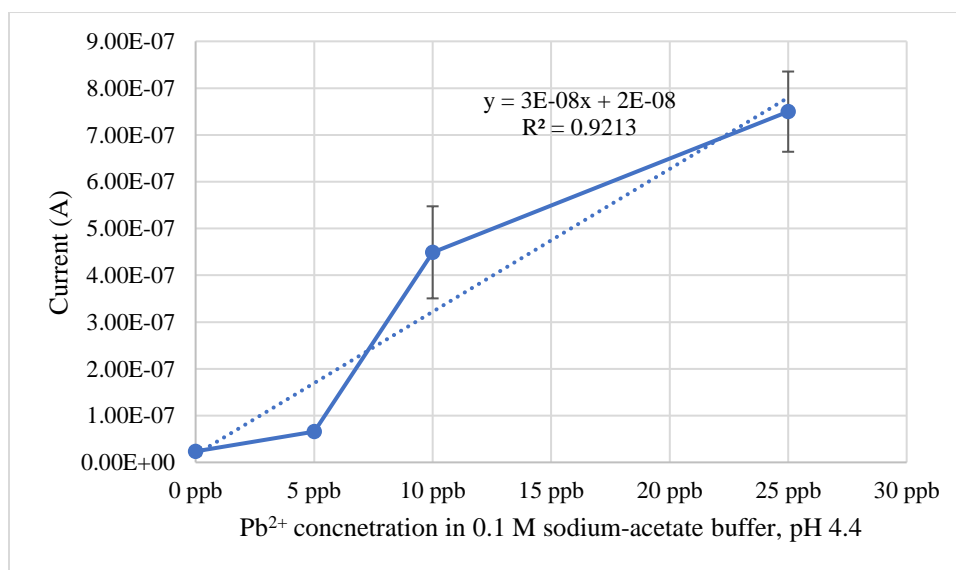


Figure 34: Plot of the peak current from the DPASV rGO-PPy modified SPE sensor in detection of Pb<sup>2+</sup> in 0 ppb - 25 ppb concentrated solution of Pb<sup>2+</sup> in 0.1 M sodium-acetate buffer (pH 4.4) with 10 min (600 sec) deposition cycle

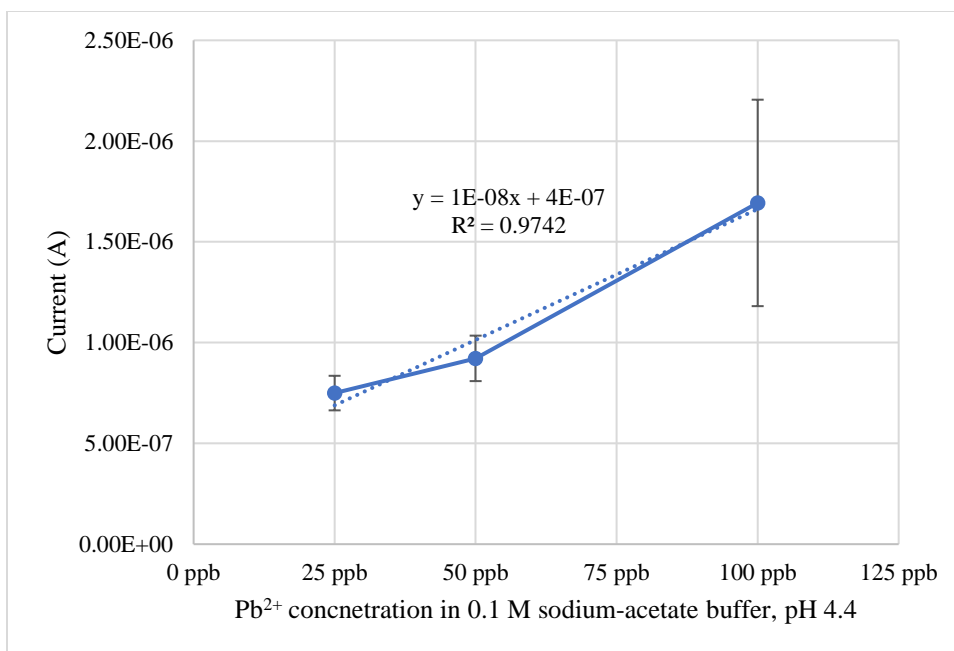


Figure 35: Plot of the peak current from the DPASV rGO-PPy modified SPE sensor in detection of  $Pb^{2+}$  in 25 ppb - 100 ppb concentrated solution of  $Pb^{2+}$  in 0.1 M sodium-acetate buffer (pH 4.4) with 10 min (600 sec) deposition cycle

Figure 34 shows the plot of the peak current in 0 ppb - 25 ppb concentrated solution of  $Pb^{2+}$  with the corresponding trendline/calibration curve with  $R^2 = 0.9213$ . Technically, there shouldn't be a definite peak current for the 0 ppb analytes, which is only the sodium-acetate buffer (pH 4.4) solution. But, in our study we found a peak current for 0 ppb solution which showed the in Figure 34. A similar trendline/calibration curve for the 25 ppb - 100 ppb concentrated solution of  $Pb^{2+}$  showed in Figure 36 with  $R^2 = 0.9742$ . With the error bar standard deviation, it shows very close values for the 50 ppb and 100 ppb signal.

The peak current from the range for 250 ppb - 1000 ppb concentrated solution of  $Pb^{2+}$  in 0.1 M sodium-acetate buffer (pH 4.4) using the rGO-PPy modified SPE sensor is showed in Figure 36. The corresponding trendline/calibration curve with  $R^2 = 0.9624$  is also shown here. Because of the

change in slope based on the concentration, the calibration curves for  $Pb^{2+}$  were determined using three linear concentration ranges 0 to 25 ppb, 25 to 100 ppb and 0 to 1000 ppb.

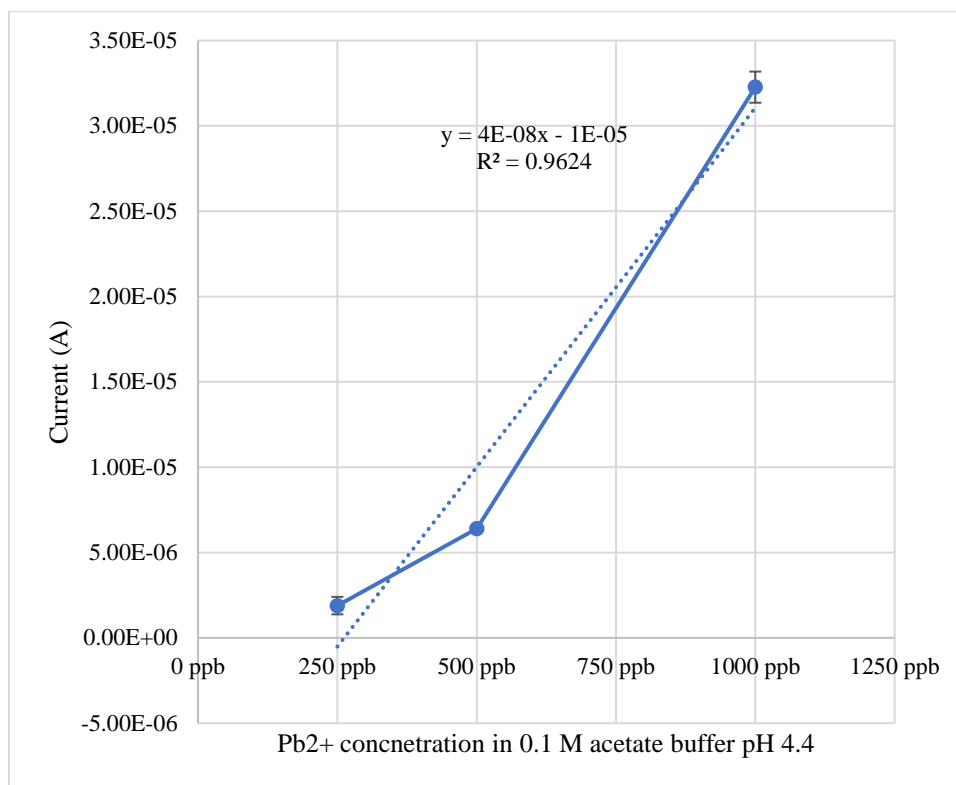


Figure 36: Plot of the peak current from the DPASV rGO-PPy modified SPE sensor in detection of  $Pb^{2+}$  in 250 ppb - 1000 ppb concentrated solution of  $Pb^{2+}$  in 0.1 M sodium-acetate buffer (pH 4.4) with 10 min (600 sec) deposition cycle

The peak current from the DPASV response during the test using rGO-PPy modified SPEs for the detection of  $Pb^{2+}$  for the total range (0 – 1000 ppb) of  $Pb^{2+}$  in 0.1 M sodium-acetate buffer at pH 4.4 is also shown in the Figure 37. The corresponding trendline/calibration curve has the  $R^2 = 0.8953$ . The trendline equation for the total range was  $y = 3E-08x - 1E-06$ , which doesn't reflect the different stages of the slope based on the  $Pb^{2+}$  concentration change. Using the calibration equation on the total range will hinder the detection of lower concentration less 35 ppb. The equation will return a negative value of peak current for any concentration on or below 35 ppb as it can be seen from the y intercept and x intercept value. And the value for that lower range won't

meet the standardize curve to the 0-25 ppb and 25-100 ppb. The linear equations for the lower range validate the measured peak current using DPASV step and it is possible to calculate the peak current for the corresponding  $\text{Pb}^{2+}$  concentrations. In the equation  $y = 3\text{E-}08x + 2\text{E-}08$  (from Figure 34),  $y$  is the peak current corresponding to the  $\text{Pb}^{2+}$  concentration in particles per billion (ppb) or  $\mu\text{g/L}$ . For example, for 1 ppb  $\text{Pb}^{2+}$  concentration, the peak current would be  $5.00\text{E-}8$  (from the equation) while the average peak current for 0 ppb  $\text{Pb}^{2+}$  concentration (i.e. buffer only) was  $2.336\text{E-}8$ .

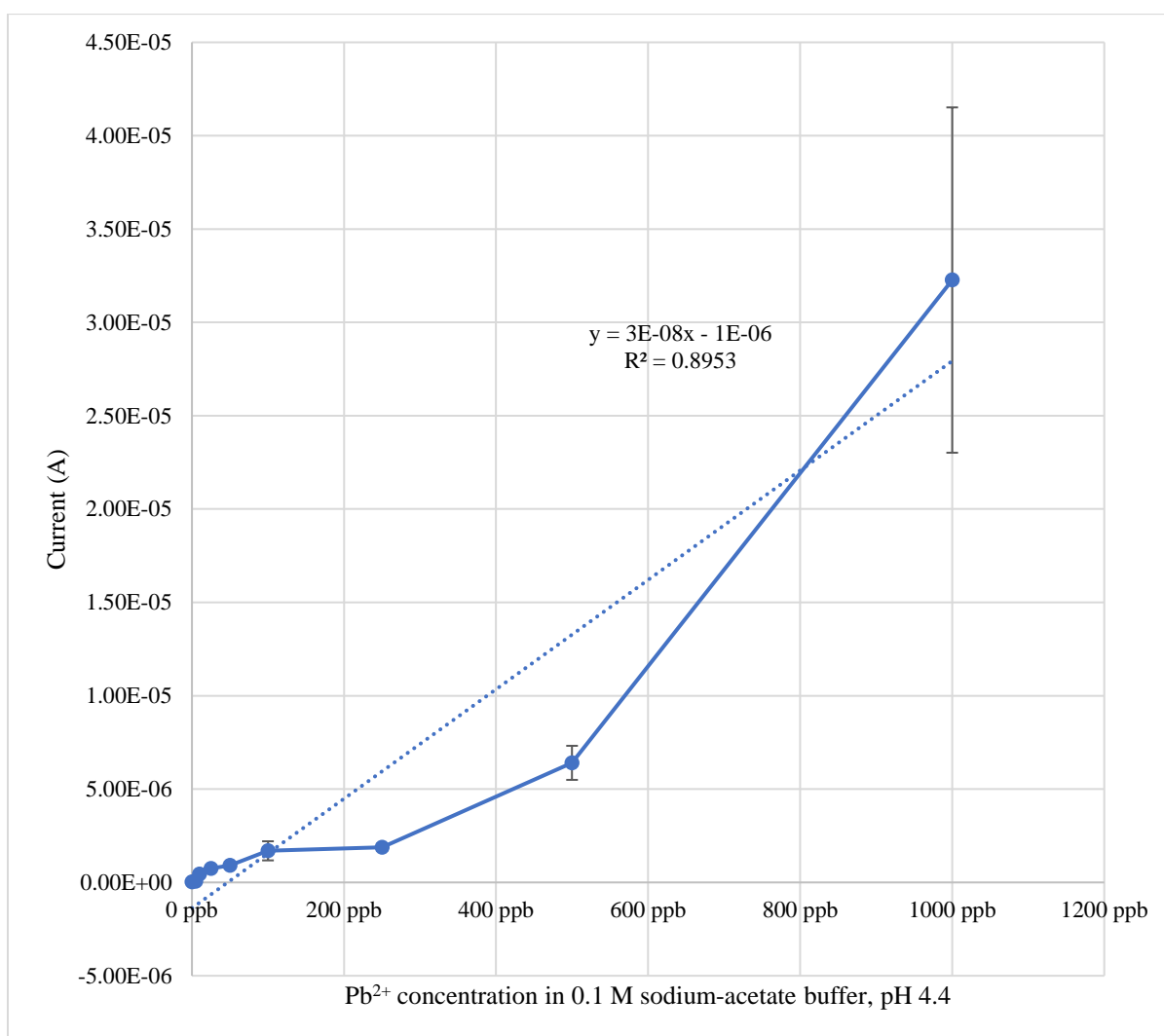


Figure 37: Plot of the peak current from the DPASV rGO-PPy modified SPE sensor in detection of  $\text{Pb}^{2+}$  in 0 ppb - 1000 ppb concentrated solution of  $\text{Pb}^{2+}$  in 0.1 M sodium-acetate buffer (pH 4.4) with 10 min (600 sec) deposition cycle

#### 4.12 Effect of physical parameters (temperature) on electrochemical detection of $\text{Pb}^{2+}$ in 0.1 M sodium-acetate buffer, pH 4.4 using rGO-PPy modified SPE

The electrochemical detection method used in this study was based on the reduction and oxidation behavior of the target heavy metal molecules i.e.  $\text{Pb}^{2+}$  and the analytical solution/supporting electrolytes in the voltammetry process. Temperature is one of the most important parameters that affect the oxidation-reduction potential (ORP). In electrochemistry, thermodynamics of oxidation and reduction reactions is governed by equation developed by the 1920 Nobel Prize winner Walther H. Nernst (1864-1941) [85]. The Nernst equation relates the reduction potential of an electrochemical reaction to the standard electrode potential, temperature, and activities (often scaled by concentrations) of the chemical species undergoing reduction and oxidation. According to the Nernst equation:

$$E (ORP) = E_0 - \frac{2.3RT}{nF} \times \log \frac{[reductant]}{[oxidant]}$$

Here,  $E (ORP)$  is the is the half-cell reduction potential at the temperature of interest

$E_0$  is the standard reduction potential of the system of interest

T is temperature (Kelvin)

R is the universal gas constant

F is the Faraday constant

n is the number of electrons transferred in the reaction

Considering the constant value of R, F and with the smallest value of  $n = 1$  (i.e. 1 electron) for water ( $\text{H}_2\text{O}$ ) then the difference between the ORP between the freezing point (273 K) and the boiling point (373 K) would be about 200 millivolts. Temperature changes the  $\text{pK}_a$  of water which in turn affects the concentrations of  $[\text{H}_3\text{O}^+]$  and  $[\text{OH}^-]$  and that affects both reduction and oxidation

potential of water.  $pK_a$  is the acid dissociation constant which is a quantitative measure of the strength of an acid in solution. It is also defined as the equilibrium constant for a chemical reaction.

As discussed in Chapter 2, metals, metalloids and their complexes can exist in the environment in several valence forms. They can also exist as organometallic compounds with a metal/metalloid-carbon bond. The temperature plays important role on the fate of the state of the metal in the environment. For example, with a lead service line in the water supply, hot water can leach more lead compared to cold water.

The effect of temperature was studied using the different operating condition to affect the reduction step (pre-concentration/deposition) and the oxidation step (stripping).

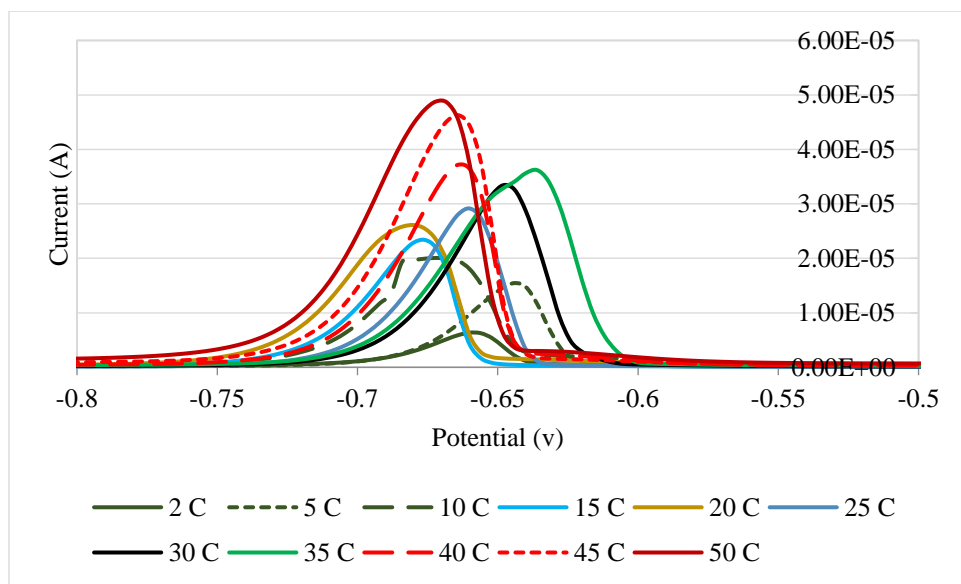
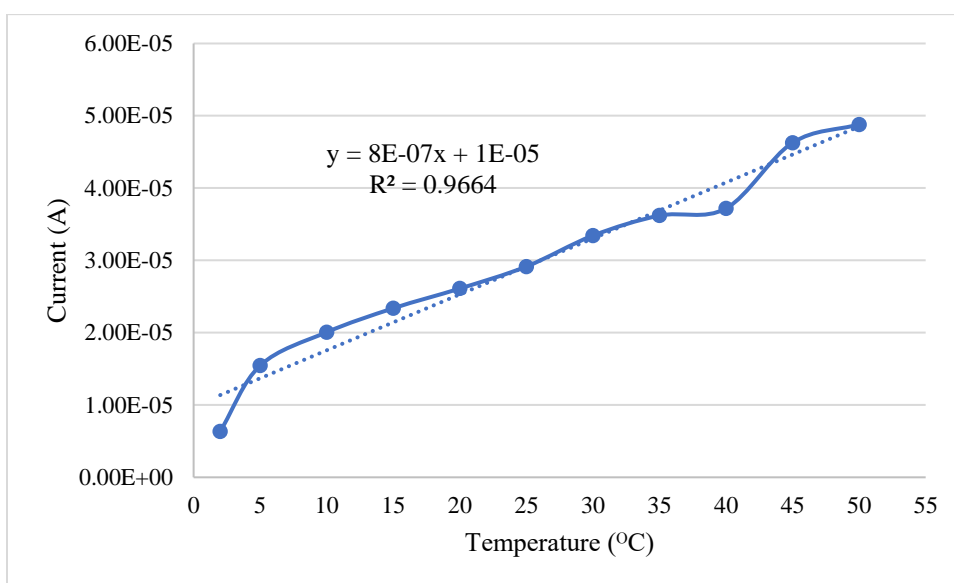


Figure 38: Effect of temperature on  $Pb^{2+}$  detection: 1000 ppb  $Pb^{2+}$  in 0.1 M sodium-acetate buffer, pH 4.4 with rGO-PPy SPE deposition and stripping at the same temperature

Figure 38 shows the DPASV results with varying temperature. The deposition step and the stripping step, both done at the same temperature. It can be seen from the Figure 39 that the peak current increased with increase temperature. At the same time, the oxidation potential for the peak current also changed in respect to change in temperature (Figure 38). The increase in stripping currents with higher temperatures is attributed to increased mass transport and enhanced electrochemical reaction kinetics, which acted as a catalyst for the electrolytic accumulation to stripping of metal ions back into the solution [86].



*Figure 39: Peak current from the DPASV step for 1000 ppb Pb<sup>2+</sup> in 0.1 M sodium-acetate buffer, pH 4.4, with rGO-PPy SPE deposition and stripping at the same temperature*

A similar test was done with different temperature for the oxidization state i.e. the DPASV/stripping step while the reduction/deposition step was performed in the room temperature. The stripping current increased with the increase in temperature as it shows in Figure 41. However, the potential corresponding to the peak current changed in wider range (Figure 40) comparing to the first case where both deposition and stripping was done in the same temperature over the range.

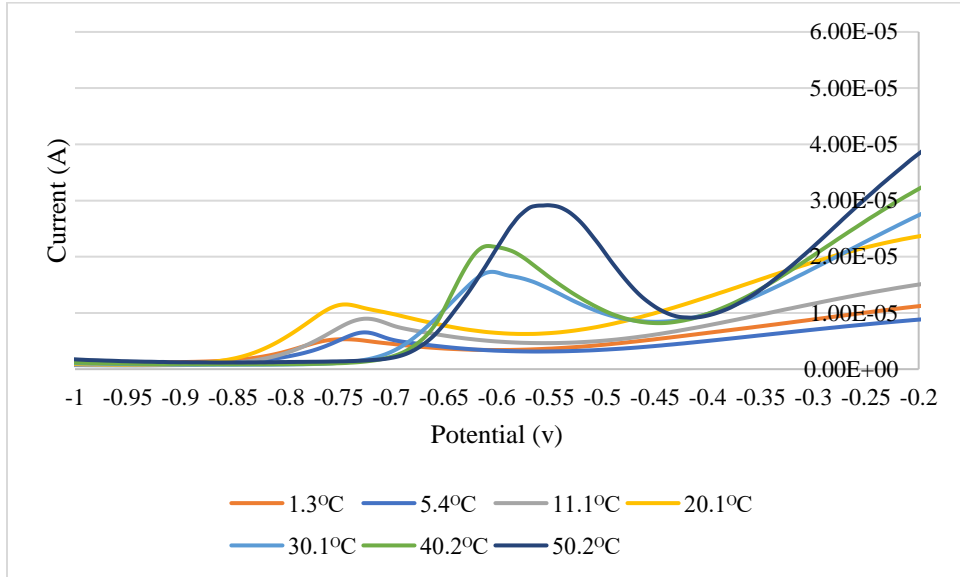


Figure 40: Effect of temperature on  $Pb^{2+}$  detection: 1000 ppb  $Pb^{2+}$  in 0.1 M sodium-acetate buffer, pH 4.4 with rGO-PPy SPE deposition at room temperature and stripping at different temperature

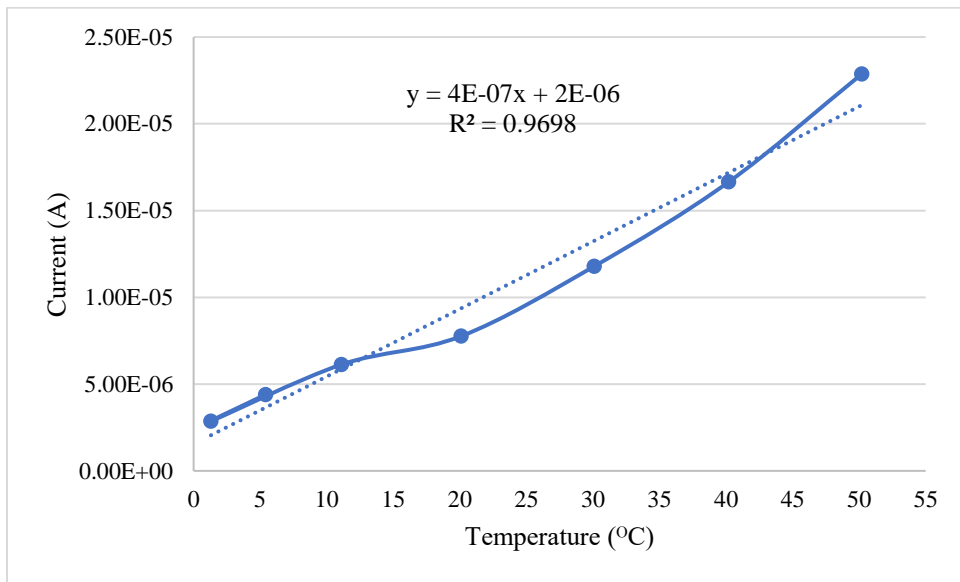


Figure 41: Peak current from the DPASV step for 1000 ppb  $Pb^{2+}$  in 0.1 M sodium-acetate buffer, pH 4.4, with rGO-PPy SPE deposition at room temperature and stripping at different temperature

The response from the DPASV step for 1000 ppb  $Pb^{2+}$  in 0.1 M Acetate Buffer, pH 4.4, with rGO-PPy SPE deposition at room temperature and stripping at different temperature and deposition and stripping at the same temperature is compared in the Figure 42 along with the trendlines. The slope of the trendlines were very similar with a noticeable difference in the y-intercept. At a given temperature, for example at 50°C, the peak current is almost twice when the deposition was done at the same temperature as the stripping step compare to deposition at room temperature and stripping at the varying temperature. The effect of temperature on the sensor structure i.e. reduced graphene oxide-polypyrrole (as layer) were not studied. As these tests were conducted up to 50°C, no noticeable change (or degradation) was found on the sensor surface.

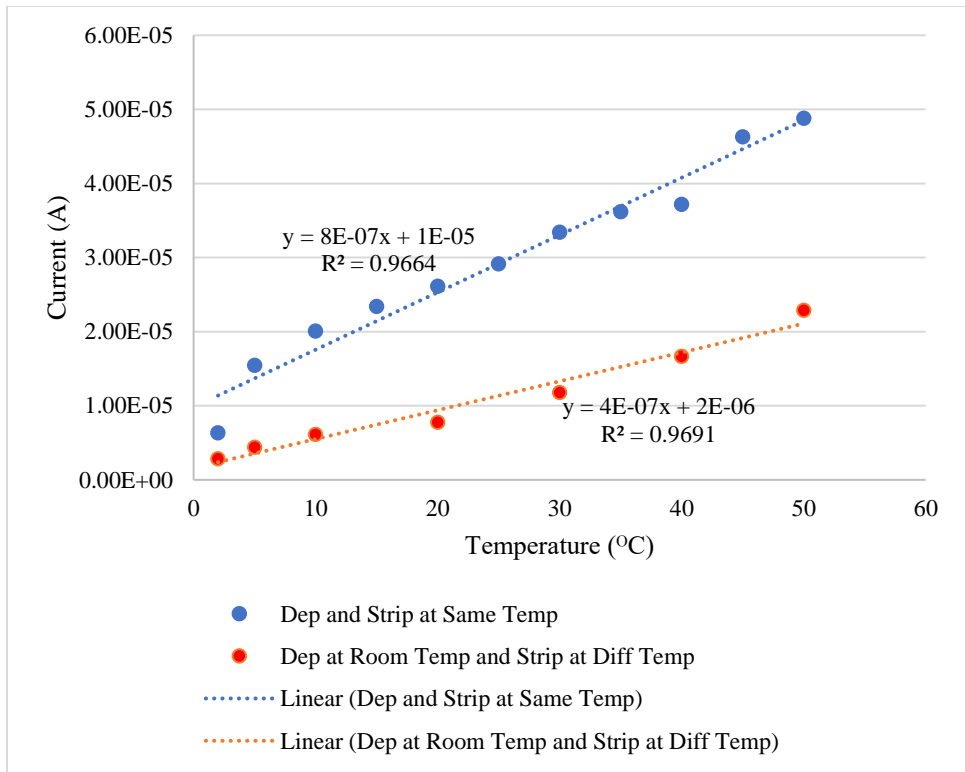


Figure 42: Comparison between the peak current from the DPASV step for 1000 ppb  $Pb^{2+}$  in 0.1 M sodium-acetate buffer, pH 4.4, with rGO-PPy SPE deposition at room temperature and stripping at different temperature and deposition and stripping at the same temperature

#### 4.13 Selectivity test of rGO-PPy modified SPE in presence of $\text{Cu}^{2+}$ (as interfering metal ions) on electrochemical detection of $\text{Pb}^{2+}$ :

As discussed earlier in the electrochemical detection method and the importance of pH in electrochemical detection, the other metal ions and their complexes make it difficult to identify and quantify  $\text{Pb}^{2+}$  with the similar signal interferences. For any given source of water, the total analytical concentration of a given metal in water is the sum of the concentrations of its free ion and its complexes and any metal associated with suspended solids, organic or mineral. In most natural waters, the concentration of free lead ion  $\text{Pb}^{2+}$ , is less than the sum of the molal concentrations of its complexes, which in this case are lead complexes with hydroxyl, carbonate, bicarbonate, and sulfate ions. Other metals that are found in natural waters most often as complexes and not as free ions include  $\text{Al}^{3+}$ ,  $\text{Ag}^+$ ,  $\text{Cu}^{2+}$ ,  $\text{Fe}^{3+}$ , and  $\text{Hg}^{2+}$ . Among these, identification or signal interference with the  $\text{Cu}^{2+}$  is very important for the tap water supply. Copper pipe is a very common choice for the plumbing and one of the most commonly used materials for water pipes in the United States and Europe. It is lightweight, very malleable, durable and recyclable. Because of the joints, fillers and corrosion over time, some  $\text{Cu}^{2+}$  are always present in tap water. The EPA Lead and Copper Rule (LCR) established an action level of 0.015 mg/L (15 ppb) for lead and 1.3 mg/L (1300 ppb) for copper based on the 90<sup>th</sup> percentile level of tap water samples [14]. The Figure 43 shows one of the test report on “Lead/Copper Samples” by Wisconsin Department of Natural Resources [87]. The 90<sup>th</sup> percentile level of copper was 68  $\mu\text{g/L}$  and 90<sup>th</sup> percentile level of lead was 5.9  $\mu\text{g/L}$  on the test on August 2014. The presence of copper in tap water was almost 10 times more in compare to lead for the 90<sup>th</sup> percentile level. Even it was double for the individual sample test.

**Lead/Copper Samples**

PWS ID 24106071 SHOREWOOD WATERWORKS

Sample Date: 08/27/2014  
 Sample ID: 815634  
 Sample Time: 655  
 Type: Compliance  
 Reported Date: 09/30/2014  
 Source: Distribution System  
 Reason: SDWA  
 # Samples: 1  
 Lab ID: 721026460  
 Lab Name: Northern Lake Service Inc. (Crandon)  
 Collector: D BERGE

**Lead/Copper Results**

| Code | Description | Result | 90th percentile value | Units | Qualifier |
|------|-------------|--------|-----------------------|-------|-----------|
| 1022 | COPPER      | 7.2    | 68                    | UG/L  |           |
| 1030 | LEAD        | 2.7    | 5.9                   | UG/L  |           |

**Lead/Copper Results**

Code: 1030 Description: LEAD  
 Store Code: 1051 Description: LEAD TOTAL  
 Result: 2.7 90th percentile value: 5.9  
 Units: UG/L Qualifier:  
 Limit of Detection: 0.10 Limit of Quantification: 0.20  
 MCL: MCL Units: UG/L

Last Revised: 10/13/2016

**Lead/Copper Results**

Code: 1022 Description: COPPER  
 Store Code: 1042 Description: COPPER TOTAL  
 Result: 7.2 90th percentile value: 68  
 Units: UG/L Qualifier:  
 Limit of Detection: 1.0 Limit of Quantification: 2.0  
 MCL: MCL Units: UG/L

Last Revised: 10/13/2016

Figure 43: Tap water test report on “Lead/Copper Samples” by Wisconsin Department of Natural Resources [87]

4.13.1 Selectivity test in presence of Cu<sup>2+</sup> on electrochemical detection of Pb<sup>2+</sup> using rGO-PPy modified SPE

Considering the presence and effect of copper in tap water, the proposed sensor was tested to evaluate the possible interference with the detection of trace amount of Pb<sup>2+</sup> in the presence of Cu<sup>2+</sup>. CuCl<sub>2</sub> was used as a source of Cu<sup>2+</sup>. As in most cases, the presence of Cu<sup>2+</sup> is more than the Pb<sup>2+</sup>, the solutions prepared for this test were 1,000 ppb Pb<sup>2+</sup> in presence of 5,000 ppb Cu<sup>2+</sup> and 500 ppb Pb<sup>2+</sup> in presence of 2,500 ppb Cu<sup>2+</sup> in 0.1 M sodium-acetate buffer (pH 4.4). The rGO-PPy modified SPE sensor was tested under the optimum operating conditions and the response from the DPASV cycle presented in Figure 44 and Figure 45. Though the oxidation potential changed for Pb<sup>2+</sup> detection peak current, it is possible to identify and differentiate the signal for Cu<sup>2+</sup> in the buffer solution. The peak current from the 500 ppb Pb<sup>2+</sup> bit suppressed due to the

presence of  $\text{Cu}^{2+}$ , but the peak current 1000 ppb  $\text{Pb}^{2+}$  is very close to the peak current without  $\text{Cu}^{2+}$ .

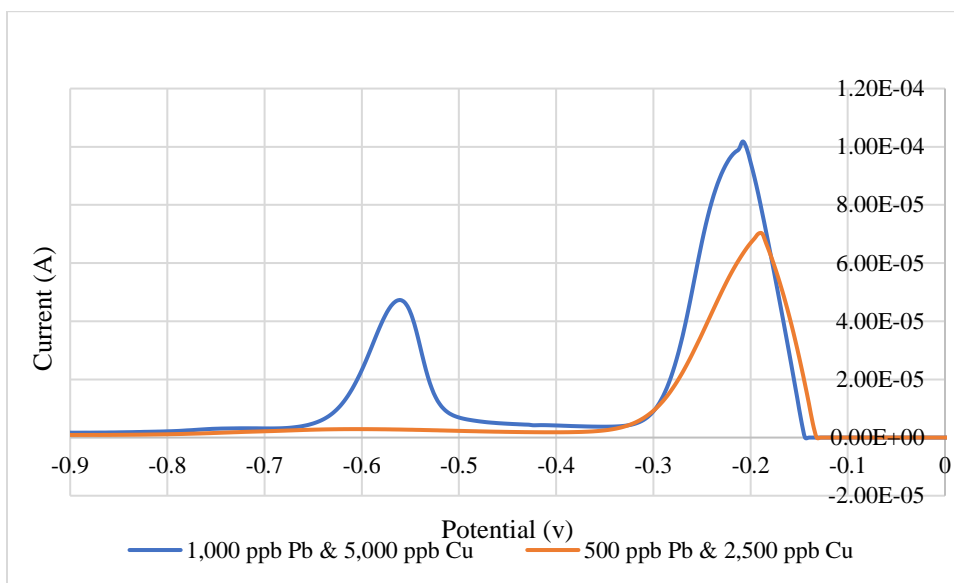


Figure 44: Electrochemical detection of  $\text{Pb}^{2+}$  in presence of  $\text{Cu}^{2+}$  using rGO-PPy modified SPE sensor in 0.1 M sodium-acetate buffer (pH 4.4) with 10 min (600 sec) deposition cycle (Blue line: 1,000 ppb  $\text{Pb}^{2+}$  in presence of 5,000 ppb  $\text{Cu}^{2+}$  and Orange line: 500 ppb  $\text{Pb}^{2+}$  in presence of 2,500 ppb  $\text{Cu}^{2+}$ )

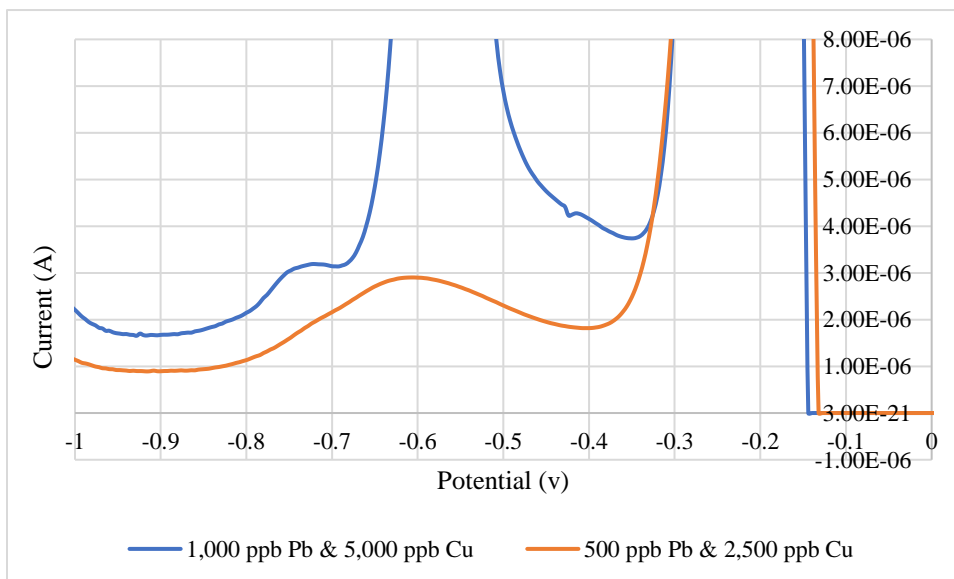


Figure 45: Electrochemical detection of  $\text{Pb}^{2+}$  in presence of  $\text{Cu}^{2+}$  using rGO-PPy modified SPE sensor in 0.1 M sodium-acetate buffer (pH 4.4) with 10 min (600 sec) deposition cycle (with smaller maximum value in y-axis to zoom in the peak current for the orange line: 500 ppb  $\text{Pb}^{2+}$  in presence of 2,500 ppb  $\text{Cu}^{2+}$ )

#### 4.14 Electrochemical detection of Pb<sup>2+</sup> using rGO-PPy modified SPE in tap water test

The rGO-PPy (as layers) modified screen printed electrode exhibits high sensitivity and good selectivity (in presence of Cu<sup>2+</sup>) towards the determination of Pb<sup>2+</sup> under the optimum laboratory conditions (0.1 M sodium-acetate buffer, pH 4.4 made with DI water). To evaluate the practicability of the proposed and developed SPE sensor, it was used to detect Pb<sup>2+</sup> in local tap water sample.

As from the data of the “Lead/Copper Samples” test on the tap water by Wisconsin Department of Natural Resources [87], it can be seen that in most cases the level of lead is very low (about 1-2 µg/L or ppb) to maintain the water quality standard to meet the USEPA and Department of Natural Resources drinking water quality regulations. Since the concentration level of Pb<sup>2+</sup> in tap water collected from our laboratory was extremely low [88, 89], which showed no signals during the detection, spiked sample were inspected at different level of Pb<sup>2+</sup> for detection and quantification of Pb<sup>2+</sup> using the developed rGO-PPy sensor. The Pb<sup>2+</sup> concentrated solution with 0.1 M sodium-acetate buffer (pH 4.4) was suitably diluted with the tap water sample and maintained the pH at 7.6, as the median pH value of the tap water from the water distribution system of Milwaukee Water Works is 7.62 [89]. After the proper dilution procedure, multiple measurements were performed under the same conditions to illustrate its application in practical analysis.

| <b>Lead and Copper</b> |             | <b>Maximum</b> | <b>Minimum</b> | <b>90th percentile</b> |
|------------------------|-------------|----------------|----------------|------------------------|
| Copper (2014)          | See note 2. | 0.130          | <0.001         | 0.038                  |
| Lead (2014)            | See note 2. | 0.0210         | <0.0010        | 0.0082                 |

*Figure 46: Tap water test report on “Lead/Copper” by Milwaukee Water Works [89]*

As it can be seen in Figure 47, the tap water spiked with 1 ppb  $Pb^{2+}$  shows flat line (blue line) without any defined peak signal. However, the DPASV response for the 10 ppb  $Pb^{2+}$  spiked solution with higher current (orange line) but without a specific peak signal. The signal line from the 25 ppb  $Pb^{2+}$  shows a peak (black line) but around -0.18 V as oxidation potential for the peak current.

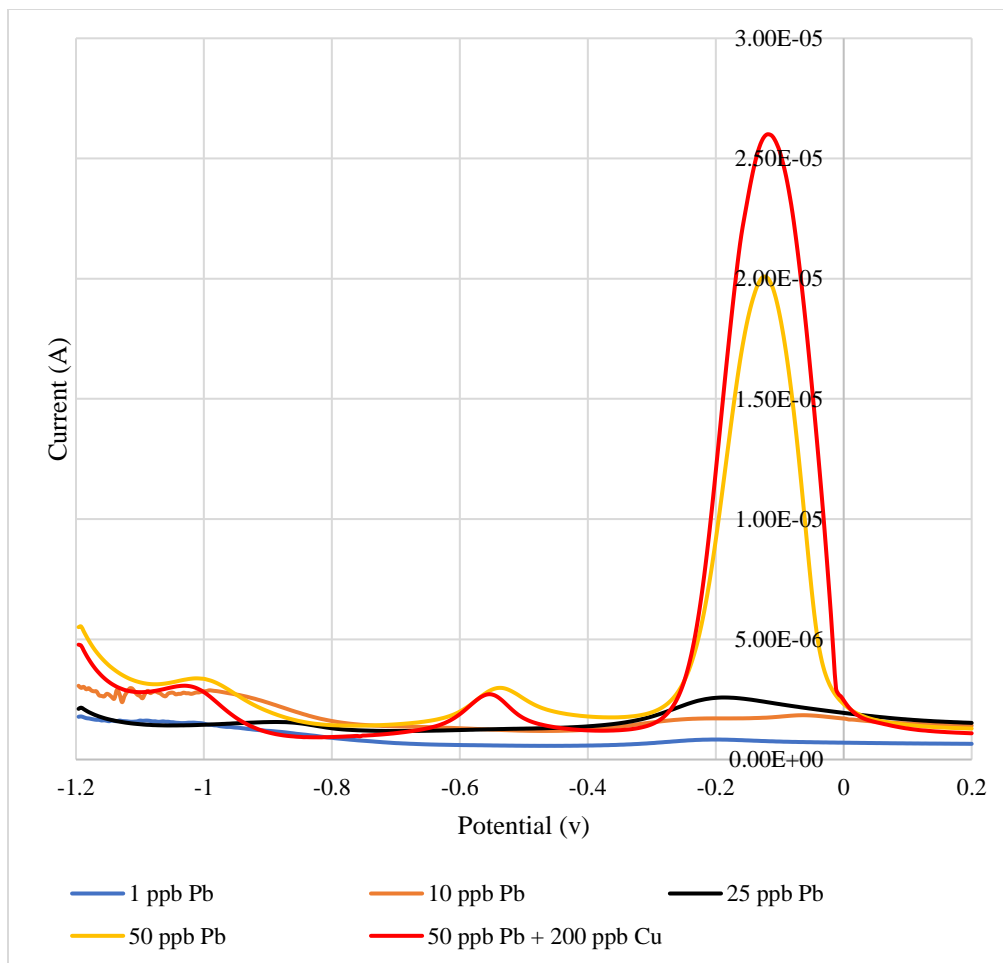


Figure 47: Electrochemical detection of  $Pb^{2+}$  in tap water with spiked  $Pb^{2+}$  and  $Cu^{2+}$  using rGO-PPy modified SPE with 10 min (600 sec) deposition cycle (blue line: 1 ppb  $Pb^{2+}$ , orange line: 10 ppb  $Pb^{2+}$ , black line: 25 ppb  $Pb^{2+}$ , yellow line: 50 ppb  $Pb^{2+}$ , red line: 50 ppb  $Pb^{2+}$  in presence of 200 ppb  $Cu^{2+}$ )

Finally, for 50 ppb  $Pb^{2+}$  spiked solution shows a peak (yellow line) around -0.55 V as oxidation potential for the peak current with another well-defined peak around -0.1 V. And for a spike

solution of 50 ppb  $\text{Pb}^{2+}$  in presence of 200 ppb  $\text{Cu}^{2+}$ , the peaks are at -0.55 V and -0.1 V. A possible explanation for the two peaks might be interpreted from the information of the available organic, inorganic and microbiological constituent in tap water as well the operating principle of stripping voltammetry method. The common sources of drinking water — both tap and bottled water — include rivers, lakes, streams, ponds, and reservoirs (surface water), and wells and springs (groundwater). As water travels over the surface of the land (as rain water, waste water etc.) or through the ground, it washes off and dissolves organic and inorganic substances, naturally-occurring minerals and radioactive material in some rare cases in some specific area in the earth. The organic or inorganic substances are from the human activity (chemical waste, mining waste, pesticides, etc.) and from the presence of animals. In potable water i.e. drinking water (tap water, bottled water) a very small amount of some contaminants can also be found, which is not harmful for human or poses a health risk as long as they are within the safe limit set by the drinking water supply authority. In a “2015 Drinking Water Report” by Washington Water Service Company (WWSC) mentioned [90], they have identified and described in five groups as the source/type of water contaminants:

- **Microbial contaminants** (viruses, parasites, and bacteria): sewage treatment plants, septic systems, agricultural livestock operations, and wildlife are source of this contaminants.
- **Inorganic contaminants** (salts and metals): industrial or domestic wastewater discharges, mining, or farming, oil and gas production and naturally-occurring or result from urban storm water runoff.
- **Pesticides and herbicides:** agriculture, urban storm water runoff, and residential uses, these are the main source of this type of contaminants.

- **Radioactive contaminants:** only the oil and gas production and mining activities are the sources of this type of contaminants and the naturally-occurring events (such as earthquake, volcano) sometimes initiate a source for the radioactive contaminants.
- **Organic chemical contaminants:** the byproducts of industrial processes and petroleum production including synthetic and volatile organic chemicals, and can also come from gas stations, urban storm water runoff, and septic systems.

From the “2016 Distribution System Water Quality” by Milwaukee Water Works [89], the total number of parameters to test for the tap water is more than 250 in twelve different groups namely- Clarity, Microbiological, Chemical & Physical Parameters, Inorganic Chemicals, Organic Chemicals, Estrogens and Other Hormones (EDCs), Perfluorinated Compounds, Phosphate Flame Retardants, Nitrosamines, Phenolic Endocrine Disruptors (EDCs), Pharmaceuticals & Personal Care Products, Radionuclides (pCi/L) and UCMR-3 (2013).

| Q582FLUR<br>11/12/2017<br>10:50:37 AM     |           | Wisconsin Department of Natural Resources<br>Drinking Water System<br>Fluoride Sample History |           |            |                   |                    |            |           | Page 2 of 4                                  |                 |
|---|-----------|---|-----------|------------|-------------------|--------------------|------------|-----------|--|-----------------|
| Samples between 11/12/2016 and 11/12/2017 |           |   |           |            |                   |                    |            |           |  |                 |
| System Name:                              | PWS ID:   | Collected:  | Samp Id:  | Typ:       | Lab Result/Units: | Site Result/Units: | Reported:  | Lab Id:   | Location Desc:                               | Collector:      |
| Region:                                   |           |   |           |            |                   |                    |            |           |  |                 |
| Type:                                     |           |   |           |            |                   |                    |            |           |  |                 |
| County:                                   |           |   |           |            |                   |                    |            |           |  |                 |
| CUDAHY WATERWORKS                         | 24101693  | 10/11/2017  | 348723001 | D          | 0.75 MG/L         | 0.72 MG/L          | 10/23/2017 | 113133790 | KITCHEN SINK                                 | MICHAEL OLLMANN |
|   |           | 09/11/2017  | 341961001 | D          | 0.73 MG/L         | 0.74 MG/L          | 09/21/2017 | 113133790 | KITCHEN SINK                                 | MICHAEL OLLMANN |
|   |           | 08/02/2017  | 333408001 | D          | 0.77 MG/L         | 0.73 MG/L          | 08/14/2017 | 113133790 | KITCHEN SINK                                 | MICHAEL OLLMANN |
|   |           | 07/05/2017  | 326049001 | D          | 0.71 MG/L         | 0.71 MG/L          | 07/13/2017 | 113133790 | KITCHEN SINK                                 | MICHAEL OLLMANN |
|   |           | 06/05/2017  | 319800001 | D          | 0.73 MG/L         | 0.75 MG/L          | 06/09/2017 | 113133790 | KITCHEN SINK                                 | MICHAEL OLLMANN |
|   |           | 05/08/2017  | 314952001 | D          | 0.73 MG/L         | 0.73 MG/L          | 05/17/2017 | 113133790 | KITCHEN SINK                                 | MICHAEL OLLMANN |
|   |           | 04/04/2017  | 308266001 | D          | 0.70 MG/L         | 0.72 MG/L          | 04/10/2017 | 113133790 | KITCHEN SINK                                 | MICHAEL OLLMANN |
|   |           | 03/06/2017  | 302940001 | D          | 0.71 MG/L         | 0.72 MG/L          | 03/09/2017 | 113133790 | KITCHEN SINK                                 | MICHAEL OLLMANN |
|   |           | 02/09/2017  | 299538001 | D          | 0.74 MG/L         | 0.75 MG/L          | 02/17/2017 | 113133790 | KITCHEN SINK                                 | MICHAEL OLLMANN |
|   |           | 01/10/2017  | 296069001 | D          | 0.73 MG/L         | 0.75 MG/L          | 01/17/2017 | 113133790 | KITCHEN SINK                                 | MICHAEL OLLMANN |
|   |           | 12/07/2016  | 292197001 | D          | 0.79 MG/L         | 0.78 MG/L          | 12/20/2016 | 113133790 | KITCHEN SINK                                 | MICHAEL OLLMANN |
|   |           | MILWAUKEE WATERWORKS  | 24101000  | 10/05/2017 | 348544001         | D                  | 0.53 MG/L  | 0.54 MG/L | 10/23/2017                                   | 113133790       |
| 09/07/2017                                | 342438001 |   |           | D          | 0.51 MG/L         | 0.52 MG/L          | 09/21/2017 | 113133790 | FIRE STATION LAUNDRY SINK 1ST FLT VANDENBUSH |                 |
| 08/03/2017                                | 334528001 |   |           | D          | 0.54 MG/L         | 0.62 MG/L          | 08/14/2017 | 113133790 | FIRE STATION LAUNDRY SINK 1ST FLS. BINTER    |                 |
| 07/06/2017                                | 327943001 |   |           | D          | 0.52 MG/L         | 0.50 MG/L          | 07/14/2017 | 113133790 | FIRE STATION LAUNDRY SINK 1ST FLS. BINTER    |                 |
| 06/01/2017                                | 320274001 |   |           | D          | 0.54 MG/L         | 0.54 MG/L          | 06/09/2017 | 113133790 | FIRE STATION LAUNDRY SINK 1ST FLS. BINTER    |                 |
| 05/04/2017                                | 314951001 |   |           | D          | 0.53 MG/L         | 0.56 MG/L          | 05/17/2017 | 113133790 | FIRE STATION LAUNDRY SINK 1ST FLS. BINTER    |                 |
| 04/06/2017                                | 309450001 |   |           | D          | 0.54 MG/L         | 0.59 MG/L          | 04/20/2017 | 113133790 | FIRE STATION LAUNDRY SINK 1ST FLT SUSAC      |                 |
| 03/02/2017                                | 302931001 |   |           | D          | 0.51 MG/L         | 0.53 MG/L          | 03/09/2017 | 113133790 | FIRE STATION LAUNDRY SINK 1ST FLS. BINTER    |                 |
| 02/02/2017                                | 299272001 |   |           | D          | 0.52 MG/L         | 0.59 MG/L          | 02/16/2017 | 113133790 | FIRE STATION LAUNDRY SINK 1ST FLS. BINTER    |                 |
| 01/05/2017                                | 295239001 |   |           | D          | 0.54 MG/L         | 0.56 MG/L          | 01/19/2017 | 113133790 | FIRE STATION LAUNDRY SINK 1ST FLS. BINTER    | S. BINTER       |
| 12/01/2016                                | 291853001 |   |           | D          | 0.57 MG/L         | 0.56 MG/L          | 12/13/2016 | 113133790 | FIRE STATION LAUNDRY SINK 1ST FLT SUSAC      |                 |

Figure 48: : Tap water test report on “Fluoride Sample History” by Wisconsin Department of Natural Resources [87]

There are few organic and inorganic constituent are allowed up to certain level (such as CaCO<sub>3</sub>, Barium, Chlorine, Chlorite, Fluoride, Adipate, di(2-ethylhexyl), Bromodichloromethane etc.) to maintain the quality and for disinfection purpose. Figure 48, shows Tap water test report on “Fluoride Sample History” by Wisconsin Department of Natural Resources [87]. And because of the disinfection chemicals used at the water treatment plants, there are some disinfection byproducts which also has significant impact on the water quality. Figure 49 shows tap water test report on “Disinfection Byproducts” as a result of the chemicals applied to the natural water (lake/river/ground water) by Wisconsin Department of Natural Resources.

| Wisconsin Department of Natural Resources  |                                      |        |       |                     |                    |                         |     |           |
|--|--------------------------------------|--------|-------|---------------------|--------------------|-------------------------|-----|-----------|
| Wisconsin DNR Drinking Water data          |                                      |        |       |                     |                    |                         |     |           |
| <b>Other (non-bacteriological) Samples</b> |                                      |        |       |                     |                    |                         |     |           |
| PWS ID 24106071 SHOREWOOD WATERWORKS       |                                      |        |       |                     |                    |                         |     |           |
| Sample Group:                              | Disinfection Byproducts (TTHM, HAA5) |        |       |                     |                    |                         |     |           |
| Source ID:                                 | (none)                               |        |       |                     |                    |                         |     |           |
| Well #:                                    | (none)                               |        |       |                     |                    |                         |     |           |
| Sample ID:                                 | 942874                               |        |       |                     |                    |                         |     |           |
| Sample Date:                               | 09/01/2016                           |        |       |                     |                    |                         |     |           |
| Sample Time (24-hour clock):               | 1030                                 |        |       |                     |                    |                         |     |           |
| Type:                                      | Compliance                           |        |       |                     |                    |                         |     |           |
| Reported Date:                             | 09/14/2016                           |        |       |                     |                    |                         |     |           |
| Reason:                                    | SDWA                                 |        |       |                     |                    |                         |     |           |
| Source:                                    | Distribution System                  |        |       |                     |                    |                         |     |           |
| # Samples:                                 | 1                                    |        |       |                     |                    |                         |     |           |
| Collector:                                 | B NOWAK                              |        |       |                     |                    |                         |     |           |
| Lab Id:                                    | 721026460                            |        |       |                     |                    |                         |     |           |
| Lab Name:                                  | Northern Lake Service Inc. (Crandon) |        |       |                     |                    |                         |     |           |
| <b>Sampling Results</b>                    |                                      |        |       |                     |                    |                         |     |           |
| Code                                       | Description                          | Result | Units | Qualifier           | Limit of Detection | Limit of Quantification | MCL | MCL Units |
| 2943                                       | BROMODICHLOROMETHANE                 | 3.3    | UG/L  |                     | .23                | .81                     | 80  | UG/L      |
| 2942                                       | BROMOFORM                            | .26    | UG/L  | Between LOD and LOQ | .21                | .74                     | 80  | UG/L      |
| 2941                                       | CHLOROFORM                           | 2.9    | UG/L  |                     | .25                | .9                      | 80  | UG/L      |
| 2454                                       | DIBROMOACETIC ACID                   | .63    | UG/L  |                     | 0.061              | 0.20                    |     | UG/L      |
| 2944                                       | DIBROMOCHLOROMETHANE                 | 2      | UG/L  |                     | .17                | .61                     | 80  | UG/L      |
| 2451                                       | DICHLOROACETIC ACID                  | 2.4    | UG/L  |                     | 0.048              | 0.16                    |     | UG/L      |
| 2456                                       | HAA5                                 | 3.8    | UG/L  |                     |                    |                         | 60  | UG/L      |
| 2453                                       | MONOBROMOACETIC ACID                 | .14    | UG/L  | Between LOD and LOQ | 0.097              | 0.32                    |     | UG/L      |
| 2450                                       | MONOCHLOROACETIC ACID                | 0      | UG/L  | Non-detect          | 0.65               | 2.2                     |     | UG/L      |
| 2452                                       | TRICHLOROACETIC ACID                 | .63    | UG/L  |                     | 0.11               | 0.35                    |     | UG/L      |
| 2950                                       | TTHM                                 | 8.46   | UG/L  |                     |                    |                         | 80  | UG/L      |

Figure 49: Tap water test report on “Disinfection Byproducts” as a results of the chemical applied to the natural water (lake/river/ground water) by Wisconsin Department of Natural Resources [87]

All these microbiological, inorganic chemicals and organic chemicals can affect the electrochemical detection by altering the phase of the  $\text{Pb}^{2+}$  in water. As in the DPASV test for the spiked tap water sample (Figure 48), it can be said that the free  $\text{Pb}^{2+}$  in the sample produced the peak signal around -0.6 V, and the peak around -0.1 V might be from the lead complexes with the other constituents available in that tap water sample. The copper might also form a complex ligand and increase that peak at -0.1 V. Only a portion of total  $\text{Pb}^{2+}$  ion used to spike the tap water sample might remain as  $\text{Pb}^{2+}$  ion and produced that peak current around -0.6 V. The redox potential also changed based on the metal complex formed in the solution due to the available elements presents in the tap water.

## **Chapter 5: Conclusion**

## 5.1 Overall summary

The aim of this study was to develop an electrochemical sensor for speedy, selective and sensitive detection of  $\text{Pb}^{2+}$  using reduced graphene oxide and polypyrrole (rGO-PPy) nanocomposite. The rGO-PPy modified electrode possessed a large effective area because of unique 3D porous architectures and displayed excellent selectivity for determination of  $\text{Pb}^{2+}$ . The sensor structure and the fabrication method of the developed sensor is rapid and simple to follow compared to complex and time consuming electrochemical synthesis process. With the optimum operating conditions, the developed rGO-PPy nanocomposite modified SPE can be used to identify and quantify  $\text{Pb}^{2+}$  up to 5 ppb and with the linear range from calibration curve up to 1 ppb. Moreover, this fabrication process can be easily modified and implemented using a printing device for inexpensive mass production. Graphene oxide can be reduced chemically and can be applied on the working electrode of the sensor in one step process. Mabrook et. al. [91] has already reported a successful application of the polypyrrole layer using a conventional inkjet printer with some simple modification.

As the tap water/drinking water comes from groundwater (wells and springs) and surface water (rivers, lakes, streams), the developed sensor can be applied with few additional steps. The detection method can be applied using the following steps:

1. The standard calibration curves (Figure 34, 35 and 36) described above for testing in the optimum operating conditions with different concentration of  $\text{Pb}^{2+}$  can be used as a scale for identifying and quantifying the  $\text{Pb}^{2+}$  in water sample.

2. For tap water or surface water, the water sample need to be filtered using fast and quantitative filtering paper, removing particles in the water sample and then the pH measurement needed to be done. After that following the standard pH buffer guide, the pH needed to be adjusted to 4.4 using the sodium-acetate buffer. One of the most important task in this process is to use a fixed/known volume ratio for the water sample to adjust the pH as well as to consider the dilution factor to calculate the correct concentration range. Once the sample water solution is filtered and adjusted to pH 4.4 the deposition cycle and the DPASV cycle be applied using the three-electrode electrochemical station. The measured peak height values at the potential range can be compared with the standard curve to quantify the amount of  $\text{Pb}^{2+}$  in water sample.

## 5.2 Future direction

As described in the optimal operating conditions and the results, this developed sensor can be used with modified pH solution for a reliable detection and quantification of  $\text{Pb}^{2+}$  in water. Most of the current studies (including this) only confirmed water sensor applications that could detect heavy metals in buffer solutions or after a certain filtration and addition of certain chemical solution (separation or pre-concentration for sample preparation). The main challenge to apply the rGO-PPy sensor to real-world samples (tap water, waste water or river water) without changing the pH or other operating conditions for real-time, on-site detection of heavy metals is the severe interference of organic-inorganic chemicals and biological constituent in a solution such as tap water, waste water. The sensing signals will be complicated because of the formation of metalloid and metal complexes and will affect the redox potential range for the deposition and stripping steps.



*Figure 50: Solubility of lead salt ( $PbCl_2$ ) in water with different pH, pH 4.4 buffer in the jar (on the left) and tap water pH 7.38 in the conical flask (on the right) with same of amount lead salt in 100 mL water*

As in Figure 50, the solubility of the lead salt in water depends on the pH of the water.  $PbCl_2$  was used in this experiment as a source of the  $Pb^{2+}$ . With the metalloids and metal complexes already in the tap water, the added lead salt  $PbCl_2$  are being rapidly degraded and sediment in the form of hard soluble carbons, sulfates and sulfides on the bottom. And with the pH 7.38 of tap water, it wasn't possible to produce homogeneous solution of the  $PbCl_2$  a tap water even with a concentration 100 ppb or 100  $\mu\text{g/L}$ . The small amount metal and metalloids in tap water appear in different chemical forms and in different oxidizing conditions which depends on the source of the water (ground well, river or lake) [16], the treatment process and the environmental change (seasonal change-winter/summer). The tap water is slightly basic [89] and contains some dissolved mineral salts, most likely calcium and magnesium carbonates and bicarbonates. The anions of those salts consume some of the  $H^+$  maintain the pH in slightly basic forms. Lower atmospheric pressure causes the evaporation of the dissolved  $CO_2$  in water. In that case, the

equilibrium with the carbonic acid and carbon di oxide changes, and that caused a change in pH of water. At higher temperature, the bicarbonates in water decomposes in carbonate and carbon di oxide, the resultant dissociation of any dissolved carbonic acid change the pH of water.

The environmental chemistry of water or the solution of interest plays an important role on metal behavior including the formation of metal complexes, and the importance of pH and oxidation-reduction reactions to metal mobility. To develop a versatile sensor to work with any source of water would be very complicated. However, a more specific sensor can be developed targeting a specific source by analyzing water chemistry for the specific reduction-oxidization potentials for possible interfering elements.

## References

- [1] E.-E. C. O and O. W. O, "Heavy Metal Assessment of Ground, Surface and Tap Water Samples in Lagos Metropolis Using Anodic Stripping Voltammetry," *Resources and Environment*, vol. 2, pp. 82-86, 2012.
- [2] J. H. Duffus, "Heavy Metals - A meaningless term?," *Pure and Applied Chemistry*, vol. 74, p. 14, 2002 2002.
- [3] L. Järup, "Hazards of heavy metal contamination," *British medical bulletin*, vol. 68, p. 167, 2003.
- [4] "U.S. Environmental Protection Agency - Framework for Metals Risk Assessment," *EPA 120/R-07/001, Office of the Science Advisor, Risk Assessment Forum, Washington, D.C.*, 2007.
- [5] W. H. Organization, "Biological Monitoring of Metals," 1994.
- [6] G. Aragay, J. Pons, and A. Merkoci, "Recent trends in macro-, micro-, and nanomaterial-based tools and strategies for heavy-metal detection," *Chem Rev*, vol. 111, pp. 3433-58, May 11 2011.
- [7] M. Banchelli, C. Guardiani, R. B. Sandberg, S. Menichetti, P. Procacci, and G. Caminati, "Media effects in modulating the conformational equilibrium of a model compound for tumor necrosis factor converting enzyme inhibition," *Journal of Molecular Structure*, vol. 1091, pp. 65-73, 2015.
- [8] H. Bouziane, B. Messabih, and A. Chouarfia, "Effect of simple ensemble methods on protein secondary structure prediction," *A Fusion of Foundations, Methodologies and Applications*, vol. 19, pp. 1663-1678, 2015.
- [9] W. H. Organisation, "Ten chemicals of major public health concern," *International Programme on Chemical Safety-Health impacts of chemicals*, 10/21/2017 2014.
- [10] D. M. Whitacre, *Reviews of Environmental Contamination and Toxicology Volume 232*. Dordrecht: Dordrecht : Springer, 2014.
- [11] C. R. Chowdhury BA, "Biological and health implications of toxic heavy metal and essential trace element interactions," *Prog Food Nutr Sci, US National Library of Medicine, National Institutes of Health* vol. 11, pp. 55-113, 1987.
- [12] E. Mitchell, S. Frisbie, and B. Sarkar, "Exposure to multiple metals from groundwatera global crisis: Geology, climate change, health effects, testing, and mitigation," *Metallomics*, vol. 3, pp. 874-908, 2011.
- [13] A. Navas-Acien, E. Guallar, E. Silbergeld, and S. J. Rothenberg, "Lead exposure and cardiovascular disease - A systematic review," in *Environ. Health Perspect.* vol. 115, ed, 2007, pp. 472-482.
- [14] U. S. E. P. Agency, "Lead and Copper Rule: Basic Information about Lead in Drinking Water," 2017.
- [15] W. H. Organization, "Lead poisoning and health," *Fact sheet*, 2017.
- [16] M. Torrice, "How Lead Ended Up In Flint's Tap Water," *Chemical & Engineering News, American Chemical Society*, vol. 94, p. 4, 10/21/2017 2016.
- [17] U. S. EPA, "U.S. EPA to strengthen protection from lead in drinking water.(Environmental Protection Agency)," *Journal of Environmental Health*, vol. 68, p. 42, 2005.

- [18] G. Plumlee, J. Durant, S. Morman, A. Neri, R. Wolf, C. Dooyema, *et al.*, "Linking Geological and Health Sciences to Assess Childhood Lead Poisoning from Artisanal Gold Mining in Nigeria," *Environmental Health Perspectives (Online)*, vol. 121, p. 744, 2013.
- [19] U. S. EPA, "DETERMINATION OF TRACE ELEMENTS IN WATERS AND WASTES BY INDUCTIVELY COUPLED PLASMA - MASS SPECTROMETRY," *ENVIRONMENTAL MONITORING SYSTEMS LABORATORY - OFFICE OF RESEARCH AND DEVELOPMENT* vol. 200.8, 1994.
- [20] Z. Li, J. Chen, M. Liu, and Y. Yang, "Supramolecular solvent-based microextraction of copper and lead in water samples prior to reacting with synthesized Schiff base by flame atomic absorption spectrometry determination," *Anal. Methods*, vol. 6, pp. 2294-2298, 2014.
- [21] M. Zougagh, A. Garc'ia de Torres, E. Vereda Alonso, and J. M. Cano Pavón, "Automatic on line preconcentration and determination of lead in water by ICP-AES using a TS-microcolumn," vol. 62, ed: Talanta, 2003, pp. 503-510.
- [22] Y. Izumi, F. Kiyotaki, T. Minato, D. Masih, and Y. Seida, "Monitoring trace amounts of lead and arsenic adsorption by x-ray absorption fine structure combined with fluorescence spectrometry," *Physica Scripta*, vol. 2005, pp. 933-935, 2005.
- [23] Y. Izumi, F. Kiyotaki, T. Minato, and Y. Seida, "X-ray absorption fine structure combined with fluorescence spectrometry for monitoring trace amounts of lead adsorption in the environmental conditions," *Anal. Chem.*, vol. 74, pp. 3819-3823, 2002.
- [24] M. A. Rahman, M.-S. Won, and Y.-B. Shim, "Characterization of an EDTA bonded conducting polymer modified electrode: its application for the simultaneous determination of heavy metal ions," *Analytical chemistry*, vol. 75, p. 1123, 2003.
- [25] N. Zhou, H. Chen, J. Li, and L. Chen, "Highly sensitive and selective voltammetric detection of mercury(II) using an ITO electrode modified with 5-methyl-2-thiouracil, graphene oxide and gold nanoparticles," *An International Journal on Analytical Micro-and Nanochemistry*, vol. 180, pp. 493-499, 2013.
- [26] Y. Wei, R. Yang, J.-H. Liu, and X.-J. Huang, "Selective detection toward Hg(II) and Pb(II) using polypyrrole/carbonaceous nanospheres modified screen-printed electrode," *Electrochimica Acta*, vol. 105, pp. 218-223, 2013.
- [27] X. Gong, Y. Bi, Y. Zhao, G. Liu, and W. Y. Teoh, "Graphene oxide-based electrochemical sensor: a platform for ultrasensitive detection of heavy metal ions," *RSC Adv.*, vol. 4, pp. 24653-24657, 2014.
- [28] A. Martín, J. Hernández-Ferrer, M. T. Martínez, and A. Escarpa, "Graphene nanoribbon-based electrochemical sensors on screen-printed platforms," *Electrochimica Acta*, vol. 172, pp. 2-6, 2015.
- [29] S. Wu, Q. He, C. Tan, Y. Wang, and H. Zhang, "Graphene-Based Electrochemical Sensors," *Small*, vol. 9, p. 1160, 2013.
- [30] R. Seenivasan, W. J. Chang, and S. Gunasekaran, "Highly Sensitive Detection and Removal of Lead Ions in Water Using Cysteine-Functionalized Graphene Oxide/Polypyrrole Nanocomposite Film Electrode," *ACS Appl Mater Interfaces*, vol. 7, pp. 15935-43, Jul 29 2015.
- [31] B. Wu, N. Zhao, S. Hou, and C. Zhang, "Electrochemical Synthesis of Polypyrrole, Reduced Graphene Oxide, and Gold Nanoparticles Composite and Its Application to Hydrogen Peroxide Biosensor," *Nanomaterials (Basel)*, vol. 6, Nov 21 2016.

- [32] W. Zhang, J. Wei, H. Zhu, K. Zhang, F. Ma, Q. Mei, *et al.*, "Self-assembled multilayer of alkyl graphene oxide for highly selective detection of copper(ii) based on anodic stripping voltammetry," *Journal of Materials Chemistry*, vol. 22, p. 22631, 2012.
- [33] F. Tang, F. Zhang, Q. Jin, and J. Zhao, "Determination of Trace Cadmium and Lead in Water Based on Graphene-modified Platinum Electrode Sensor," *Chin. J. Anal. Chem.*, vol. 41, pp. 278-282, 2013.
- [34] X. Zhang, Y. Zhang, D. Ding, J. Zhao, J. Liu, W. Yang, *et al.*, "On-site determination of Pb 2+ and Cd 2+ in seawater by double stripping voltammetry with bismuth-modified working electrodes," *Microchemical Journal*, vol. 126, pp. 280-286, 2016.
- [35] E. Chow and J. J. Gooding, "Peptide Modified Electrodes as Electrochemical Metal Ion Sensors," *Electroanalysis*, vol. 18, pp. 1437-1448, 2006.
- [36] B. Çeken, M. Kandaz, and A. Koca, "Electrochemical metal-ion sensors based on a novel manganese phthalocyanine complex," *Synthetic Metals*, vol. 162, pp. 1524-1530, 2012.
- [37] J. Chang, G. Zhou, E. R. Christensen, R. Heideman, and J. Chen, "Graphene-based sensors for detection of heavy metals in water: a review," *Anal Bioanal Chem*, vol. 406, pp. 3957-75, Jun 2014.
- [38] J. Li, S. Guo, Y. Zhai, and E. Wang, "High-sensitivity determination of lead and cadmium based on the Nafion-graphene composite film," *Analytica Chimica Acta*, vol. 649, pp. 196-201, 2009.
- [39] Y. Shao, J. Wang, H. Wu, J. Liu, I. A. Aksay, and Y. Lin, "Graphene Based Electrochemical Sensors and Biosensors: A Review," *Electroanalysis*, vol. 22, pp. 1027-1036, 2010.
- [40] T. Gan and S. Hu, "Electrochemical sensors based on graphene materials," *An International Journal on Analytical Micro- and Nanochemistry*, vol. 175, pp. 1-19, 2011.
- [41] S. Wang, P. K. Ang, Z. Wang, A. L. L. Tang, J. T. L. Thong, and K. P. Loh, "High mobility, printable, and solution-processed graphene electronics," *Nano letters*, vol. 10, p. 92, 2010.
- [42] J. Gong, T. Zhou, D. Song, and L. Zhang, "Monodispersed Au nanoparticles decorated graphene as an enhanced sensing platform for ultrasensitive stripping voltammetric detection of mercury(II)," *Sensors & Actuators: B. Chemical*, vol. 150, pp. 491-497, 2010.
- [43] Z. Li and Q. Xia, "Recent advances on synthesis and application of graphene as novel sensing materials in analytical chemistry," *Rev. Anal. Chem.*, vol. 31, pp. 57-81, 2012.
- [44] D. A. C. Brownson and C. E. Banks, "Graphene electrochemistry: an overview of potential applications," *Analyst*, vol. 135, pp. 2768-2778, 2010.
- [45] Y. Iwai, A. Hiroki, M. Tamada, and T. Yamanishi, "Radiation deterioration in mechanical properties and ion exchange capacity of Nafion N117 swelling in water," *Journal of Membrane Science*, vol. 322, pp. 249-255, 2008.
- [46] C. Moore, S. Hackman, T. Brennan, and S. D. Minteer, "Effect of mixture casting phosphonium salts with Nafion (R) on the proton exchange capacity and mass transport through the membranes," *J. Membr. Sci.*, vol. 254, pp. 63-70, 2005.
- [47] T. Y. Chen and J. Leddy, "Ion exchange capacity of Nafion and Nafion composites," *Langmuir*, vol. 16, 2000.
- [48] I. I. Emmanuel, G. B. Priscilla, J. Nazeem, T. Khotso, and M. W. Chandre, "Metallo-Graphene Nanocomposite Electrocatalytic Platform for the Determination of Toxic Metal Ions," *Sensors*, vol. 11, pp. 3970-3987, 2011.

- [49] G. Williams, B. Seger, and P. V. Kamat, "TiO<sub>2</sub>-graphene nanocomposites. UV-assisted photocatalytic reduction of graphene oxide," *ACS nano*, vol. 2, p. 1487, 2008.
- [50] J. Liu, S. Fu, B. Yuan, Y. Li, and Z. Deng, "Toward a universal adhesive nanosheet for the assembly of multiple nanoparticles based on a protein-induced reduction/decoration of graphene oxide," *Journal of the American Chemical Society*, vol. 132, p. 7279, 2010.
- [51] C. Chen, X. Niu, Y. Chai, H. Zhao, and M. Lan, "Bismuth-based porous screen-printed carbon electrode with enhanced sensitivity for trace heavy metal detection by stripping voltammetry," *Sensors and Actuators B: Chemical*, vol. 178, pp. 339-342, 2013.
- [52] Z.-q. Zhao, X. Chen, Q. Yang, J.-h. Liu, and X.-j. Huang, "Selective adsorption toward toxic metal ions results in selective response: electrochemical studies on a polypyrrole/reduced graphene oxide nanocomposite," *Chem. Commun.*, vol. 48, pp. 2180-2182, 2012.
- [53] R. Rong, H. Zhao, X. Gan, S. Chen, and Q. Xie, "An Electrochemical Sensor Based on Graphene-Polypyrrole Nanocomposite for the Specific Detection of Pb (II)," *NANO*, vol. 12, 2016.
- [54] M. Choi and J. Jang, "Heavy metal ion adsorption onto polypyrrole-impregnated porous carbon," *Journal of Colloid And Interface Science*, vol. 325, pp. 287-289, 2008.
- [55] R. Xu, L. Xiao, L. Luo, H. Jia, C. Wang, and F. Wang, "High Electrochemical Performance for Pb(II) Detection Based on N,S Co-Doped Porous Honeycomb Carbon Modified Electrodes," *J. Electrochem. Soc.*, vol. 164, pp. B382-B389, 2017.
- [56] Z. Wang, L. Li, and E. Liu, "Graphene ultrathin film electrodes modified with bismuth nanoparticles and polyaniline porous layers for detection of lead and cadmium ions in acetate buffer solutions," *Thin Solid Films*, vol. 544, pp. 362-367, 2013.
- [57] R. María-Hormigos, M. J. Gismera, J. R. Procopio, and M. T. Sevilla, "Disposable screen-printed electrode modified with bismuth-PSS composites as high sensitive sensor for cadmium and lead determination," *Journal of Electroanalytical Chemistry*, vol. 767, pp. 114-122, 2016.
- [58] "World Health Organization, Guidelines for drinking-water quality [electronic resource]: incorporating 1st and 2nd addenda, Vol.1, Recommendations.– 3rd ed.," *Silver, Geneva, Switzerland*, pp. 434-435, 2008.
- [59] Y. Wei, C. Gao, F.-L. Meng, H.-H. Li, L. Wang, J.-H. Liu, *et al.*, "SnO<sub>2</sub>/Reduced Graphene Oxide Nanocomposite for the Simultaneous Electrochemical Detection of Cadmium(II), Lead(II), Copper(II), and Mercury(II): An Interesting Favorable Mutual Interference," *The Journal of Physical Chemistry C*, vol. 116, pp. 1034-1041, 2012.
- [60] J. Wang, C. Bian, J. Tong, J. Sun, and S. Xia, "L-Aspartic acid/L-cysteine/gold nanoparticle modified microelectrode for simultaneous detection of copper and lead," *Thin Solid Films*, vol. 520, pp. 6658-6663, 2012.
- [61] X. C. Fu, J. Wu, J. Li, C. G. Xie, Y. Liu, Y. Zhong, *et al.*, "Electrochemical determination of trace copper(II) with enhanced sensitivity and selectivity by gold nanoparticle/single-wall carbon nanotube hybrids containing three-dimensional L-cysteine molecular adapters," *Sens. Actuator B-Chem.*, vol. 182, pp. 382-389, 2013.
- [62] L. Zhu, L. Xu, B. Huang, N. Jia, L. Tan, and S. Yao, "Simultaneous determination of Cd(II) and Pb(II) using square wave anodic stripping voltammetry at a gold nanoparticle-graphene-cysteine composite modified bismuth film electrode," *Electrochimica Acta*, vol. 115, pp. 471-477, 2014.

- [63] J. Morton, N. Havens, A. Mugweru, and A. K. Wanekaya, "Detection of Trace Heavy Metal Ions Using Carbon Nanotube- Modified Electrodes," *Electroanalysis*, vol. 21, pp. 1597-1603, 2009.
- [64] S. Tolani, A. Mugweru, M. Craig, and A. K. Wanekaya, "Rapid and efficient removal of heavy metal ions from aqueous media using cysteine-modified polymer nanowires," *Journal of Applied Polymer Science*, vol. 116, pp. 308-313, 2010.
- [65] B. Devadas, M. Rajkumar, S. M. Chen, and R. Saraswathi, "Electrochemically Reduced Graphene Oxide/Neodymium Hexacyanoferrate Modified Electrodes for the Electrochemical Detection of Paracetamol," *Int. J. Electrochem. Sci.*, vol. 7, pp. 3339-3349, 2012.
- [66] Z. Wang, J. Zhang, P. Chen, X. Zhou, Y. Yang, S. Wu, *et al.*, "Label-free, electrochemical detection of methicillin-resistant staphylococcus aureus DNA with reduced graphene oxide-modified electrodes," *Biosensors and Bioelectronics*, vol. 26, pp. 3881-3886, 2011.
- [67] S. Yang, B. Xu, J. Zhang, X. Huang, J. Ye, and C. Yu, "Controllable Adsorption of Reduced Graphene Oxide onto Self-Assembled Alkanethiol Monolayers on Gold Electrodes: Tunable Electrode Dimension and Potential Electrochemical Applications," *J. Phys. Chem. C*, vol. 114, pp. 4389-4393, 2010.
- [68] M. Jasinski, P. Gründler, G.-U. Flechsig, and J. Wang, "Anodic Stripping Voltammetry with a Heated Mercury Film on a Screen-Printed Carbon Electrode," *Electroanalysis*, vol. 13, pp. 34–36, 2001.
- [69] J. Barton, M. B. G. García, D. H. Santos, P. Fanjul-Bolado, A. Ribotti, M. McCaul, *et al.*, "Screen-printed electrodes for environmental monitoring of heavy metal ions: a review," *Microchimica Acta*, vol. 183, pp. 503-517, 2015.
- [70] A. Hayat and J. L. Marty, "Disposable screen printed electrochemical sensors: tools for environmental monitoring," *Sensors (Basel)*, vol. 14, pp. 10432-53, Jun 13 2014.
- [71] A. Odobasic, "Determination and Speciation of Trace Heavy Metals in Natural Water by DPASV," *University of Tuzla, Faculty of Technology, Bosnia and Herzegovina*, 2016.
- [72] F. A. Settle, "Handbook of Instrumental Techniques for Analytical Chemistry " *Prentice Hall (June 4, 1997)*, 1997.
- [73] A. P. Ruas de Souza, C. W. Foster, A. V. Koliopoulos, M. Bertotti, and C. E. Banks, "Screen-printed back-to-back electroanalytical sensors: heavy metal ion sensing," *Analyst*, vol. 140, pp. 4130-6, Jun 21 2015.
- [74] Q. Li, C. Yu, R. Gao, C. Xia, G. Yuan, Y. Li, *et al.*, "A novel DNA biosensor integrated with Polypyrrole/streptavidin and Au-PAMAM-CP bionanocomposite probes to detect the rs4839469 locus of the vangl1 gene for dysontogenesis prediction," *Biosensors and Bioelectronics*, vol. 80, pp. 674-681, 2016.
- [75] B. Haghghi and M. A. Tabrizi, "Direct electron transfer from glucose oxidase immobilized on an overoxidized polypyrrole film decorated with Au nanoparticles," *Colloids and Surfaces B: Biointerfaces*, vol. 103, pp. 566-571, 2013.
- [76] "Graphite and Its Awesome Properties," <http://www.electroboom.com/?p=835>, last accessed: 11/13/2017.
- [77] "Properties of Graphene Oxide."
- [78] L. J. Cote, F. Kim, and J. Huang, "Langmuir-Blodgett assembly of graphite oxide single layers," *Journal of the American Chemical Society*, vol. 131, p. 1043, 2009.
- [79] W. S. Hummers and R. E. Offeman, "Preparation of Graphitic Oxide," *Journal of the American Chemical Society*, vol. 80, pp. 1339-1339, 1958.

- [80] M. H. Chakrabarti, C. T. J. Low, N. P. Brandon, V. Yufit, M. A. Hashim, M. F. Irfan, *et al.*, "Progress in the electrochemical modification of graphene-based materials and their applications," *Electrochimica Acta*, vol. 107, pp. 425-440, 2013.
- [81] J. Gensheimer, J. Broaddus, Y.-C. Lin, and Y. Cao, "Scalable Production of Reduced Graphene Oxide (rGO) from Graphite Oxide (GO)," *Young Scientist, Vanderbilt Center for Science Outreach, Vanderbilt University* 2014.
- [82] J. Kauppila and A. Viinikanoja, *University of Turku, Faculty of Mathematics and Natural Sciences, Department of Chemistry, Laboratory of Materials Chemistry and Chemical Analysis*.
- [83] S. J. Deverel, S. Goldberg, and R. Fujii, "Chemistry of trace elements in soils and groundwater," *ASCE Manual and Reports on Engineering Practice, No. 71, Agricultural Salinity Assessment and Management (2nd Edition), Chapter 4*, pp. 89-137, 2012.
- [84] L. Zhu, C. Tian, R. Yang, and J. Zhai, "Anodic Stripping Voltammetric Determination of Lead in Tap Water at an Ordered Mesoporous Carbon/Nafion Composite film Electrode," *Electroanalysis*, vol. 20, pp. 527-533, 2008.
- [85] M. V. Orna and J. T. Stock, "Electrochemistry, past and present," *American Chemical Society, Division of the History of Chemistry*, vol. ACS symposium series, 390, p. 606, 1989.
- [86] S. B. Hočevár, B. Ogorevc, J. Wang, and B. Pihlar, "A Study on Operational Parameters for Advanced Use of Bismuth Film Electrode in Anodic Stripping Voltammetry," *Electroanalysis*, vol. 14, pp. 1707-1712, 2002.
- [87] "Wisconsin Department of Natural Resources, Wisconsin DNR Drinking Water data, Lead/Copper Samples," 2017.
- [88] "2016 Treated Water from Water Treatment Plants Water Quality Report, Milwaukee Water Works," 2016.
- [89] "2016 Distribution System Water Quality Report, Milwaukee Water Works," 2016.
- [90] "2015 Drinking Water Report, Washington Water Service Co., Allyn Shopping Center Water System, State ID #01695Q, MasonCounty," p. 5.
- [91] M. F. Mabrook, C. Pearson, and M. C. Petty, "Inkjet-printed polypyrrole thin films for vapour sensing," *Sensors and Actuators B: Chemical*, vol. 115, pp. 547-552, 23 May 2006 2006.